Digital Comprehensive Summaries of Uppsala Dissertations
from the Faculty of Pharmacy 373

Mechanistic Studies of Membrane Permeation of Peptides

ROSITA KNEISZL

ACTA UNIVERSITATIS
UPSALIENSIS
2025

ISSN 1651-6192
ISBN 978-91-513-2407-4
urn:nbn:se:uu:diva-552025

UPPSALA
UNIVERSITET

Dissertation presented at Uppsala University to be publicly examined in A1:107a, BMC, Husargatan 3, 75123, Uppsala, Thursday, 24 April 2025 at 13:00 for the degree of Doctor of Philosophy (Faculty of Pharmacy). The examination will be conducted in English. Faculty examiner: Professor Maija Lahtela-Kakkonen (University of Eastern Finland, Finland).

Abstract

Kneiszl, R. 2025. Mechanistic Studies of Membrane Permeation of Peptides. *Digital Comprehensive Summaries of Uppsala Dissertations from the Faculty of Pharmacy* 373. 92 pp. Uppsala: Acta Universitatis Upsaliensis. ISBN 978-91-513-2407-4.

Oral administration of drugs is often preferred over injections due to its convenience, and therapeutic peptides offer significant advantages, including high activity, specificity, and low toxicity. However, oral delivery of peptide drugs presents significant challenges such as low permeability across the gastrointestinal epithelium. A promising strategy to improve bioavailability is co-formulating peptides with permeation enhancers (PEs) to facilitate transcellular transport. In this thesis, the interactions between peptides, PEs, and lipid membranes have been investigated using both the atomistic all-atom (AA) and coarse-grained (CG) molecular dynamics (MD) simulations. We investigated the interactions between PE and membrane using AA-MD. The PEs studied were different medium-chain fatty acids, such as laurate, caprate (C10), and caprylate, and the caprylate derivative SNAC all with a negative charge and neutral caprate and neutral sucrose monolaurate. Our results indicated that the PEs, once incorporated into the membrane, induce membrane leakiness in a concentration-dependent manner. The results also indicated that a PE concentration of at least 70−100 mM is needed to strongly affect transcellular permeability. We then studied the colloidal structures of different peptide therapeutics in the presence and absence of two different PEs, C10 and SNAC and bile salt, taurocholate. The simulations provided insights into molecular-level interactions, highlighting the specific contacts between peptide residues responsible for aggregation and the interactions between peptide residues and permeability enhancers/taurocholates that are crucial within the mixed colloids. Our simulations also showed that the PEs can promote the release of hydrophobic peptides while restrict the release of water-soluble peptides. Finally, we also performed umbrella sampling simulations to calculate the effective permeability coefficients (Peff) for three different peptides: octreotide, desmopressin, and triptorelin, using CG-MD in the presence of C10 and SNAC in the membrane. The results show that C10 can increase the Peff, of the peptides included in orders of magnitude in a concentration-dependent manner, compared to the peptide systems without C10 present. These molecular-level insights can guide the design of improved permeability enhancer-based dosage forms, allowing for selecting the best possible peptide-PE combination and precise control of peptide release profiles near the intended absorption site.

Keywords: Molecular dynamics (MD) simulations, Umbrella sampling (US) simulations, membrane permeation, drug delivery, oral peptide therapeutics, peptide permeability, permeation enhancers, salcaprozate sodium (SNAC), capric acid (C10)

Rosita Kneiszl, Department of Pharmacy, Box 580, Uppsala University, SE-75123 Uppsala, Sweden.

ISSN 1651-6192
ISBN 978-91-513-2407-4
URN urn:nbn:se:uu:diva-552025 (http://urn.kb.se/resolve?urn=urn:nbn:se:uu:diva-552025)

Till Philip och Isabella

List of Papers

This thesis is based on the following papers, which are referred to in the text by their Roman numerals.

I. Larsson, P., Kneiszl, R., Marklund E. G. (2020) MkVsites: A tool for creating GROMACS virtual sites parameters to increase performance in all-atom molecular dynamics simulations. *Journal of Computational Chemistry,* 41(16):1564-1569

II. Kneiszl, R.*, Hossain, S.*, Larsson, P. (2022) *In Silico*-based experiments on mechanistic interactions between several intestinal permeation enhancers with a lipid bilayer model. *Molecular Pharmaceutics,* 19(1):124-137. Article of the Day (Dec. 16, 2021), Editors' Choice.

III. Hossain, S., Kneiszl, R., Larsson, P. (2023) Revealing the interaction between peptide drugs and permeation enhancers in the presence of intestinal bile salts. *Nanoscale*, 15:19180-19195

IV. Kneiszl, R., Hossain, S., Larsson P. (2025) Concentration-dependent effects from the permeation enhancers capric acid and SNAC on peptide permeability. *Submitted*

*Equal contributions

Author's contribution statement:
In paper I, I was involved in the data analyses. In paper II, I performed the simulations, validation, data analysis, visualisation, and wrote the original draft manuscript. In paper III, I performed the *in vitro* experiment and carried out some of the data analyses, and took part in the writing process regarding the *in vitro* experiments. In paper IV, I carried out the simulations, validation, data analysis, visualisation, and wrote the original draft manuscript.

Other contributions not included in the thesis:

I. Hossain, S., Parrow, A., Kabedev, A., Kneiszl, RC., Leng, Y., Larsson, P. (2022) Explicit-pH Coarse-Grained Molecular Dynamics Simulations Enable Insights into Restructuring of Intestinal Colloidal Aggregates with Permeation Enhancers. *Processes*, 10(1), 29.

II. In a collaborative project on cellular uptake and permeability of cyclic peptides, we performed molecular dynamics simulations to explain *in vitro* data on peptide permeability kinetics in Caco-2 cells. Some cyclic peptides that displayed unexpectedly high permeability with regards to their size and polar surface were found to fold in upon themselves, creating intramolecular hydrogen bonds and shielding polar groups. It thus seems that these cyclic peptides achieve high permeability by a mechanism reminiscent of Cyclosporin A permeability. A collaboration within the Dept. of Pharmacy, Uppsala University, and a pharmaceutical company.

III. Involved in a collaborative project to explore the atomistic modes of action of the structural salcaprozate sodium isomers, at various concentrations and charges, by employing all-atom molecular dynamics, and umbrella sampling simulations. A collaboration within the SweDeliver consortium with a pharmaceutical company.

Contents

Abbreviations

AA	All-atom
API	Active pharmaceutical ingredient
APL	Area per lipid
C8	Caprylic acid (neutral form), sodium caprylate (neg. charge)
C10	Capric acid (neutral form), sodium caprate (neg. charge)
C12	Lauric acid (neutral form), sodium laurate (neg. charge)
CG	Coarse-grain
CHOL	Cholesterol
FF	Force field
GI	Gastrointestinal (GI) tract
GLP-1 RA	Glucagon-like peptide 1 receptor agonist
ISDM	Inhomogeneous solubility-diffusion model
MD	Molecular dynamics
MM	Molecular mechanics
PBC	Periodic Boundary Conditions
P_{app}	Apparent permeability
P_{eff}	Effective permeability
PEs	Permeation enhancers
PME	Particle Mesh Ewald
POPC	1-palmitoyl-2-oleoyl-sn-glycero-3-phosphocholine
TAUR	Taurocholate
US	Umbrella sampling
VMD	Visual molecular dynamics

Introduction

With computational approaches in the 'dry laboratory', such as molecular dynamics (MD) simulations, – referred to as a 'computational microscope'[1,2] – the possibility to mechanistically study and explore dynamical and temporal processes at an atomic level exists, not accessible through traditional wet laboratory experiments[3]. Traditional wet laboratory experiments provide invaluable empirical data; however, it can be challenging to study fast or very small-scale events. Furthermore, MD simulations can complement wet laboratory experiments[3,4,5,6,7], when studying membrane permeation of peptides, for instance.

Membrane permeation of peptides

Permeability refers to the ability of a molecule to cross a cell membrane, and the rate at which it does so, typically expressed in cm/s. To study the passive absorption of drugs *in vitro*, the human intestinal epithelial cell line, Caco-2, can be used as a model. With this model, the obtained absorption rate constants are typically expressed as apparent permeability coefficients (P_{app}). Artursson and Karlsson[8] studied 20 drugs and peptides and found that the obtained P_{app} values ranged from 5×10^{-8} to 5×10^{-5} cm/s, with higher values for substances that have a higher oral absorption percentage in human. Moreover, drugs and peptides that are absorbed to <1% had P_{app} values $\leq 1 \times 10^{-7}$ cm/s. For instance, the orally administered peptide desmopressin had a P_{app} value of 0.13×10^{-6} cm/s[8]. The apparent permeability gives a value on the overall permeability, including passive diffusion and active transporters, and is measured in cell-based models that mimic *in vivo* conditions. In contrast, the effective permeability (P_{eff}) reflects specifically the passive diffusion, representing the intrinsic ability of a molecule to cross a membrane. The value of P_{eff} depends on factors such as molecular size, polarity, charge, and lipophilicity, as well as membrane characteristics like thickness, lipid composition, and sterol content.

The majority of therapeutic peptides are administered via injection, as oral delivery is limited by the physiology of the gastrointestinal (GI) tract and the inherent physicochemical properties of peptides. The oral route of administration is generally preferred for various reasons, as injectable formulations can

cause discomfort and pain at the injection site, reduce patient adherence, and result in higher healthcare and manufacturing costs compared to orally administered peptides. However, there are several obstacles associated with oral delivery of peptide drugs, such as maintaining stability in the GI tract, low permeability, and a narrow absorption window in the intestine.

Challenges with absorption of peptides

Therapeutic peptide molecules are important in the treatment of severe diseases such as cancer, hypercholesterolemia, and diabetes mellitus[9]. However, the vast majority of marketed orally delivered drugs are small molecules (in molecular size) and qualify into the Biopharmaceutical Classification System[10] (BCS) class II, being of low solubility and high permeability, and typically following the criteria in Lipinski's rule of five for optimal properties for absorption, distribution, metabolism and excretion (ADME). Lipinski's rule states that the molecular weight (MW) should be under 500 g/mol (also, Dalton (Da)), a calculated Log P<5, hydrogen bond donors should be <5, and <10 hydrogen bond acceptors, for good absorption of small molecules[11]. Note that, Lipinski formulated these rules in 1995[12] when 11% of the included 2245 compounds had a MW over 500 Da. Therapeutic peptides generally fall into the third category of the BCS, mainly being of high aqueous solubility and low permeability. Moreover, not surprisingly, peptides generally do not conform to Lipinski's rule of five. The molecular weight of a therapeutic peptide is typically in the range of 500-5000 Da[13]. They are molecules "beyond the rule of 5".

Peptides are linear sequences of up to 50 amino acids (AA), with insulin being an exception consisting of 51 AA. An amino acid consists of a central carbon atom (the α-carbon) bonded to a hydrogen atom (H), a side chain (residue, -R) that determines the amino acid's polarity, charge, and reactivity, a carboxyl group (-COOH, C-terminus), and an amino group ($-NH_2$, N-terminus). In the mammalian cell, the pH is close to neutral (pH 7), and both the carboxylic group and the amino group are fully charged. The order of amino acids in a sequence, of connected amino acids, starts at the N-terminal and ends at the C-terminal. The carboxyl group of one amino acid and the amino group of another form a covalent peptide bond, linking amino acids together to create peptide or protein (>50 AA) sequences (primary structure). Sometimes, a peptide has a secondary structure, folding patterns, such as α-helices and β-sheets, stabilized by hydrogen bonds, as in insulin, studied in Paper III. Peptides are often too short to have a stabilizing tertiary structure, determined by the amino acid sequence, and a quaternary structure such as proteins have, stipulating functionalities. However, peptides can form simple dimers and aggregates despite being a single chain.

Peptides can aggregate in different ways depending on their sequence, environment, and concentration. Hydrophobic residues tend to promote aggregation by clustering together to avoid water. In addition, aromatic residues can interact via $\pi - \pi$ stacking, stabilising aggregates. Specific sequences are prone to β-sheet-rich aggregates, for instance in amyloid-β peptides. MD simulations can provide information on the mechanistic behavior of the aggregation, but also support in the search for appropriate anti-aggregation drugs[14]. Moreover, atomistic MD simulations can identify key hydrophobic residues and the formation of hydrogen bonds responsible for influencing the aggregation propensities of structurally similar decapeptides[15].

The challenges associated with oral administration of peptides include the following:

1. The peptide bond is susceptible to hydrolysis by protease and peptidase enzymes in the GI tract. The machinery of the human body is inherently designed to enzymatically degrade proteins and peptides in the stomach and intestine to absorb amino acids, and di-, and tripeptides to utilize them as building blocks. Digestive enzymes such as pepsin in the stomach, and trypsin and chymotrypsin in the small intestine, cleave the peptide bonds connecting amino acids in peptides and proteins. Additionally, peptides are susceptible to metabolism by peptidases present in the brush border of the epithelium. Also, peptides such as cyclosporine A can undergo metabolism by cytochrome 450 (CYP450) enzymes in the brush-border. Cyclosporin, and other peptides, can also be targeted by efflux proteins like P-glycoprotein (P-go)[16] limiting their permeation. One approach to enhance the peptide stability is to alter the chirality of the constituent amino acids, changing them from the naturally occurring L-amino acid enantiomer to the D-enantiomer. Another approach is to change the naturally occurring amino acid to an unnatural one. Furthermore, to co-formulate the peptide with a P-gp inhibitor can also be an approach. The acidic pH in the stomach, which serves to protect the body from harmful bacteria and viruses, can also denature or hydrolyse peptides, rendering them inactive. Additionally, bile salts can destabilize peptide structures. One formulation strategy to mitigate this challenge is to protect it with an enteric coating.

2. The intestinal mucus layer lining the intestinal wall can trap and slow down the diffusion of peptides, functioning as a barrier. The main glycoproteins in mucus is mucin, which carry a net negative charge at neutral pH that can interact with positively charged peptides, limiting their mobility and preventing them from reaching epithelial cells[17].

3. Poor permeability. Peptides are in general more hydrophilic than lipophilic, challenging the partitioning into lipophilic cell membranes, resulting in low permeability. There is a correlation between high permeation and high hydrophobicity[18], although too high is not good either as it tends to interact more with the membrane lipid tail region (by adsorption). In addition, slow diffusion in the aqueous layer, and low solubility are other characteristics of too hydrophobic compounds. Tight junctions between epithelial cells further restrict the passage of large molecules (MW>500Da), such as peptides to pass through the paracellular route. One formulation approach to improve permeability is to co-formulate the peptide with permeation enhancers (PEs).

4. First-pass metabolism. After absorption, the splenic vein and the hepatic portal vein transports substances from the GI tract to the liver for processing. In the liver, peptides, like small-molecular drugs, undergo first-pass metabolism, reducing their bioavailability. Chemical structural modifications can be relevant in order to minimize first-pass metabolism by CYP450 enzymes (Phase I), and to minimize the risk of Phase II first-pass metabolism, in which conjugation processes take place to enhance the molecule's water solubility for excretion[17].

Oral therapeutic peptides

A handful of peptide drugs are marketed for oral administration, of which two are based on the permeation enhancer (PE) formulation technology, such as octreotide co-formulated with caprylate (C8) in Mycapssa® and semaglutide co-formulated with SNAC in Rybelsus®. Permeation enhancers have been studied since the 1960s[19] and are molecules that enhance the absorption of hydrophilic molecules with low permeability over the epithelium in the GI tract, including peptides[20], and for instance, vitamin B12[21] (cobalamin). The oral peptide therapeutics currently approved on the market contain the following active pharmaceutical ingredients (API): (i) desmopressin, (ii) cyclosporine A and voclosporin, (iii) the first approved marketed peptide drug based on PE formulation design: Semaglutide, (iv) the second approved peptide drug on the market based on PE formulation design: Octreotide.

Desmopressin is a structure analogue of the endogenous antidiuretic hormone arginine vasopressin that regulates the water balance in the body. Desmopressin has been modified such that the N-terminal α-amino group has been replaced by a hydrogen (deamination of 1-cysteine), and the L-arginine at position 8 has been replaced by D-arginine. Desmopressin is available for oral delivery for the treatment of central diabetes insipidus, nocturnal enuresis and

other conditions. It has a molecular weight of 1069 Da and an amino acid sequence of deamino-Cys(1)-Tyr-Phe-Gln-Asn-Cys(1)-Pro-D-Arg-Gly-NH_2. The number in parenthesis denotes a disulphide bond between the two cysteine residues. This short sequence makes it stable and less susceptible to degradation by human intestinal fluid (HIF) in the gastrointestinal (GI) tract, unlike large linear peptides, such as insulin. It has a high potency with an oral bioavailability of only 0.17% from a 1–4 microgram dose, 0.2 mg/tablet. It has a Log P value of –4.2[16]. The permeability of desmopressin over a mixed POPC-cholesterol membrane (70:30 ratio), in the presence and absence of permeation enhancers, has been studied by employing umbrella sampling simulations, in the work in Paper IV. Desmopressin is presented in Figure 1.

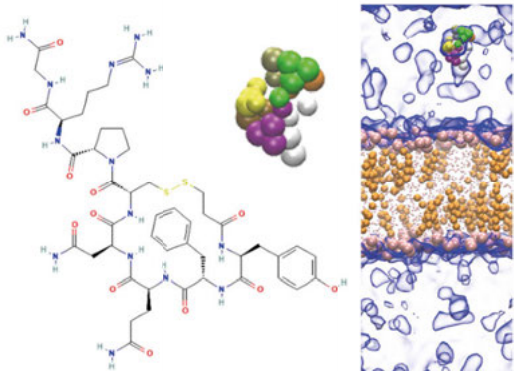

Figure 1. Coarse-grained (CG) desmopressin peptide molecule structure (top, middle), CG molecular simulation (MD) snapshot of desmopressin in the aqueous phase, created in the visual software Visual Molecular Dynamics[22] programme (VMD), (right), Paper IV. Molecular structure of desmopressin (left), PubChem.

Key features, among others, needed for successful oral delivery of peptide therapeutics are high potency, as seen for desmopressin[16], and high permeability, as seen for cyclosporine A[16,18]. Furthermore, it is beneficial if the peptide is able to adopt another conformation by shielding polar groups and reducing intermolecular hydrogen bonding while passing through the more hydrophobic membrane. Once in the aqueous phase again, in the cytosol, it can adopt to other, more hydrophilic conformations again. This has been observed with nuclear magnetic resonance (NMR) spectroscopy[23,24,25]. In addition, with computational MD simulation experiments, it was reported that a peptide's flexibility is of importance for membrane permeation, as seen for the cyclic peptide cyclosporine[23].

Cyclosporine A, and voclosporin (MW: 1214 Da) with improved affinity to the target site, are immunosuppressant peptides given by oral administration, indicated for organ transplantations. These peptides have not been studied in this thesis, but serve as examples of the possibilities and challenges orally

delivered peptide drugs face. Cyclosporin is a neutral, lipophilic cyclic peptide with stable bonds, consisting of eleven amino acids (MW 1203 Da). It can permeate through cell membranes and interact with intracellular targets[18]. Up to 86% of the administered dose permeates the intestinal epithelium, however, due to brush border metabolism and efflux, the fraction absorbed (F_a) is 35%. Furthermore, 8% is metabolised in the liver, yielding an oral bioavailability (F) of 27% in general, however, in the range of 20–50%[16]. Furthermore, cyclosporine induces aggregation of gel-forming mucins – the intestinal mucus barrier of glycoproteins[26]. Although cyclosporin's lipophilicity differs from desmopressin's, yet, interestingly, they have comparable diffusivity[16].

Semaglutide is the first approved oral peptide therapeutic based on PE formulation design – one of two to this day. Semaglutide is a glucagon-like peptide 1 (GLP-1) receptor agonist (RA) present in the oral tablet Rybelsus®[27], indicated for type 2 diabetes mellitus. It was brought to the market as a result of the PIONEER clinical trials programme[27], and was approved on the market by the Food and Drug Administration (FDA) in September 2019, followed by the European Medicine Agency (EMA) in April 2020. In the oral tablet, semaglutide is co-formulated with the permeation enhancer SNAC, known also as salcaprozate sodium, developed with the Eligen carrier technology[28] by Emisphere Technologies, USA, (Figure 6). Semaglutide is a linear peptide with a linker and a fatty acid part (molecular weight: 4114 Da). It has an oral bioavailability of 0.4-1.2%, compared to 87% of that from the subcutaneous injection of semaglutide. However, with the oral treatment, a steady state is reached in almost everyone, due to a half-life of seven days[29]. Semaglutide has not been studied in this thesis. However, the permeation enhancer SNAC has been studied in Papers II-IV.

Octreotide is the second approved peptide drug based on PE formulation design. It is the API present in the oral capsule in the marketed drug Mycapssa®[30], which was approved in June 2020 by FDA, for the treatment of acromegaly. Octreotide is a synthetic cyclic octapeptide analogue to the endogenous hormone somatostatin, and was developed during the 1980s[31]. In Mycapssa, it is co-formulated with the transient permeability enhancer (TPE™) technology – an oily suspension of different pharmaceutical excipients, including a medium-chain fatty acid (MCFA) caprylate (C8, (Figure 4)) as the main permeation enhancer[31]. Octreotide has a molecular weight of 1019 Da, and its amino acid sequence can be found in the SI of Paper III. The positively charged residues are D-Phe and Lys. The hydrophobic residues D-Phe, Phe, and D-Trp show significant contact interaction pattern with the PEs and the taurocholate bile salt studied in Paper III.

Information on peptide concentration in oral dosage forms is limited in the literature. However, Berg *et al.*[32] studied a solid oral dosage form containing

18 mg of octreotide, which can yield approximately 0.35 mM to 3.5 mM of octreotide peptide concentration in an intestinal water pocket, assuming the release of the dose occurs within 1–5 pockets with a volume of approximately 5–10 millilitres[32]. Octreotide has been studied in Papers III-IV included in this thesis. In Paper III, the aggregation behaviour, among other, of octreotide, in the presence and absence of the permeation enhancers capric acid (C10) and salcaprozate sodium (SNAC), has been investigated with all-atom MD simulations. In Paper IV, the permeability of octreotide over the mixed POPC-cholesterol model membrane has been studied, in the presence and absence of the permeation enhancers C10 and SNAC by employing coarse-grained (CG) MD simulations. Octreotide is presented in Figure 2.

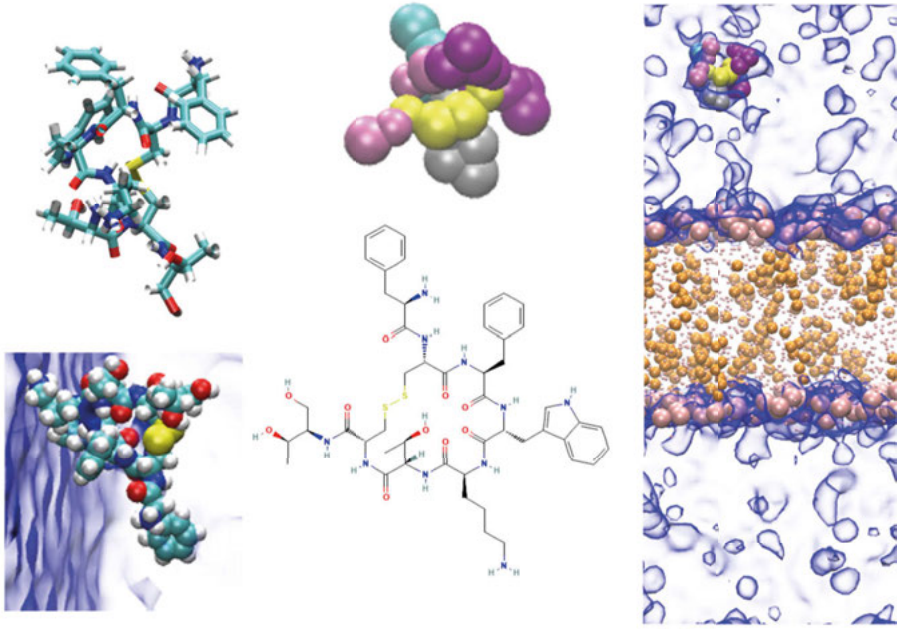

Figure 2. All-atom (AA) molecular dynamics (MD) simulation snapshot of an octreotide peptide molecule in aqueous solution (lower left corner, Paper III). AA-MD simulation snapshot of the octreotide molecule, visualized with VMD (Paper III). Coarse-grained (CG) octreotide peptide molecule structure (top, middle), CG-MD snapshot of desmopressin in the aqueous phase (right), Paper IV. All molecular visualizations were created in the software visual molecular dynamics (VMD), apart from the molecular structure of octreotide, (bottom, middle), (PubChem).

Permeation enhancers

Permeation enhancers (PEs) are molecules with the ability to enhance the absorption of hydrophilic molecules with low permeability over the intestinal epithelium, such as peptides. Permeation enhancers (PEs) can also be termed

absorption enhancers or promotors, and in some cases, as in the work included in this thesis, intestinal permeation enhancers or transient permeation enhancers, and as found in some literature specifying it to oral peptide permeation enhancers. A thorough review on approximately 250 PEs by Maher *et al.*[16] is available in the literature. Intestinal PEs transiently alter the intestinal epithelial barrier to facilitate permeation of substances with low oral bioavailability. The increase in bio-availability of the peptides in the presence of PEs, have resulted in low, single-digit numbers (around 1-5%). For both octreotide and semaglutide, an oral bioavailability around 1% have been sufficient for effective treatment, however, PEs should at least increase the bioavailability of peptides to 10% due to variability between individuals[29].

Intestinal permeation enhancers can be categorized as tight junction selective (paracellular PEs) and/or membrane perturbing (transcellular PEs)[33]. The permeation enhancers that act as tight junction (TJ) openers can be classified as 1st generation, which mediate an indirect effect, or 2nd generation, which mediate a direct effect on the tight junctions[16]. C10, having a multimodal effect, belongs to the 1st generation TJ openers[34]. In a study by Li *et al.*[35], the authors reported on the apparent permeability coeffcient value (P_{app}) of intestinal octreotide absorption in Caco-2 cell monolayers, in the presence of a tight junction modulator, sinomenine, with an octreotide concentration of 10 µM and 0.5% w/v of sinomenine (SN). The obtained P_{app} values were determined to 5.89×10^{-6} cm/s for octreotide and SN, compared to the control (octreotide alone): 2.67×10^{-6} cm/s. In a model of Everted gut sacs studies in rats, the octreotide concentration of 10 µM and 0.5% w/v of sinomenine resulted in a non-linear increase in octreotide absorption, compared to that of octreotide alone – approximately a 2.15-fold increase of octreotide with sinomenine. Sinomenine mediated the opening of tight junctions in a reversible and transient way[35]. Transcellular PEs can be categorized as surfactants that alter the integrity of the enterocyte membrane, as complexing agents, and as non-surfactant PEs[16]. The surfactant PE group can be further divided into subgroups, where medium-chain fatty acids (MCFAs) belong to the first, and bile salts to the second.

Human intestinal fluids (HIF) help with digestion and nutrient absorption. One key component is bile, consisting of bile salts, secreted into the duodenum during digestion. Bile salts are synthesized in the liver with cholesterol as precursor molecule. The function of bile salts is to emulsify large fat droplets into smaller droplets, and to aid in the absorption of fat and that of fat-soluble molecules, by forming micelles to transport components across the intestinal lining into the bloodstream. Cholic acid and taurocholate molecules are key components in bile salts as emulsifiers and in enabling fat digestion. Bile salts can be classified as transcellular intestinal permeation enhancing molecules.

Different molecular representations of taurocholic acid and taurocholate are illustrated in Figure 3.

The work presented in this thesis focuses on studying PEs belonging to the transcellular category, rather than the tight junction selective PEs, apart from medium-chain fatty acids (MCFAs) having multimodal modes of action (Papers II-IV), and sucrose monolaurate (Paper II). Additionally, taurocholate has been studied, in the fasted and in the fed state, together with permeation enhancers and peptides in the work included in Paper III.

In vitro diffusion studies have demonstrated that the interaction between peptides and bile salts or PEs can lead to a reduction in the availability of free peptide monomers. These findings highlight the complex interplay between peptide-colloid interactions and peptide stability, all of which ultimately affect peptide absorption and bioavailability[36,37]. Pabois *et al.*[38] conducted AA-MD simulations to study the aggregation behaviour of different bile salts, confirming their self-assembly driven by the hydrophobic steroid region. The simulations revealed that the ionic chain of the hydroxyl groups of the bile salts predominantly interact with the bulk water[38].

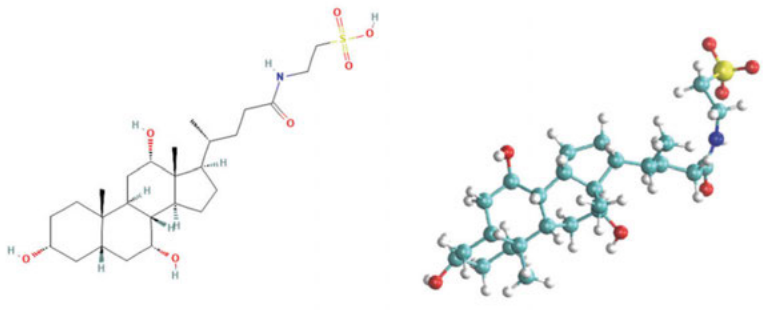

Figure 3. Left: Molecular structure of taurocholic acid (PubChem), and to the right: Atomistic representation of taurocholate from MD simulation (Paper III).

Monoglycerides (MGs) and medium-chain fatty acids (MCFAs) are single-chained saturated lipids containing six to twelve carbon atoms, with a carboxylic acid headgroup (-COOH). MGs contain a glycerol backbone bound to a single fatty acid with an ester bond (-COO-). Both MGs and MCFAs exhibit amphiphilic properties, allowing for self-assembly into micelles and vesicles, above their critical micelle concentrations (CMC). This can disrupt model and biological membranes, contributing to their potential antibacterial properties and relevance in drug delivery. In this thesis, only the potential of MCFAs as

permeation enhancers for hydrophilic molecules, such as peptides, is explored, not MGs. A thorough review on fatty acids (FAs) and monoglycerides (MGs) by Joon and Jackman[39] is available in the literature.

MCFAs are weakly ionizable molecules sensitive to changes in pH, as opposed to the non-ionic MGs. The bulk pK_a value, defined as the concentration where half of the carboxylic headgroups are deprotonated and the other half protonated – of MCFA monomers is around 4.8, which slightly increases with hydrocarbon chain length. They will have another pK_a value, the surface pK_a value, within a phospholipid membrane, which can be remarkedly higher compared to the bulk pK_a value, due to the local dielectric environment[40]. Reported[41] surface pK_a values (air/water interface) for C8 and C10 were 4.9 and 6.4, respectively. The higher surface pK_a value for C10 was reasoned to be because of stronger intermolecular interactions preventing the acidic hydrogen atom in the carboxylic group to easily dissociate[40]. A study by Hossain *et al.*[42] in which molecular dynamics simulations were employed on CMC values for C8, C10, and C12, revealed that in the ionized state the CMC were 32, 15, and 1 mM, respectively, and in the non-ionized state, they were 9, 5, and 1 mM, respectively. Here, CMC was defined as the concentration were half of the MCFA molecules were in the micellar state. The lower concentrations needed for micelle formation in the non-ionized state is reasoned to be because of the hydrophobic effect, which increases with increasing hydrocarbon chain length[42]. A pivotal *in vitro* study[43] on C10, reported that at lower C10 concentrations, the initial incorporation rate into phosphatidylcholine vesicles (DMPC), was quicker at lower concentrations than at higher. This was argued to be because of the monomeric form of C10 at lower concentrations as opposed to the micellar state at higher concentrations, where the C10 molecules first have to dissociate from the micelle into monomers, and then insert into the vesicles. Thus, it was established that FA monomers and micelles interact differently with membranes[43]. In a molecular dynamics study, Kang *et al.*[44] simulated C10 micelles near the membrane interface and they found that the micelles do not cause membrane disruption, rather acting as a C10 molecule reservoir by releasing C10 monomers into the bilayer, creating localized mass imbalances between the two leaflets, where smaller sized micelles more efficiently transferred C10 monomers to the membrane[44].

The amphiphilic nature of MGs and MCFAs, makes them prone to partition into membranes, which can affect membrane properties and alter permeability. However, the results of their insertion depend on if they assembled into the formation together with the cylindrical shaped membrane phospholipids, or if they inserted with their coned-shaped geometry, into the already formed phospholipid membrane. The former scenario creates an energetically favourable equilibrium state, and the latter a non-equilibrium state. In the former, the likelihood of disrupting the membrane is lower as compared to in the latter. In

both, the effect on permeability is comparable[40]. In the latter, when a positively curved single-chained lipid inserts into the outer leaflet of a bilayer, it creates a mass imbalance between the outer and the inner leaflet, which might cause transverse diffusion (flip-flop) of the inserted molecule, from the outer to the inner leaflet. This is a fast event for the non-ionic MGs and a slower one for anionic FAs. In addition, the insertion might cause the membrane to bend or bud with bilayer curvatures to accommodate for the space taken by the inserted molecules[40].

The sodium salts of the MCFAs are studied as permeation enhancers in oral drug delivery, such as caproic acid (C6:0, hexanoic acid), caprylic acid (C8:0, octanoic acid), capric acid (C10:0, decanoic acid), and lauric acid (C12:0, dodecanoic acid), Figure 4. To this day, capric acid is not present in any marketed oral peptide therapeutic, to the best of my knowledge. However, it has been included in various preclinical and clinical trials with biomolecules, such as desmopressin, and insulin. Moreover, C10 is the main PE component in the Gastrointestinal Permeation Enhancement Technology (GIPET™, Merrion Pharmaceuticals, Ireland)[16].

PEs can enhance the absorption by direct, and/or indirect modes of action. C12 is believed to mediate a paracellular effect at low concentrations and a mucosal damaging effect at high concentrations. Sucrose monolaurate is described to work by an indirect effect by opening the tight junctions via membrane perturbation. C10 is believed to both have a transcellular perturbation such as altering the fluidity of the plasma membrane and a mucosal perturbation at a high concentration and by direct and indirect paracellular mechanisms at a low concentration. The mode of action by C8 is assumed to be to fluidize the plasma membrane[16,45,46]. C8, C10, and C12 have been studied in Paper II, and C10 has been studied in Papers III-IV.

A comparison made by Brayden *et al.* between C8, C10, and C12 FAs in relation to CMC, permeability enhancement, and cytotoxicity, studied *in vitro* in monolayers, revealed that for permeability enhancement the highest concentration was needed for C8 (highest CMC) > C10 (mid CMC) > C12 (lowest CMC). However, C12 resulted in the highest cytotoxicity and C8 in the lowest[47]. Tran *et al.*[48] studied C10 and a GLP1 co-agonist peptide, with enteric coating in a minipig model. They reported a relative bioavailability of ~2%, and that C10 worked by increasing the membrane fluidity[48]. The macrocyclic peptide enlicitide chloride (MK-0616), selected as the molecule of the year 2023[49], is a peptide currently in clinical trials formulated with the medium-chain fatty acid C10 as a permeation enhancer, for the treatment of hypercholesterolemia and coronary artery disease. It functions as a proprotein convertase subtilisin/kexin-type 9 (PCSK9) inhibitor[50,51].

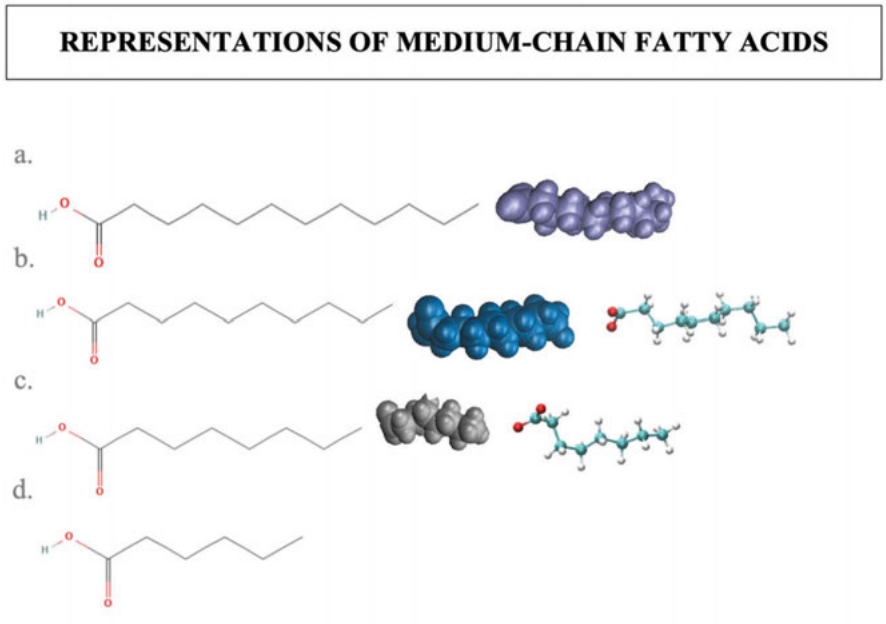

Figure 4. Molecular representations of medium-chain fatty acids (MCFAs), from the most upper panel: a) lauric acid (C12) molecular representations 1) molecular structure (PubChem), 2) atomistic molecular representation with VDW representation, 3) with licorice representation, in VMD. Molecules in b-d) follow the same pattern. In b) capric acid C10), in c) caprylic acid (C8), and in d) caproic acid (C6). The sodium salts of lauric acid, capric acid, and caprylic acid: sodium laurate, caprate, and caprylate, and capric acid have been studied in Paper II; C10 has been studied in Papers III-IV.

A non-ionic surfactant molecule, sucrose monolaurate, has been studied in the work of McCartney *et al.*[52] in which they identified it to be a potential permeation enhancer, mediating its enhancing effect by the means of plasma membrane perturbation, resulting in the opening of tight junctions and a paracellular flux. Sucrose monolaurate (SL) achieved to enhance the relative bioavailability of insulin with 2.4% (SL concentration: 50 mM) and 8.9% (SL: 100 mM), in rat jejunal and colonic instillations, at the same values as those seen for C10[52]. Sucrose monolaurate has been included in the work in Paper II in this thesis, and is presented in Figure 5.

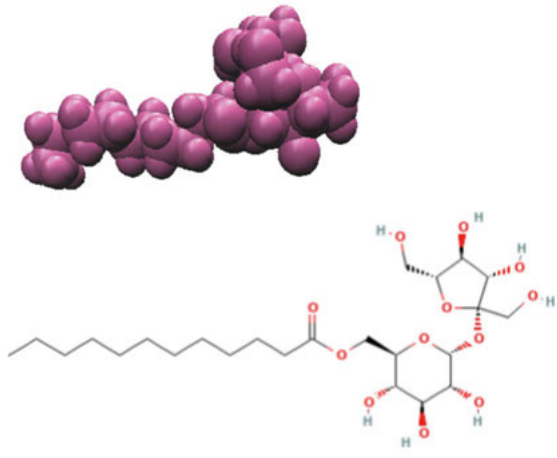

Figure 5. Molecular representations of sucrose monolaurate (SL). Upper part: atomistic molecular representation (VDW representation), created in VMD. Lower part: molecular structure obtained from PubChem.

Salcaprozate sodium (SNAC) is a synthetic *N*-acylated amino acid derivative of salicylic acid with a *pKa* around 5, (Figure 6). Although structurally similar to the MCFA caprylic acid – with its eight hydrocarbon single-chain and carboxylic acid headgroup, and with its aromatic ring structure, which the MCFAs lack – it does not behave as a surfactant in concentrations below its CMC[45], and it is not hydrophobic enough to form micelles, as MCFAs can.

SNAC has a GRAS status (Generally Recognized as Safe). As a permeation enhancer achieving around 1% bioavailability, SNAC is present in the marketed oral tablet Rybelsus®, Novo Nordisk, Denmark, co-formulated with semaglutide, and in Eligen® B12, Emisphere, USA, with vitamin B12 (cobalamin). The Eligen® carriers are the most studied substances as PEs. They are several hundred molecules that improve passive permeation across the intestinal epithelium. Apart from SNAC, (sodium *N*-[8-(4-hydroxybenzoyl)-aminocaprylate], there are also the following, among others, developed with the Eligen® carrier technology: (i) 5-CNAC (*N*-(5-chlorosalicyloyl)-8-aminocaprylic acid), and (ii) 4-CNAB (4-[(4-chloro-2-hydroxy-benzoyl)amino]butanoic acid)[16], Figure 6. SNAC has been studied in Papers II-IV.

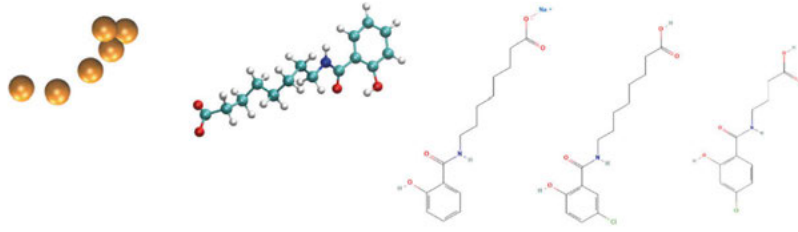

Figure 6. Molecular representations of the Eligen carriers®, from left to right: coarse-grained MD simulation representation of SNAC (Paper IV), atomistic representation of SNAC (Paper II-III), created in VMD. SNAC, 5-CNAC, and 4-CNAB structures obtained from PubChem.

The mode of actions of SNAC has been studied to a large extent, yet, not fully understood. In the following five sections, the currently believed mode of actions of SNAC are presented.

Efficient absorption of oral semaglutide is enabled by the presence of SNAC[27]. Semaglutide co-formulated with SNAC is absorbed in the stomach, achieved with controlled surface eroding of the tablet, resulting in a slower rate of tablet disintegration by the prevention of fluids from reaching the core of the tablet. The controlled release tablet minimizes the dilution of both SNAC and semaglutide, as a high local co-release close to the lining of the stomach help in enabling the uptake, thus, a spatial proximity between the two is needed. In the *in vitro* gastric epithelium model, NCI-N87, they observed a significant 7-fold (approx.) increase in the apparent permeability (P_{app}) of semaglutide in the presence of 80 mM SNAC, compared to control (no SNAC present). It was revealed that SNAC increased the pH of simulated gastric fluid (SGF) from acidic to neutral within 5 to 15 min, versus control (only semaglutide-containing tablets, no SNAC), assumably by inhibiting pepsin's activity at low pH by increasing the pH causing reduced pepsin activity[27].

Furthermore, investigations revealed that transcellular absorption of semaglutide occurs fast, in a highly localized environment in the stomach, and especially at the surface mucous epithelial cell layer, enriched within surface mucous cells. Additionally, studied in rats, paracellular-directed absorption was not occurring due to intact apical tight junctions[27], thus, classified as a transcellular PE. The interaction between SNAC and lipid membranes resulting in a transcellular effect, was established with high-sensitivity differential scanning calorimetry. With increasing SNAC concentration, the transition temperature (T_m) of DMPC reduced, indicative of SNAC incorporated in and fluidized the lipid membrane, changing the membrane permeability. Moreover, SNAC increases the monomerization of semaglutide, which is known to form

oligomers. The self-association of semaglutide was investigated with NMR spectroscopy, dynamic light scattering (DLS), and analytical ultracentrifugation, revealing a shift from semaglutide oligomers to monomers with increasing SNAC concentration, which also was confirmed not to be caused by the ionic strength from 120 mM sodium chloride in the system[27].

Initially, SNAC was believed to enhance absorption by increasing the lipophilicity of peptides by forming a noncovalent complex – a chaperone hypothesis. However, there are only limited and inconsistent evidence supporting that[27,29]. In addition, SNAC did not enhance the absorption of another GLP-1 analogue, liraglutide, studied in rats[27]. Liraglutide consists of a 16-hydrocarbon fatty acid with a L-γ-Glu-linker to obtain albumin binding and oligomerization. Semaglutide has an optimized fatty acid moiety for strong albumin binding (an 18-hydrocarbon long diacid). It also has another linker (bis-aminodiethoxyacetyl) for peptide flexibility and optimized binding to the receptor. In addition, it contains an unnatural amino acid to prevent peptidase degradation[53]. Moreover, the enhancing effect of SNAC seemed to be size dependent, decreasing as molecular size exceeds 4kDa[27].

However, how SNAC enhances permeability of peptides in the small intestine is still unclear[29]. In a study by Fattah *et al*.[54], SNAC and octreotide were studied in five intestinal tissue segments from rat, and across human colonic mucosae, mounted in Ussing chambers. The study reported that SNAC enhanced the apparent permeability of octreotide across all regions studied in both species, compared to the P_{app} coefficient value of octreotide alone. The P_{app} of octreotide in the presence of SNAC is reported to increase in various regions in the GI tract, and the values are in the order of 10^{-6} and range from 1.3 x 10^{-6} cm/s to 2.5 x 10^{-6} cm/s. These findings suggest that SNAC has potentials as a PE for octreotide. However, SNAC appears to interact with simulated intestinal buffer components[54]. In a study by Ling *et al.*, SNAC and octreotide interaction with hydrated DMPC liposomes were studied with solid-state NMR (ssNMR) spectroscopy. The study reported that SNAC increases the motion of phospholipids in one plane (uniaxial) in a concentration-dependent manner. It boosts the dynamics of lipid headgroups, which plateaus between 24- and 72-mM concentrations of SNAC. SNAC enhances the fluidity of the hydrophobic centre by 43% at 72 mM, more significantly than the interfacial region. When octreotide was introduced, these aforementioned results were less significant, which the authors reason to be the peptide-PE interactions consuming monomeric SNAC, decreasing the SNAC-membrane interactions[55].

In a preprint paper by Colston, Faivre and Schneebeli[56], scalable continuous constant pH (all-atom) molecular dynamics (CpHMD) simulations were employed to study PEs and the oral absorption of peptide drugs. They also utilized NMR, diffusion-ordered spectroscopy (DOSY), and dynamic light

scattering (DLS) experiments. The authors propose a 'sinking-in-quicksand' hypothesis, suggesting that PE-filled, that is, SNAC-filled, fluid membrane defects form, allowing polar peptide (semaglutide) to be submerged into the membrane. In the simulations, they observed how semaglutide, in the presence of SNAC and its redistribution, spontaneously incorporated into the membrane enabled by SNAC[56].

Innovatively, SNAC and C10 have been combined in the same formulation, reported in a recent paper by Niu *et al*[57]. The combination was evaluated both pre-clinically and clinically on oral peptide formulations of a GLP-1 analogue and a PCSK9 inhibitor, respectively. A synergistic effect was observed in an animal model, however, in clinical, for the combination to enhance the absorption of the PCSK9 inhibitor, the effect from C10 was missing. Hence, there are translatability issues between the specific animal model and human. They conclude that further understanding of C10-based peptide formulations, and of the mode of actions of C10 in human are needed[57].

Interestingly, from a mechanistic perspective, changing the position of the functional hydroxyl (-OH) group on the benzene ring in SNAC from *ortho*-position (as in the "effective" structure reported in Buckley *et al.*) to the *para*-position – resulting in *p*-SNAC, the *para*-isomer of SNAC – significantly diminishes the absorption-enhancing effect for semaglutide, rendering it ineffective, in comparison to SNAC (Figure 7). As a clarification, in Buckley, *et al.*[27], the "ineffective" structure of SNAC is referred to as *o*-SNAC; however, this may be *p*-SNAC, as the functional group is moved to the *para*- rather than the *ortho*-position (moved opposite to the amide group fatty acid chain and not adjacent – the "effective" isomer holds the hydroxyl group in *ortho* position). Returning to the main point, these "effective" and "ineffective" structural isomers of SNAC highlight the significance of exploring a deeper mechanistic understanding of their mechanisms of action and the differences between them.

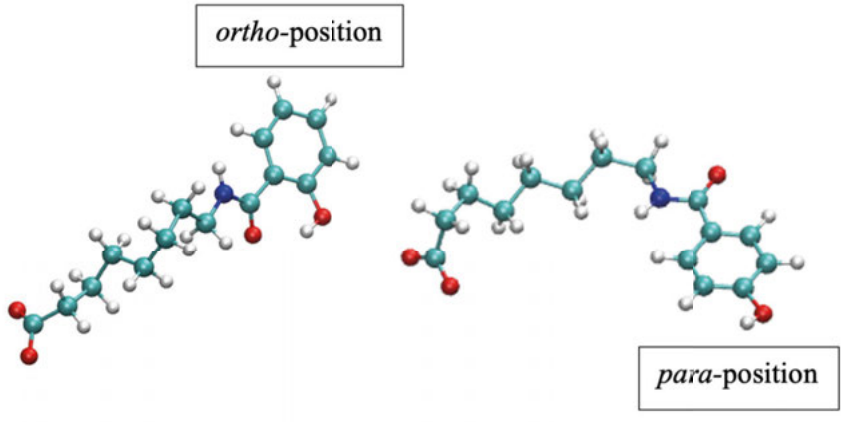

Figure 7. Structural isomers of Salcaprozate sodium (SNAC). To the left, with its hydroxyl (-OH) group in *ortho*-position, and to the right, *p*-SNAC with its hydroxyl group in *para*-position. Licorice representations created in the Visual Molecular Dynamics software (VMD) from atomistic MD simulations. The structural isomer *p*-SNAC, referred to as *ortho*-SNAC in Buckley *et al.*[27] has not been included in the work of this thesis.

Hossain *et al.*[58], studied the influence of bile composition on the membrane insertion of the PEs caprylate, caprate, and SNAC, both *in vitro* and with MD simulations. From MD simulations, they found that the amount of free PE monomers where higher in the fasted state simulated intestinal fluids (FaSSIF) than in the fed state (FeSSIF). Furthermore, that the transmembrane perturbation (insertion) of caprate (C10) and caprylate (C8) into the membrane was higher in the presence of FaSSIF than FeSSIF. The MD simulations also revealed that SNAC was instead adsorbed onto the membrane surface, as opposed to incorporation, indicating a different mode of action[58].

The plasma membrane

The spontaneous self-assembly and self-sealing of phospholipids into a bilayer in aqueous environments forms a stable barrier between the two aqueous compartments, in which the hydrophobic tails are facing each other within the bilayer – the hydrophobic core, and their polar head groups are exposed to the aqueous solution on either side (Figure 8).

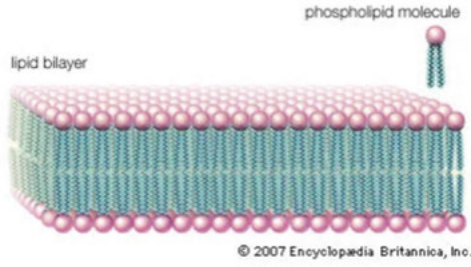

Figure 8. "Phospholipid molecules, like molecules of many lipids, are composed of a hydrophilic "head" and one or more hydrophobic "tails." In a water medium, the molecules form a lipid bilayer, or two-layered sheet, in which the heads are turned toward the watery medium and the tails are sheltered inside, away from the water. This bilayer is the basis of the membranes of living cells."[59] By courtesy of Encyclopædia Britannica, Inc., copyright 2014; used with permission.

The cell membrane is an anisotropic multicomponent system that is highly heterogeneous in the lipid distribution and composition[60]. The lipid composition of the cell membrane varies between cellular compartments such as the plasma membrane, endoplasmic reticulum, mitochondria, and between species. It is the integral membrane proteins that give the membrane its functionalities[61]. The plasma membrane also consists of approximately 65% glycerolipids, 10% sphingolipids, and 25% sterols such as cholesterol. Phospholipids are the most abundant of membrane lipids. They have a polar headgroup and two hydrophobic hydrocarbon, fatty acid tails. Typically, they contain between 14 to 24 carbon atoms (long-chain fatty acids), and one tail is usually saturated, and the other is unsaturated with one or more *cis*-double bonds, in general, creating a small kink. Differences between lipids in length and saturation influence the packing and fluidity in the membrane[62]. The membrane is asymmetrical in its composition between the two leaflets[60].

Cholesterol is as abundant as the phospholipids and are evenly distributed in both leaflets and consists of a small hydrophilic domain of a hydroxyl group, adjacent to it is a rigid planar structure composed of four fused hydrocarbon (steroid) rings, and a short single acyl chain. Cholesterol inserts its polar hydroxyl group close to the phospholipid head groups, and partly immobilize those regions in the acyl chain most adjacent to the polar headgroups, which results in a decrease in permeability to small hydrophilic molecules, such as water. To maintain optimal properties of the membrane, cholesterol impact the structure and function by influencing the membrane's fluidity, stability, and permeability[63]. The plasma membrane can undergo various curvatures and bend inwards or outwards. Membrane curvatures play a role in endocytosis, among other functions. Such active uptake mechanism might further impact the absorption rate of macromolecular drugs[64].

Koldsø *et al*.[60], created molecular dynamics simulation models with high complexity of the asymmetry of plasma membranes. One model consisted of 1500 lipids resembling the *in vivo* composition. They observed nano-clusters in the outer leaflet. With another model of 6000 lipids, they observed correlations between surface curvature of the bilayer with the clustering of lipid molecules[60]. The molecular view of the cell membrane is presented in Figure 9.

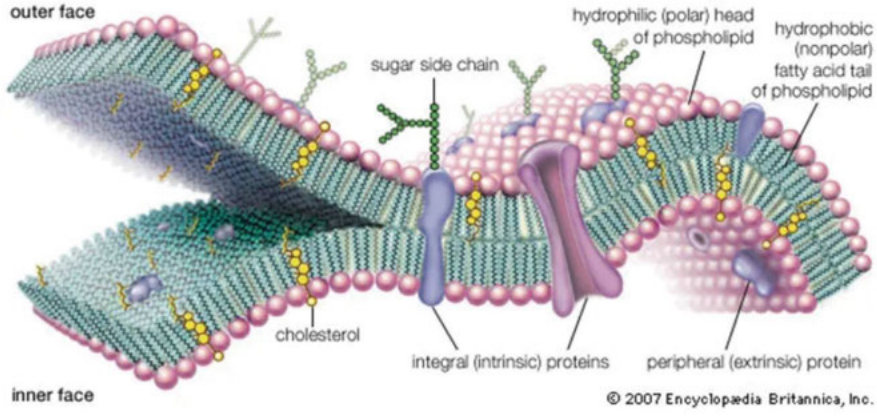

Figure 9. "Molecular view of the cell membrane. Intrinsic proteins penetrate and bind tightly to the lipid bilayer, which is made up largely of phospholipids and cholesterol and which typically is between 4 and 10 nanometres (nm; 1 nm = 10^{-9} metre) in thickness. Extrinsic proteins are loosely bound to the hydrophilic (polar) surfaces, which face the watery medium both inside and outside the cell. Some intrinsic proteins present sugar side chains on the cell's outer surface."[65] By courtesy of Encyclopædia Britannica, Inc., copyright 2017; used with permission.

Peptide drugs are generally too large and polar to permeate through the cell membrane. However, the most common mechanism for membrane permeation of high-permeable cyclic peptides is by passive diffusion[18]. Lateral diffusion is the movement of molecules within the plane of the bilayer and within a leaflet. It is a random, Brownian motion of molecules to distribute membrane components to maintain optimal properties, and it happens often and quickly – approximately 10^7 times per second, and a diffusion coefficient (D) of about 10^{-8} cm^2/second[62]. Cholesterol and membrane proteins, as the cytoskeleton actin, can reduce the overall lateral diffusion.

In transverse diffusion, also referred to as flip-flop events, a lipid molecule transverse from one leaflet to the other, within the membrane. It is essential in maintaining the asymmetry in composition of the leaflets, and to maintain its curvature, tension, and functionality. It happens slowly and rarely – less than once a month. A flip-flop event is an energy-intensive process, as the hydrophilic head group of the lipid needs to pass through the hydrophobic core of the bilayer. Cholesterol, as opposed to POPC, does not need enzyme-

assistance in order to flip-flop, and it can do so faster compared to lipids. In Figure 10, simple diffusion, lateral diffusion, and transverse diffusion are illustrated.

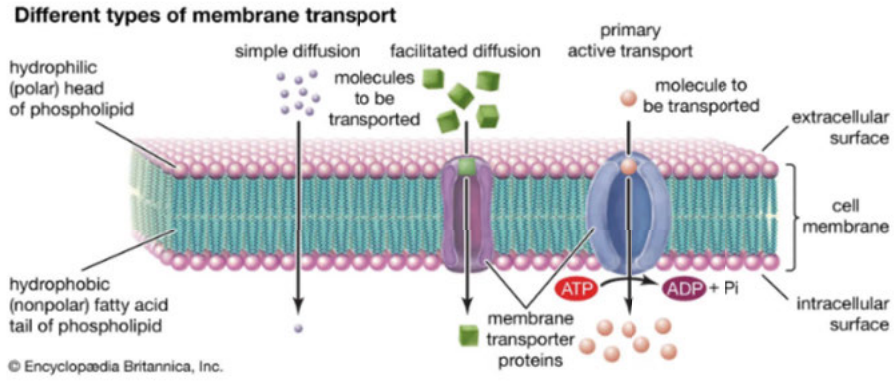

Figure 10. Different types of membrane transport, such as simple diffusion, facilitated diffusion, and active transport. By courtesy of Encyclopædia Britannica, Inc., copyright 2018; used with permission.

Molecular dynamic simulations

Despite the extensive information available regarding PEs, knowledge of their precise molecular mechanisms of action remains incomplete. Furthermore, the ways in which different PEs affect the properties of lipid bilayers are not fully understood, nor is it clear what makes a particular combination of PEs and peptides successful. Molecular dynamics (MD) simulations can capture events on the molecular level, and different analyses of the obtained trajectories can provide valuable insights into the composition of oral peptide dosage forms.

MD simulations can also be used to generate new experimentally testable hypotheses[4]. In a published review article[4], Hollingsworth and Dror explain MD simulations, and the possible applications and limitations in relation to the *in vitro* experiments to accelerate potential findings by the use of both techniques[4]. With experimental data from *in vitro* experiments, simulations can be validated and also improved. In general, macroscopic behavior of systems is easy to observe *in vitro*, while difficult to simulate. On the other hand, molecular and atomistic details and energetics can be observed in simulations, while difficult to capture *in vitro*[66]. MD simulations can be used to study molecular interactions of various PEs, nano-particles, membrane fluidity and membrane structural properties. Some of the limitations with atomic MD simulations is that they are computationally demanding, and typically can only be applied to the study of processes on very short time- and length scales. In a review article

by Moradi *et al.*[3], they go through published work on molecular dynamics simulations studying lipid bilayers in relation to important analyses of such, the technical challenges, and the existing protocols[3].

Molecular dynamics (MD) is a computational simulation technique that dates back to the 1950s. The concept of MD simulations as a tool to study particles dynamically was introduced by Alder and Wainwright in 1957[67] simulating the behaviour of hard spheres in a box varying temperature and density properties. This provided the science community with numerical evidence for phase transitions. In addition, the Verlet algorithm[68] from 1967 is still used, also as refined versions thereof, in modern MD simulations as a numerical integrator. Modern MD simulations enable the study of interactions on different time scales, achieving an atomic-level (10^{-10} meters) spatial resolution and a femtosecond (10^{-15} seconds) temporal resolution. The first molecular dynamics (MD) simulation with atomistic level details on the permeability of water over a lipid bilayer was published in 1994[69], in which the inhomogeneous solubility-diffusion model (ISDM) was reported. The ISDM account for the rate of flow across a membrane, and takes into account the local variations of the solubility and the diffusivity of a compound within a membrane[70].

Atomistic MD simulations – on the atom and molecular level (1 to 100 nm) – currently provide the most detailed molecular descriptions available on model membrane systems. Every atom included in the system is accounted for. In coarse-grained (CG) MD simulations – 10 to 100 nm, a mesoscopic length scale – atoms are grouped together into CG beads, which allows for the increase in time- and length scales from the atomistic resolution. Larger scale models such as continuum and hybrid models exist as well. In addition, restrained simulations, such as umbrella sampling simulations are applicable to capture rare events, such as a peptide molecule located in the hydrophobic core of a membrane. In this thesis work, atomistic and coarse-grained models, and umbrella sampling simulations have been employed.

In MD simulations, the use of molecular mechanics force fields (FF) is required, which is the potential energy function to describe the interaction between atoms. The pairwise interatomic energy can be of different contributions, for instance, bonded potentials, and van der Waals interactions. In short, the integration algorithm stipulates how the calculations are carried out, and the force field provides the integration algorithm with what to calculate for each timestep. The chosen force field defines the forces acting on each particle in the system, in relation to their properties and positions. There are different types of force fields, such as:

1. All-atom (AA) force fields have parameters for every single atom within a system. The time step between two consecutive force-calculations (which is the time-consuming part) is limited to 2 fs in standard atomistic simulations. The timestep is limited to 1 to 2fs due to the high-frequency vibrations of bonds and angles involving hydrogen atoms (the fastest degrees of freedom in the system). Hence, an increase in timestep is limited by the fastest vibrations. Bond stretching vibrations, especially those involving hydrogen (H) atoms, are very fast (on the order of 10 fs), thus, a very small timestep is required to accurately simulate these vibrations. The use of constraints makes this more efficient, allowing a timestep of 2fs instead of 1fs.

   The increase from the typical timestep of 2fs to up to 4–4.5fs can be achieved by the virtual interaction sites method, in which hydrogen atoms are replaced by massless virtual interaction sites. The virtual sites technique has been shown for the regular amino acids and for some lipids, and is implemented by default in MD software packages such as GROMACS[71]. The python toolkit MkVsites[72,73] enable virtual interaction site parameters in GROMACS for any molecule, such as unusual molecules, modified groups or atom types, for instance, found in drug molecules. Today, it is impossible to apply the virtual sites technique on such modified molecules and unusual atom types often present in drug molecules without the MkVsites toolkit. The proof of concept for the MkVsites tool resulted in Paper I.

2. Coarse-grained (CG) force fields, which accelerate traditional AA MD simulations, contain abstract representations of molecules by grouping heavy atoms into CG beads, with a 4:1 mapping, in general, with one single interaction center. For example, four methyl groups (4x -CH_3) are described as four CG carbon beads. This makes it possible to sample the motions of molecules on the microsecond scale (10^{-14} temporal resolution), typically with a 10 or 20 fs timestep; it can be higher. However, what is still underway, among other changes, is “the introduction of polarized particles in the peptide backbone that will allow secondary structure transitions to occur”[74]. Molecular representations for illustrative purposes can be found in Figure 11.

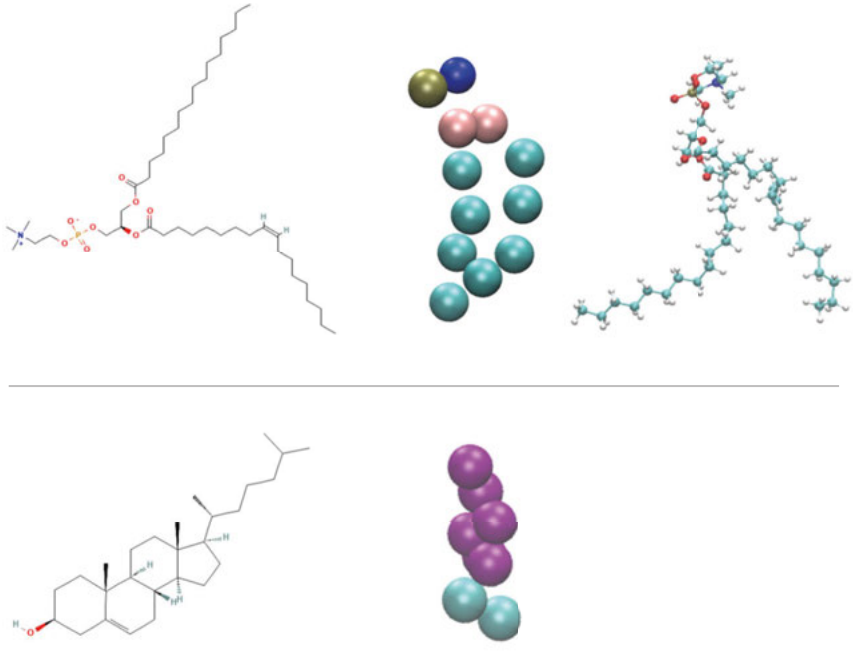

Figure 11. Molecule structures of 1-palmitoyl-2-oleoyl-sn-glycero-3-phosphocholine (POPC, upper panel: Molecule structure obtained from PubChem, coarse-grained MD molecule, atomistic MD molecule) and cholesterol (CHOL, lower panel: molecule structure, CG MD molecule representation (no study included on AA MD cholesterol = no AA MD representation)).

In summary, the force fields describe the intra- and intermolecular forces within a system. The foundation in every force field constitutes of four components that involve the bond stretching, angle bending, and the bond rotation (torsion), thus, the bonded interactions within a molecule, and forth, the non-bonded interactions in a system.

Umbrella sampling simulations

There are different free energy techniques – enhanced sampling – that can be applied for different purposes when studying rare events, such as free energy perturbation (FEP), thermodynamic integration (TI)[75], and free sampling (or enhanced sampling) such as umbrella sampling[76] (US), Meta dynamics, Adaptive biasing force (ABF), and Replica exchange molecular dynamics (REMD). Umbrella sampling (US) is one of the most traditional free energy techniques applied, used in order to obtain the potential of mean forces (PMFs). It has been employed in Papers II-IV in this thesis work.

The different thermodynamic energy states can be specified along a selected reaction coordinate, ξ, in order to separate these states. Along the reaction coordinate, the probability distribution of the system can be calculated, arriving at the free energy along the reaction coordinate – the potential of mean force, $A(\xi)$, (PMF)[77]. The PMF is obtained by monitoring the time average $P(\xi)$, the distribution of the system along the reaction coordinate[77]. The PMFs[75] are the characterization of the energetics involved in the translocation of molecules from window to window in a system.

Along the selected reaction coordinate, a series of initial configurations - umbrella windows, are created, and the applied bias potentials keep the molecule studied in each configuration during the US simulation. In this thesis, the harmonic bias potentials have been applied, and the approach to split the reaction coordinate (ξ) into a set number of umbrella windows has been taken.

Weighted Histogram Analysis Method

In order to turn the US simulation in each window into a sampling of the global free-energy, the Weighted Histogram Analysis Method[77,78,79] (WHAM), or the umbrella integration analysis can be applied as methods to analyse the umbrella sampling simulations[77,78]. The free energy in each umbrella window can be joint to a global free-energy profile as a series of umbrella windows are combined with the analysis method WHAM – a postprocessing method. With WHAM, the aim is to minimize the statistical error of the distribution. The global distribution is calculated by a weighted average of the distributions of the individual windows, under the condition that the sum of all weights equals to 1. Sufficient overlap between umbrella windows is needed for WHAM, but not required, yet desired, for umbrella integration[77]. WHAM has been implemented when postprocessing the US simulations in the work in this thesis.

Aim of the thesis

The general aim of the thesis is to investigate the molecular level interactions between peptides, permeability enhancers and cell membranes by *in silico*-based methods, such as molecular dynamics (MD) simulations, and to validate the results with appropriate experimental characterization techniques.

The specific aims of the thesis are:

1. To implement and validate the virtual interaction sites technique used to increase the length of the timestep in all-atom (AA) MD simulations for lipids.

Paper I: The aim of the study in Paper I was to compare two simulations with and without the python-toolkit MkVsites, as a proof of concept of the tool in creating virtual interactions sites for any molecule.

2. To investigate and characterize the influence of several permeation enhancers (PEs) used for oral delivery on key lipid bilayer properties.

   Paper II: The aim of the study in Paper II was to employ all-atom molecular dynamics simulations to investigate the effects of the intestinal permeation enhancers SNAC, sucrose monolaurate, and medium-chain fatty acids, (C12, C10, C8) on the structural and dynamical properties of the lipid 1-palmitoyl-2-oleoyl-sn-glycero-3-phosphocholine (POPC) bilayer model.

3. To study and characterize the binding and interactions of different PEs and peptides.

   Paper III: The aim of the study in Paper III was to employ all-atom molecular dynamics simulations to investigate the interaction patterns between two PEs (sodium caprate and SNAC) and four different peptides (octreotide, hexarelin, degarelix, and insulin) in the presence of taurocholate, an intestinal bile salt, representing the fasted and the fed state, respectively.

4. To calculate the permeation rates of peptides across lipid bilayers, in the presence of and absence of PEs, using different techniques.

   Paper IV: The aim of the study in Paper IV was to study the peptides desmopressin, triptorelin, and octreotide in a POPC-cholesterol (70:30) bilayer both with and without the permeation enhancers capric acid and SNAC present using coarse-grained molecular dynamics simulations and umbrella sampling simulations to obtain permeability coefficient values for each molecule.

Methods

Computational tools

The simulation algorithm in molecular dynamics (MD) is most widely used, and there are related algorithms such as Brownian Dynamics, Langevin Dynamics, and Dissipative Particle Dynamics (DPD)[5]. These algorithms are implemented in simulation software packages, such as GROMACS[80,71], AMBER[81], NAMD[82], CHARMM[83], LAMMPS[84], and Desmond[85].

MD simulations are based on the Newtonian equations of motion, which are solved to describe the behaviour of a simulated system in terms of the motion of individual atoms as a function of time. To solve Newton's second law in MD simulations, the motion of each particle is integrated over time, in each timestep, using numerical methods like Verlet integration[68], Leapfrog Verlet (md), and Velocity Verlet (md-vv). In the GROMACS simulation software package, the default integrator is Leapfrog.

In an ideal system with no external forces (and no friction) the total energy should remain constant over time, which is known as the conservation of energy. The conservation of energy, or stable, small fluctuations around a constant value, is important for the stability and accuracy of an MD simulation. Large drifts or changes in total energy would lead to accumulation of errors affecting the results. The deviations could be indicative of for instance, the need to change the timestep or integration method. Some integration algorithms are better than others in the conservation of energy, e.g., the Velocity Verlet (excellent), Leapfrog (good), and Beeman's algorithms over for example Euler's method. If the timestep is too large, the integration method may cause large, unphysical updates to particle positions and velocities, which may be solved with a reduced timestep.

An external thermostat, such as the Nosé-Hoover, v-rescale, or Langevin dynamics, to control the temperature as temperature fluctuations might cause energy drifts may be applied. Also, an external barostat, such as Berendsen or Parrinello-Rahman, can be used for constant pressure during simulation to alleviate energy fluctuations due to volume changes, when applicable. In biomolecular systems, the use of a thermostat and a barostat are often beneficial, to mimic real world conditions, as have been done in the work in Papers II-IV

in this thesis. However, they should be well equilibrated and fluctuate around the reference value in order not to initiate/increase energy drifts.

Maintaining periodic boundary conditions (PBC) are beneficial to eliminate artificial boundaries that could cause energy drifts. PBC are a mathematical technique to mimic an infinite system and bulk properties by repeating the simulation box in all directions, while the central box contains the particles being simulated but they can cross the PBC with their coordinates translated to maintain continuity. PBC and Particle-Mesh Ewald (PME) have been used in all simulations included in this thesis. PME treats long-range interaction cutoffs to alleviate artifacts in those due to PBC.

Molecular mechanics force fields

The most commonly used molecular mechanics force fields (FF) are Amber, Charmm, Gromos, and OPLS[86]. A widely used coarse-grained (CG) force field is Martini. In this thesis, the MD simulation software package GROMACS.v5[7] has been employed with the Leapfrog algorithm as integrator, and the Charmm36 (Papers II-III), Martini2.0 and Martini2.2 (Papers II and IV), and amber (Paper I) FFs have been applied.

The Martini force fields are coarse-grained models. The CG Martini FF for lipid and surfactant systems was reported in the literature in 2003[87] and has been developed in close connection with atomistic models, and thermodynamic experimental data, similar to quantum calculations improving AA models[88]. The reduction of the number of degrees of freedom together with short range potentials result in computational efficiency in comparison with AA-MD simulation force fields. Micrometer length scales or millisecond time scales are accessible[87]. In 2007, Marrink *et al.*[88] reported improvements, coined Martini2.0, applied in Paper II in this thesis. The basic mapping of the CG Martini2.0 FF model is by assembling four heavy atoms and its hydrogens into one CG bead with a central interaction site (4:1), with the exception of ring-like structures, as found in SNAC, for instance. There are four main types of interaction sites: polar (P), nonpolar (N), apolar (C), and charged (Q). For each of these, there are also subtypes, 18 in total, in order to gain a more accurate representation. For instance, to attribute donor properties (d), acceptor (a), both (da), or none (0), or by a number denoting the degree of polarity (from 1 = low polarity to 5 = high polarity). Four water molecules are represented as a single type P_4 CG site. The PC headgroup consists of two hydrophilic groups: the choline (type Q_0, bears a positive charge) and the phosphate group (Q_a, bears a negative charge). Cholesterol is modeled by eight particles: six representing the sterol body (3:1 mapping) and two for the short tail[88].

The Martini version 2.2, applied in Paper IV in this thesis in which peptides were being simulated, was reported in the literature by Marrink *et al.* in 2012[74] and reports on improved parameters for peptides and proteins. The exception from the average 4:1 mapping approach is for the mapping of ring-like structures or small molecules, for instance, benzene, cholesterol, and amino acid residues. These structures are mapped with a higher resolution of up to 2:1 mapping and are denoted with a prefix "S". In the Martini 2.2 version, the following improvements have been made: new topologies for proline, phenylalanine, and tryptophan. In addition, there was the implementation of an auxiliary program called *martinize.py* applied to coarse-grain an atomistic level structure[74]. This program was used in Paper IV in the creation of the peptide molecules.

Water models can be either explicit or implicit representations. In this thesis, explicit water models have been used, in which each water molecule's interactions are accounted for.

System descriptions

In Paper I, the oestrogen molecule was selected as an arbitrary molecule to serve as a model compound to test the applicability of the MkVsites python-tool, as the estrogen molecule contains atom types that are not found in the parent amber99sb force field files.

In Paper II, each system contained a POPC bilayer of 128 POPC molecules in total, with a certain type of permeation enhancer at different concentrations inserted into one monolayer before the start of the simulations. One pure system with only POPC molecules was also created. In the systems with PEs, six different PEs were used at seven different number concentrations that varied in the range of approximately 5–35% (based on the total number of lipid molecules in the leaflet (n=64)), corresponding to around 20–160 mM concentrations. The PEs studied were sodium laurate, sodium caprate, and capric acid (neutral form), sodium caprylate, negative SNAC, and sucrose monolaurate (neutral form), SI Table 1, Paper II. All systems contained a concentration of 150 mM sodium chloride, to imitate a physiological saline concentration. The systems were built with the web-based tool CHARMM-GUI[89,90] Membrane Bilayer Builder[91,92,93].

In Paper III, two PEs – 50% sodium caprate and 50% capric acid, and the same for SNAC, at a concentration of 50 mM, and four different peptides (octreotide, hexarelin, degarelix, and insulin), in two different concentrations (3.3 mM and 10 mM) in the presence of taurocholate, an intestinal bile salt, at two different concentrations (3 and 15 mM) representing the fasted (FaSSIF) and

the fed (FeSSIF) state, respectively, were studied. All systems were prepared in a cubic box (10 nm).

These simulations were initiated from two different starting (initial) configurations in order to comprehensively study the release process: randomly inserted into the simulation box, and in pre-formed aggregates. As a means to unbias the results of the simulations from the initial starting configurations, we also examined two different starting placements of the molecules for the simulations containing 10 mM peptides. In one case, all molecules, including the peptides, were randomly placed in the simulation box at the beginning of the simulations. In the other case, PEs and taurocholate (Taur) were randomly added in the presence of pre-formed peptide aggregates.

In Paper IV, two different model membrane systems were created, one with only POPC molecules, 64 in each monolayer, and one with a mixed bilayer with POPC and cholesterol molecules in a 70:30 ratio (128 POPC molecules and 38 cholesterol molecules). Systems were created with only the bilayer molecules solvated in a water box with an ionic strength of 150 mM sodium chloride concentration. Membrane only systems were created. In the PE-membrane systems, the PE molecules were inserted in both leaflets before the start of the simulations. The PEs studied were neutral C10 and neutral SNAC, in two different concentrations, approximately 30% and 50%. The exact concentrations of these varied however, and can be found in SI Table 1, Paper IV.

The peptides octreotide, desmopressin, and triptorelin were randomly placed, (n=1) in the aqueous phase in each of the equilibrated, 1000 ns run mixed membrane systems, in the presence and absence of the PEs. The peptides were selected based on structural similarities between desmopressin and octreotide, and triptorelin was selected in order to include a small, linear peptide. All systems contained a concentration of 150 mM sodium chloride, to imitate the physiological saline concentration.

Here, we only sought for obtaining the respective permeability value. For the different PE systems, apart from obtaining respective permeability values, we also investigated the impact on the structural properties of the membrane, as the area per lipid, the membrane thickness, the order parameter, PE molecule count in the membrane, and the number and rate of flip-flop events.

Molecular topologies

Atomistic topologies

PE molecular topology for laurate, caprate, and caprylic acid are readily obtained from the Charmm36 FF files. First, the topology for laurate was generated in the CHARMM-GUI online tool, from which topologies for caprate, capric acid, and caprylate were created by removing the appropriate number of atoms, bonds, and angles. The input topology for SNAC was created through the parameterization process Charmm General Force Field (CGenFF) 1.0.0 program[94,95], with subsequent refinement for two dihedrals in force field toolkit (fftk)[96] in the software visual molecular dynamics (VMD)[22]. It was obtained from the work by Hossain *et al.*[58]. The input topology for sucrose monolaurate was created by combining that of laurate with the appropriate sugar moiety from the Charmm36 force field files. The AA C10 and SNAC topologies were used in Papers II-III.

MkVsites topologies

The oestrogen molecule was parametrized through the GAFF force field[97].

Coarse-grained topologies

The coarse-grained (CG) caprate and caprylic topologies were obtained from the work by Hossain et al.[42], in which they were developed and validated by obtaining the C14 topology from the cgmartini.nl website. Three C1 beads represent the acyl chain (1 C1 bead = 4 carbon atoms) and one bead (P4 (neutral form) or Qa (negative charge)) was used to represent the carboxylic group. The CG C10 model was obtained by removing one C1 bead from C14. Thus, CG C10 consisted of two C1 beads and one Qa (negative) bead. To obtain the CG C8 topology, the inter-particle distance of the beads in the CG C10 topology was reduced, from 0.47 to 0.37 nm, as the 4:1 mapping results in two C1 beads (2x4C) for both C8 and C10 in order to differentiate between the two[42]. The CG SNAC topology was obtained from the work in Hossain et al.[58], in which they developed it from the atomistic SNAC topology and validated it by following the parameterization of new molecules described on the Martini website. The CG C8, C10, and SNAC topologies were used in Paper II, and the CG C10 and SNAC topologies were used in Paper IV. In Paper IV, the CG POPC and cholesterol topologies were obtained from the CHARMM-GUI Martini Maker Bilayer Builder online tool.

In Paper IV, the peptides octreotide, desmopressin, and triptorelin molecular topologies were generated using the Martinize tool *martinize.py* available on the Martini website. The amino acid residues for the peptides were directly

available in from the tool. However, the N-terminal residue pyroglutamyl in triptorelin was generated by following the instructions for selecting Martini particle types, and a bead type of Na was selected for the pyroglutamyl side chain (SI section Peptide topologies, Paper IV).

Simulation description

All-atom molecular dynamics simulations

In Paper II-III, AA-MD simulations were performed with the software programme GROMACS[71] 2018 using the Charmm36 force field[98,99]. All simulations were performed at 37 °C (310.15 K) to mimic body temperature, and at an average of 1 bar. After energy minimization with the steepest descent algorithm for 10 000 steps and after system equilibrations, the final production run was performed during 500 ns for each system using a 2fs timestep. Electrostatic interactions were calculated using the Particle Mesh Ewald method, while van der Waals interactions were evaluated with a force-switch ranging between 1.0 and 1.2 nm.

Coarse-grained molecular dynamics simulations

In Paper II, 4μs long CG MD simulations were run for caprate, caprylate, and SNAC (all negative charged), for comparison with the AA MD simulations. The CG MD simulations were performed using the Martini2.0 force field[88].

In Paper IV, the CG systems were simulated with the Martini2.2 FF at a temperature of 37°C (310.15 K) and an average of 1 bar. Electrostatic interactions were treated with the reaction-field method with a cut-off of 1.1 nm, and the vdW interactions were treated by applying a cutoff of 1.1 nm. Energy minimization and system equilibration followed the CHARMM-GUI protocol. The production runs were performed during 1000 ns for each system using a 20-fs timestep, apart from the peptide systems. They were energy minimized and equilibrated but not run for 1000 ns as the peptides were randomly inserted in the respective, already run mixed membrane only, and mixed membrane-PE systems, as the membrane structural properties in those systems were not to be analyzed, but the permeability.

Umbrella sampling simulations

Umbrella sampling simulations were employed in Papers II-IV to compute the potential of mean force (PMF).

In Paper II, umbrella sampling (US) simulations were to pull caprate, caprylate, and SNAC molecules from the membrane center to the water phase using both AA CHARMM36 and CG Martini FFs. Twenty initial configurations were created along the reaction coordinate (in the z-direction, bilayer normal) with 0.2 nm spacing intervals. Each configuration was energy minimized and equilibrated, followed by a 20 ns long production run.

In Paper III, umbrella sampling (US) simulations were employed to investigate the release of the respective peptides from either a homogenous peptide aggregate or from a mixed colloid. The simulations focused on the expulsion of a single peptide molecule from an aggregate into the water phase, and hence, a reaction coordinate, with initial configurations with 0.2 nm spacing intervals, went from the aggregate surface to the bulk water phase. Energy minimization and equilibration for 100 ps was performed for each window followed by 12 ns of production runs.

In Paper IV, 36 initial configurations with a 0.1 nm spacing interval were created, restraining either a PE or a peptide molecule in each umbrella window, by a harmonic distance potential in the *z*-direction, translocating the molecule along the reaction coordinate. In each initial configuration, a 120 ns long umbrella sampling simulation was performed, after energy minimization, and energy equilibrations.

Fourier transform infrared spectroscopy

In Paper III, in addition to molecular dynamics and umbrella sampling simulations, Fourier transform infrared spectroscopy (FTIR) was employed to investigate the impact of the PEs on changes in the secondary structures of insulin. Here, we prepared six samples with insulin and NaCl, three at pH 2 and three at pH 6. These had a NaCl concentration of 100 mM, 250 mM, and 500 mM, in which insulin powder was dissolved to a concentration of 5 mg mL^{-1}, this was done for validation purpose. Then, we prepared samples with 5 mg mL^{-1} insulin in the presence of the PEs (50 mM) and taurocholate (3 mM, 15 mM) also, (pH 6). A sample of 5 mg mL^{-1} insulin only was also prepared (pH 6). All samples were filtered, heated, and shaken. Then freeze-dried and a FTIR spectra was collected in the 4000-6000 cm^{-1} region. To the obtained spectra, a second-order derivative with 9 points was applied. They were then area-normalized in the amide I region.

Data analyses

Calculations on structural membrane properties

Structural properties of a membrane such as the area per lipid headgroup (APL), the membrane thickness, the order parameter, the event of possible flip-flops within the membrane, and the lateral diffusion, are all valuable in different degrees depending on the purpose to assess the impact of a molecule on a membrane's structural integrity in terms of packing/order, fluidization, leakiness, disturbance, etcetera.

The area per lipid (APL) headgroup is a structural membrane property that is a measurement of the area a lipid headgroup occupy, and how that varies with different molecules being inserted into, or expelled out of, the membrane or the leaflet. With *in vitro* experimental techniques, the APL value can be obtained by the use of neutron and X-ray scattering analyses. On MD simulations output trajectory files, different approaches can be taken to obtain the APL values. Two different approaches have been taken in the work of this thesis.

In Paper II, the APL was calculated only by considering the average area of the box (*x*- and *y*-lengths), in-plane of the bilayer. The obtained area is divided by the total number of lipids in the leaflet (n=64). In Paper IV, another approach was taken. The average APL of the POPC and the cholesterol molecules, respectively, was calculated with the open-source software FATSLiM[100], with the respective headgroup beads PO4 and ROH as reference atoms. FATSLiM is an acronym for 'Fast Analysis Toolbox for Simulations of Lipid Membranes', written and reported by Buchoux[100]. This software is written in Python and designed to work with GROMACS files. It is especially valuable for the analysis of vesicles and large membranes containing hundreds to thousands of lipids, because it takes into account the oscillations and temporal curvatures of the bilayer in the trajectory. The software estimates a normal for each lipid and once that is done it can identify which lipids belong to the same leaflet by identifying lipids close to each other and with a normal pointing in the same direction. The APL is estimated by calculating local Voronoi cells of which the area is extracted.

The thickness of the membrane is a measurement to evaluate if the impact by the presence of a certain molecule increases or decreases the thickness of the bilayer. The thickness of a membrane in the human body varies from 4 to 9 nm. In MD simulations and for a one to two component lipid membrane, it is often around a value near 4 nm. In both Paper II and IV, the membrane thickness was measured with the FATSLiM[100] tool. It was measured as the average distance between the POPC AA phosphate atoms, or the CG phosphate headgroup beads of the two leaflets in the bilayer. With FATSLiM, the thickness

of the membrane is calculated for each lipid searching for neighbours that belongs to the other leaflet. The distance is averaged between the reference lipid and its neighbours, and average values along the trajectory can be extracted. For the tool to identify the reference lipid, one selects the phosphate atoms, for example, of the headgroup in the lipid.

In addition, one can obtain the thickness of a bilayer by using a visualization programme like VMD[22], PyMol and Avogadro, or by applying the GROMACS tool gmx distance, for instance, by computing the distance between the average *z*-positions of headgroup atoms in each leaflet, obtaining the temporal average of the membrane thickness.

Lateral diffusion ($D_{L[molecule]}$) is a measurement of the membrane fluidity and is the lateral movement (in the 2D plane) of lipids, or other molecules, within a leaflet of the bilayer. This can in simulations be analysed with the tool gmx msd (mean square displacement), where a reference atom is set, for instance, the phosphate atom of the headgroup region of the lipid is selected. In wet laboratory experiments, it is measured by fluorescence recovery after photobleaching (FRAP), in which the rate of the diffusion of the impact is translated into the fluidity of the membrane. It can also be measured by tracking individual molecules in real time to study their movement patterns, by single particle tracking (SPT). In the AA-MD simulations reported in Paper II, the lateral diffusion of the phosphate atom in the headgroup of POPC (P atom) was set as a reference and the impact on the lateral diffusion of the POPC molecules was measured with the presence and absence of different permeation enhancers at various concentrations.

The order parameter (S_{CH}) of the lipid acyl chain tails is a measurement of how much disturbance there is in the packing of the lipid tails in a bilayer, and that is measured in reference to a set axis, which in simulations is usually the bilayer normal ((S_z), *z* axis). The obtained value then provides information on the alignment of the lipid tails to the bilayer normal, where a high value close to 1 corresponds to little disturbance in the packing of the lipid tails and indicates a highly ordered system, and a low value indicates much disturbance and high disorder in the system.

The order parameter, P2, of the coarse-grained POPC lipid tails were calculated by running a python script available from the Martini website, called *do-order-gmx5.py*[101]. The script calculates the second rank order parameter, *P2*, which is defined in Equation 1.

$$P2 = 0.5\ (3 < cos^2(\theta) > -1) \qquad \text{Equation 1.}$$

Where theta is the angle between each bead-bead bond and the *z*-axis (bilayer normal). An obtained P2 value of 1 corresponds to perfect alignment of the bond with the reference axis, a value of -0.5 indicates anti-alignment, and a value of 0 reflects a random orientation of the specific bond relative to the bilayer normal. The last 100 ns of each production run was analysed.

The order parameter (S_{CH}) of the lipid acyl chain tails can be accurately measured with experimental NMR techniques. The results thereof are used to correct the force field parameters, of which a simulation is highly dependent upon for the accuracy of the outcome. Thus, apart from improving the force fields, there is also ongoing research on the different simulation tools available to calculate the order parameters. One of these tools is the GROMACS implemented module gmx order, which calculates the order parameter for the lipid tails and is the one used for the results in Paper II. Piggot *et al.*[102] state that tools that work on all-atom systems and tools that work on saturated lipid tails work extremely well.

In atomistic simulations, the angle, θ, is the angle between the C-H bond vector and the bilayer normal (*z*-axis, Paper II). The angle describes the orientation of the molecular axis in relation to that reference- how well the bond vector aligns with the bilayer normal, averaged over all of the lipids in the system during the entire course of the simulation (described by the brackets).

Molecule count

In Paper IV, the number of PE molecules inside the mixed membrane was calculated as a PE molecule being within a distance of 0.9 nm of any of the phosphate headgroup beads (PO4) of the POPC molecules in the leaflets.

In Paper II, an expulsion event of a PE molecule was defined as a PE molecule not being within a distance of 0.9 nm of any of the phosphate atoms of the POPC molecules in the leaflet (gmx select tool of GROMACS 2016). It was not counted if the PE molecule transversed to the other leaflet. It was only counted if it expelled to the aqueous phase.

The flip-flop events (transverse diffusion) in the atomistic simulations in Paper II were calculated by following the procedure in the work of Zawada *et al.*[103]. With periodic boundary conditions (PBCs), molecules can reach the other leaflet by crossing the PBC, rather than flip-flopping within the membrane. If a molecule reached the other leaflet through PBC, then it was not counted as a flip-flop event.

In Paper IV, the flip-flop events of cholesterol and PE molecules were identified by tracking the movement of the molecule's headgroup beads, ROH and

COO, respectively, relative to the midplane of the membrane, calculated as the average *z*-coordinate of all membrane beads. Cholesterol or PE molecules were assigned to either the upper or the lower leaflet based on their *z*-position. The criteria for a flip-flop event were when a molecule transitioned from one leaflet to the other and remained in there for at least ten consecutive frames. The flip-flop rate was calculated as the number of flip-flop events divided by the product of the total number of lipid molecules (found in SI Table 1, Paper IV) and the time of the simulation, which was 1μs.

Number of contacts

In Paper II, the normalized fractional interactions were calculated as the relative number of contacts between the POPC and PE molecules present in the membrane leaflet, to better understand the interactions of the PEs that remain in the inserted leaflet during the simulation with the lipid molecules. For a two-component system as our study, a fraction of 0.5 indicates a randomly mixed membrane.

In Paper III, the peptide residue-residue contact map was created based on the criterion that two residues were in contact if the distance between any pair of atoms from the respective residues was less than 0.5 nm, same for the peptide and PEs and taurocholate contacts.

Other analyses

In Paper I, the trajectories of the simulations were analysed on the number of hydrogen bonds (hbond) and the root mean square deviation (rms), respectively, in the software Gromacs version 2018.4, using the gmx rms and hbond modules, respectively.

In Paper III, the number of hydrogen bonds was analysed by applying the gmx hbond module, and the solvent-accessible surface area (SASA) was calculated using the gmx sasa module, and the secondary structure analysis was done using the gmx dssp module, all in Gromacs.

Applicable to Papers II and IV: The percentage number concentrations have been used for the permeation enhancer molecules. However, in order to translate these to molar concentrations, the volume can be obtained from the *x*-, *y*-, and *z*-box lengths. Note that, the molar concentration can vary between systems due to different lengths of the *z*-axis. In SI, Paper II, details on the molar concentrations for each system can be found.

Water permeability

In Paper II, the water permeability values were obtained by counting water molecules. In order to capture any permeation of water molecules deep into the core of the hydrophobic membrane region, the three last carbons of the POPC lipid tails and their hydrogens were selected. All water molecules within 0.5 nm from those were counted, as a measure of how permeable the membrane was to water molecules in the presences of different types of PEs.

Permeability calculation for PE and peptide molecules

In Paper IV, the squared variance of the molecule's position in each umbrella window was calculated. By dividing each variance with that window's tau value, a diffusion coefficient value was obtained, according to the procedure in Hummer's article[104]. With the obtained diffusion coefficient values and the obtained PMFs, the ISD model was used to calculate the effective permeability coefficient P_{eff} (cm/s). The ISD model is presented in Equation 2.

$$\frac{1}{P_{eff}} = \int_{z1}^{z2} R(z)dz = \int_{z1}^{z2} \frac{exp^{(\Delta G(z))/kT}}{D(z)} dz \qquad \text{Equation 2.}$$

Where P_{eff} is the permeability, R(z) is the z-position dependent local resistance value, ΔG is the free energy difference, and kT is the product of the Boltzmann constant and the temperature[104,105,106].

Results and Discussion

Interactions of permeation enhancers with the model membrane

To characterize changes in different membrane structural properties of the POPC and the mixed POPC-Cholesterol membrane, respectively, the changes in area per lipid headgroup (APL), membrane thickness, lateral diffusion coefficients of POPC molecules (D_L), and order parameters of POPC molecules (S_{CH}) and the order parameters of the POPC CG lipid tails (P2) in the presence and absence of permeation enhancers at different concentrations, were investigated, (Paper II and IV).

In Paper II, the membrane was composed of POPC only, which is abundantly available in the mammalian cells in general. However, phosphatidylethanolamine (POPE), and other components such as sterols as cholesterol are also typically present in the mammalian membrane. In addition, membrane proteins also. In Paper IV, the mixed membrane consisted of POPC and cholesterol in 70:30 ratio. To what extent different PEs impact the membrane structural properties composed of various lipids, membrane proteins and cholesterol demands further exploration. In Paper II, another simplification made in the current study was the absence of any drug molecules. Therefore, only the absolute effect of the PEs on the membrane properties in the absence of drugs was obtained in this computational study. In both Papers II and IV, neither were different pH values nor the effect of sink conditions taken into consideration. The relevant human intestinal fluids, enzymes, and the mucus normally present in the stomach and in the lumen were also missing, as was the possibility of exploring the paracellular route, as well as the permeation enhancing effect indirectly mediating the paracellular route.

In Paper II, the changes in area per lipid are presented in Figure 12a. For each PE, the APL values increase with increasing PE concentration. The maximum changes in APL value were observed for sucrose monolaurate among different PEs at all concentration levels, and its APL value at 35% concentration increased with 14.6 % compared to the pure POPC system. The changes in APL for negatively charged caprylate, caprate and laurate followed the same order as their chain length, with higher increase in APL happening for PEs with

longer carbon chains: C12-n > C10-n > C8-n. This increase can be assumed to be a direct consequence of the increased number of charged molecules in the bilayers, which would lead to more repulsive interactions between the PE and POPC molecules. It might also be rationalized in light of the expulsion events described below (Figure 16b) for the PEs during the simulations where shorter chain PEs expelled from the membrane to a larger extent, which in turn translates to a reduced impact on the changes of membrane APL. Capric acid molecules showed the lowest increase in APL among the PEs in this study, and the flip-flop events of capric acid molecules (Figure 16c) means that molecules become more evenly distributed in both leaflets, resulting in a lower increase in APL value. For the pure POPC membrane, that is, without any PE molecules, had an APL value of approximately 0.65 nm^2 (Figure 12a).

In Paper IV, the area per lipid (APL) was determined for both POPC and cholesterol in each system (Figure 14a-b). For the system without any PE molecules, that is, only containing a membrane of POPC and cholesterol, the APL values for POPC and cholesterol were 58.05 ± 1.07 $Å^2$ and 42.3 ± 2.40 $Å^2$, respectively. In our study, an increase in the APL values for both POPC and cholesterol were observed in the presence of PEs. However, in the systems with SNAC, the increase was smaller than that in the corresponding systems containing the same percentage of capric acid molecules. In addition, a very small difference was observed between the systems containing 30% and 50% SNAC molecules. In contrast, an almost linear increase in the APL values of POPC and cholesterol was observed with increasing concentrations of capric acid in the membrane.

In Paper II, changes in membrane thickness showed almost the opposite behaviour compared to the changes in APL with the exception of neutral caprate (Figure 12b). For each PE, there was a decrease in membrane thickness with the increasing PE % concentration. This decrease is mainly due to the presence of PE molecules near the headgroup region of the membrane, which tends to push the POPC molecules apart from each other. When this happens, packing of the lipid tails is disrupted, translated into a reduction of the effective length of the tails, reducing bilayer thickness. However, for the neutrally charged caprate, a slightly increasing trend in thickness was observed with increasing PE concentration. Additionally, the location of the neutral caprate molecules was much deeper inside the membrane compared to the other fatty acid molecules that had negatively charged headgroups. We calculated the average distance, *d*, between the membrane centre and the centre of mass for caprate molecules (both negatively charged and neutral headgroups) in the membrane normal direction. The value of *d* was found to be 1.49 and 1 nm for the caprate molecules with negatively charged and neutral headgroups, respectively.

In Paper IV, the membrane thickness for each model system can be found in Figure 14c. Similar to the APL values, a clear trend was observed in membrane thickness profiles in the presence of PEs. For both capric acid and SNAC, the thickness decreased with increasing PE concentration. In the system without PEs, the membrane thickness was 4.07 ± 0.05 nm. In the 30% capric acid system, the thickness decreased to 3.89 ± 0.04 nm, and in the 50% system, it decreased further to 3.67 ± 0.05 nm. The decrease in the membrane thickness with increasing PE concentration was nearly linear. In the 30% SNAC system, the membrane thickness decreased to 3.89 ± 0.06 nm, similar to the 30% capric acid system. However, in the 50% SNAC system, the membrane thickness decreased only slightly further to 3.85 ± 0.06 nm, indicating a less pronounced effect at higher concentrations compared to the corresponding capric acid system (Figure 14c).

In Paper II, to further understand the changes in membranes' structural integrity, the lateral diffusion coefficient (D_L) for the membrane POPC molecules in the presence of different PEs at various concentrations was also calculated (Figure 12c). Unlike the other properties discussed, we did not see a clear trend in changes of D_L with the changes in PEs' concentration. However, for most cases, the maximum value was observed for SNAC. This is due to SNAC's location and orientation at the membrane surface. As SNAC mostly remains near the POPC headgroup region, it can induce more lateral movement of the POPC headgroup atoms and increase the D_L value of the POPC molecules. Sucrose monolaurate also showed higher D_L values compared to the other fatty acid PEs, which is mainly due to its relatively larger size (Figure 12c).

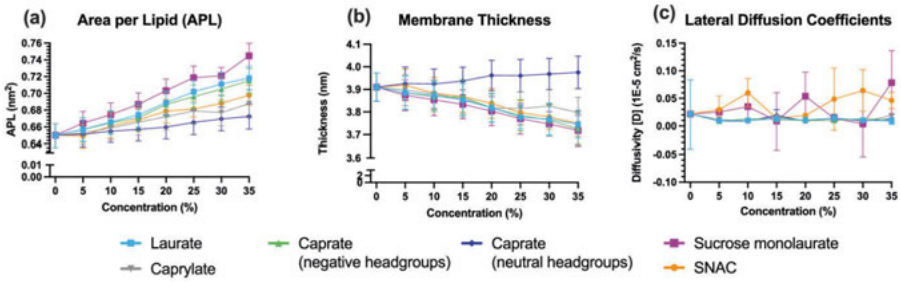

Figure 12. PEs effect on membrane structural properties. The changes in different structural properties (a) APL, (b) thickness, (c) lateral diffusion coefficient (D_L) for membrane POPC molecules calculated in the presence of different PEs at various number concentrations, Paper II.

In Paper II, the changes in order parameter (S_{CD}) values for the POPC lipid tails are presented in Figure 13. The POPC lipid tail order parameter can characterize the membrane structure, with a lower order parameter representing higher disruption within the membrane. For the negatively charged PEs, we

observed slightly decreasing POPC tail S_{CD}-values with increasing concentration, indicating a concentration-dependent PE effect on bilayer fluidity. The fatty acids with negatively charged headgroups showed a trend according to their chain length, with longer chain fatty acids causing less disruption compared to shorter chain fatty acids. The neutral molecules showed an opposite trend, most highly pronounced for capric acid (neutral form, Figure 13d). This is in agreement with a slightly increasing trend in thickness that was observed with increasing PE concentration for capric acid (neutral form). This is consistent with the increase in acyl chain order parameters seen for this particular case. Additionally, the location of the neutral caprate molecules was much deeper inside the membrane compared to the other fatty acid molecules that had negatively charged headgroups. We calculated the average distance, *d*, between the membrane centre and the centre of mass for caprate molecules (both negatively charged and neutral headgroups) in the membrane normal direction. The value of *d* was found to be 1.49 and 1 nm for the caprate molecules with negatively charged and neutral headgroups, respectively. SNAC qualitatively follows the behaviour of the other negatively charged PE concentration-induced changes to the order parameter, but the effect appears to be somewhat reduced. This is mainly due to the inability of SNAC molecules to remain incorporated into the membrane, as well as to penetrate deeper inside the membrane. This is mainly due to the inability of SNAC molecules to remain incorporated into the membrane, as well as to penetrate deeper inside the membrane. Note that the value of *d* (the average distance between the centre of the bilayer and the PE molecules) was found to be 1.9 nm for SNAC, which is relatively high compared to, for example, caprate molecules. To estimate the PE penetration ability inside the membrane, in addition to *d*, the average order parameter of the PE molecules themselves was also calculated and is presented in Figure S3, Paper II. This analysis, with the average order parameter for SNAC found to be 20% lower compared to the caprate molecules, suggests that the SNAC molecules typically remain relatively parallel to the membrane surface and interact with the POPC headgroup region without inducing significant disruption in the membrane POPC tail region compared to the other PEs.

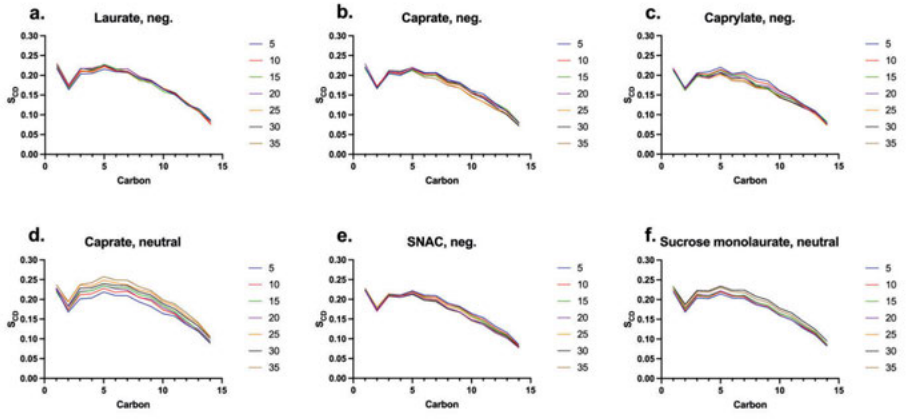

Figure 13. Carbon-deuterium order parameter for the *sn*-1 acyl lipid chain of POPC (S_{CD}), plotted for each PE in number concentrations: (a) sodium laurate, (b) sodium caprate, (c) sodium caprylate, (d) capric acid, (e) SNAC, negative charge, and (f) sucrose monolaurate (neutral form), Paper II.

In Paper IV, the order parameters of the POPC lipid tails for each model system were investigated (Figure 14d). As in line with expectations, cholesterol was observed to increase the order of the POPC lipid tails, as seen in the mixed POPC-cholesterol model system without PEs present, compared to the POPC-only membrane (SI Fig. 1c). This observation aligns with previous studies, which reported that cholesterol enhances bilayer order. The most ordered system was the one without any PEs. When PEs were added, the results indicated that higher concentrations of PEs in the membrane increased the disorder within the system, suggesting increased fluidization of the bilayer. A continuous decrease in the order parameter values was observed with increasing capric acid concentrations in the membrane. However, the transition from 30% to 50% SNAC concentration resulted in nearly identical order parameter values, which is consistent with the APL and membrane thickness results (Paper IV). SNAC reduced the order of the bonds closer to the membrane surface (GL1-C1A, C1A-D2A, GL2-C1B, and C1B-C2B) more significantly than the corresponding capric acid systems for both lipid tails. However, for bonds closer to the membrane centre (D2A-C3A, C3A-C4A, C2B-C3B, and C3B-C4B), the 50% capric acid system exhibited the lowest order parameter values among all systems (Figure 14d).

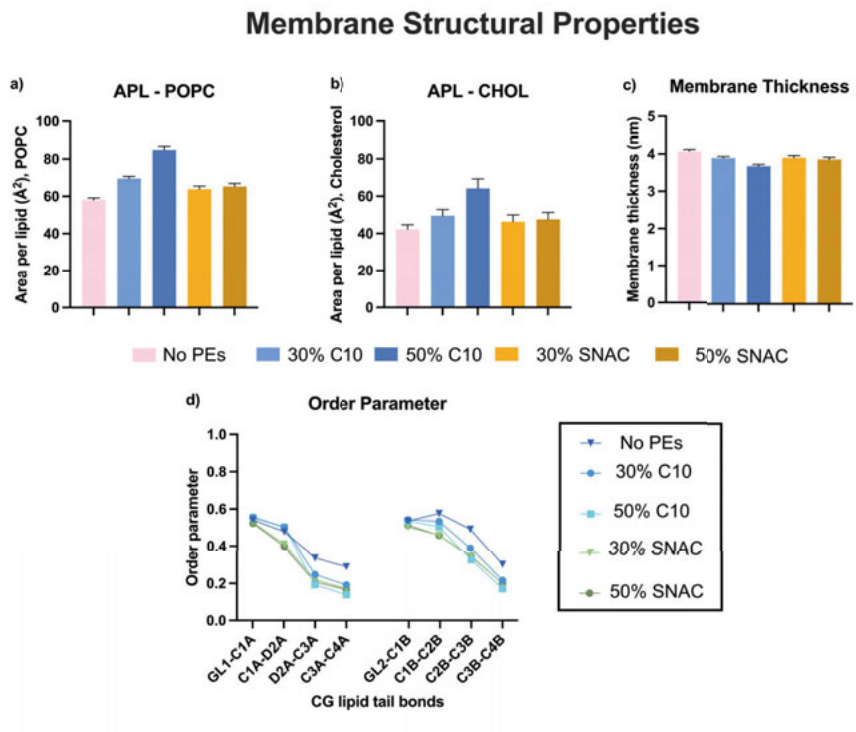

Figure 14. Structural properties of various mixed membrane systems in the presence and absence of different PEs: (a) area per lipid (APL) for POPC and (b) cholesterol, (c) membrane thickness, and (d) order parameter of the POPC lipid tails, Paper IV.

In Paper II, initial snapshots (1–10 ns) and final snapshots of the six different PEs, at 35% concentration are shown in Figure 15a-b. The results in Figure 15 were also quantified and are presented in Figure 16a-c. At the beginning of the simulations (at 0-10 ns, Figure 15a), all the permeation enhancers (PEs) remained near the headgroup region of the membrane POPC molecules. During the course of the simulations, different interaction patterns were observed for different PEs. The PEs with relatively long chain lengths, such as sucrose monolaurate and sodium laurate, were found to remain mostly in the same membrane leaflet for the complete 500 ns long simulations. In other words, they did not expel from the membrane or flip-flop within the membrane. However, for sodium caprate (neutral form and negatively charged), sodium caprylate, and SNAC, expulsion or flipflop events from the membrane occurred for a number of molecules during the complete 500 ns simulations. Final snapshots (at 500 ns, Figure 15b), it is evident that a number of caprylate, caprate, and SNAC molecules (those with a negative charge), had expelled to the water phase from the membrane leaflet. The molecules that inserted in the lower leaflet did so by first expelling into the water phase from the upper leaflet, then moving through the periodic boundary condition (PBC) to then insert into

the lower leaflet from there, hence, considered as an expulsion event and not a flip-flop event. On the other hand, caprate molecules in its neutral form changed their location from one leaflet to another through indeed flip-flop events (transverse diffusion, Figures 16b-c).

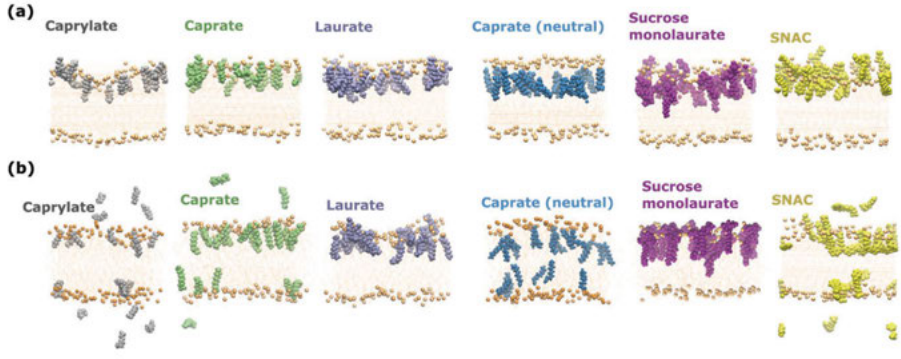

Figure 15. Interactions of different PEs with POPC membrane. Snapshot of (a) the initial, representative states, up to 10 ns and (b) final (after 500 ns simulations) system configurations of POPC membrane with 35% concentrations of the PEs. The pale orange spheres are the phosphate headgroups of the POPC molecules, and the even paler orange in between the upper and lower rows with spheres is representing the phospholipid acyl chains of the POPC molecules, Paper II.

The variation in the number (concentration) of PE molecules that remained in the initial leaflet during the simulations for the 35% PE concentration systems is presented in Figure 16a. The opposite, that is, the number of PE molecules that expelled from the membrane during the simulations, for all concentrations, is presented in Figure 16b. The profile for caprylate (C8), shows a reduction of 68% of the C8 molecules expelling from the membrane leaflet. For caprate (C10), 36% and 40% of the SNAC molecules expelled from the membrane leaflet (Figure 16b). If the PE molecules moved into the lower leaflet within the membrane, it was not considered as an expulsion event, but as a flipflop event. Sodium caprate molecules with neutral headgroups (capric acid) changed leaflet through flip-flopping, and in contrast to the other PEs, we did not observe the presence of such molecules in the water phase and also no crossing event through the periodic boundary (Figure 16c). An increasing number of expulsion events with increasing concentration for caprylate, caprate and SNAC can be observed, the same is valid for neutral caprate and flip-flop events, along with occasional expulsion events occurring for laurate and no expulsion or flip-flop events for sucrose monolaurate molecules (Figures 16b-c).

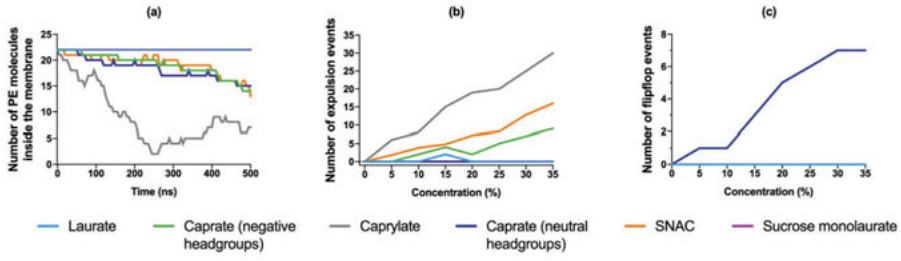

Figure 16. PEs interaction with model POPC membrane. (a) the number of PE molecules that remains incorporated in the initial leaflet (upper leaflet) of the membrane when 35 % concentration of PEs were added in each system and (b) number of expulsion events occurred during the simulation for different PEs, and (c) number of flipflop events, Paper II.

In Paper IV, PE molecules were incorporated into both leaflets of the membrane from start. To better understand the dynamic interactions of PEs with the mixed model membranes, we calculated the number of PEs that remained incorporated into the membrane throughout the simulation (Figure 17a-b). During the simulation (including the equilibration), several SNAC molecules were expelled from the membrane surface and moved into the water phase. The variation in the number of PE molecules incorporated into the membrane over time is in Figure 17a. After approximately 100 ns, a similar number of SNAC molecules (~40-50) remained incorporated into the membrane for both the 30% and the 50% SNAC systems (Figure 17a). This suggests a concentration threshold for SNAC molecules capable of interacting with the model membrane at any given time. In contrast, almost all capric acid molecules remained incorporated into the membrane throughout the simulation for both the 30% and 50% concentration systems. Furthermore, no concentration limit was observed within this concentration range, for capric acid molecules. Thus, this result aligns with that of capric acid in Paper II.

To gain further insight into the dynamic environment within the membrane, we calculated the flip-flop rate of cholesterol in the presence and absence of PEs as well as the flip-flop rate of the PEs themselves. The results presented in Figure 17b show that the cholesterol flip-flop rate increases almost linearly with the addition of capric acid. Similar to the structural properties, there was only a slight increase in the cholesterol flip-flop rate when the SNAC concentration was increased from 30% to 50%. The flip-flop rate of the capric acid molecules increased by nearly 83% as the capric acid concentration increased from 30% to 50%. As in the results of Paper II, no flip-flop events were observed for SNAC molecules in either the 30% or the 50% systems (Paper IV).

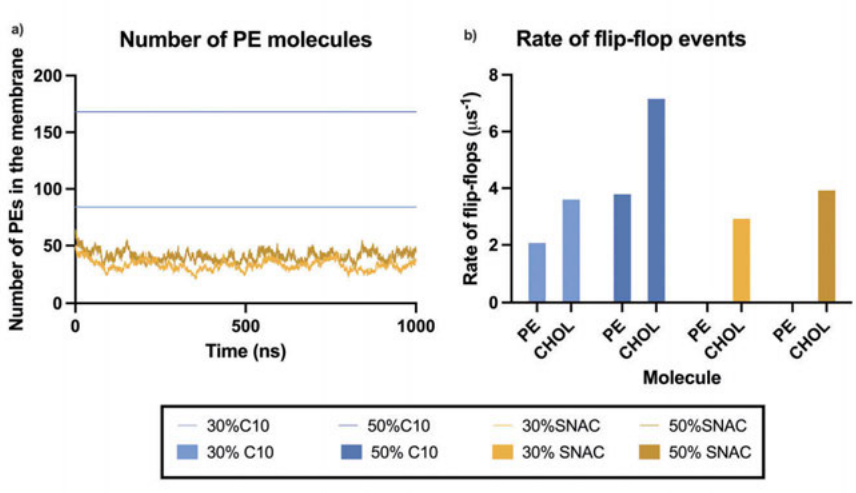

Figure 17. The number of PEs incorporated in the membrane over time, and the number and rate of flip-flop events over time, a) Number of PE molecules remaining in the membrane over time and, b) rate of flip-flop events, Paper IV.

Fractional interactions between permeation enhancers and the POPC model membrane (Number of contacts)

To better understand the interactions of the PEs that remained in the inserted leaflet during the simulation with the membrane lipid molecules, the fractional interactions between them were calculated for all simulated PE systems for the 5% and 35% system concentrations (Figure 18). At 5% concentrations, the results indicate that PEs interact preferably with the POPC molecules with >50% of total contact between PE-POPC for each PE. However, at 35% concentration, the PE-PE contact frequency increases for each PE, indicating formation of larger clusters of PE molecules, which was also observed visually in the simulations. At 35% concentration, capric acid (neutral caprate) showed the highest percentage of PE-PE contact (with 55%), which suggests that these molecules prefer to interact with themselves within the membrane. PE-PE contact of sucrose monolaurate became 50% at 35% concentration. The presence of neutral PE aggregates within the membrane is displayed in Figure 19. Although the PE-PE fractional contacts for other charged PEs increase at 35% concentration compared to 5%, PEs still interact preferably with the POPC molecules with >50% of total contact between PE and POPC. Therefore, we did not observe any aggregates of negatively charged PEs during simulations. SNAC showed the lowest PE-PE contact percentage among the PEs, which is again mainly due to their location and orientation within the membrane.

At 5 % concentrations (to the left in Figure 18), the PEs preferably interact with the POPC molecules (all above 0.5, PE-POPC, darkest colour). At 35 %

concentrations (to the right in Figure 18), PE-PE contact frequency increases for each PE, indicating formation of larger clusters of PE molecules, which was also observed visually in the simulations (Figure 19). At 35 % concentration, capric acid showed the highest percentage of PE-PE contact (55%), which suggests that the molecules prefer to interact with themselves within the membrane (Figure 18). We did not observe any aggregates of negatively charged PE molecules, although the preference to interact between PE-PE increased at 35 % compared to 5 %. SNAC showed the lowest PE-PE contact percentage among the PEs, which is again mainly due to their location and orientation within the membrane. The results suggest that PEs' charged state plays the most important role in their contact interaction pattern within the membrane.

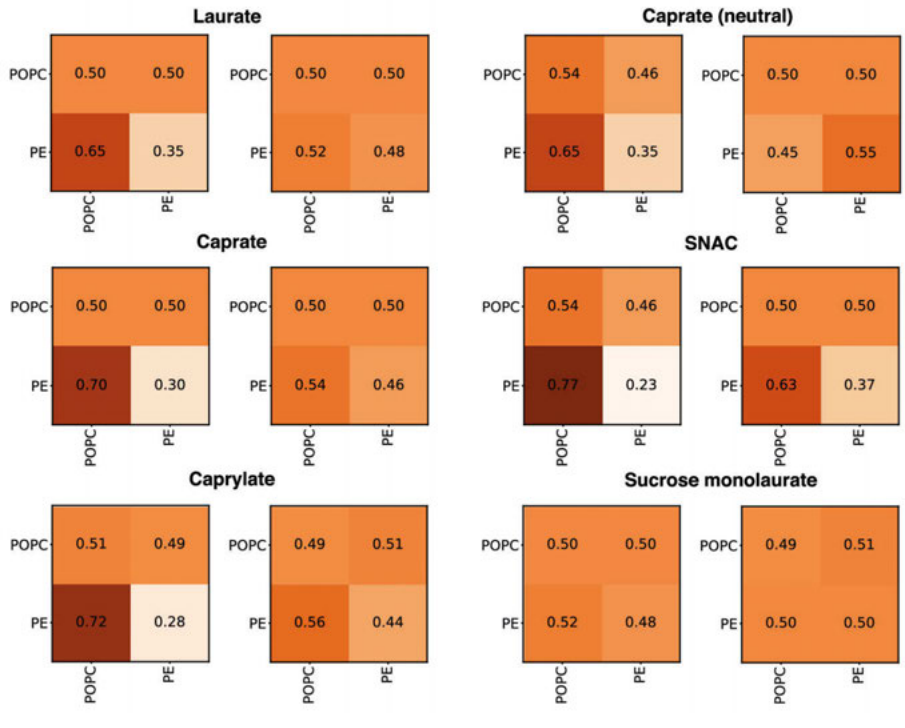

Figure 18. Fractional interaction matrix of different PEs and membrane POPC molecules. The matrix shows the fractional interaction as the relative number of contacts between PEs and/or POPC molecules compared to all other contacts. If the POPC/PE has more than one contact with another POPC/PE, this interaction is only counted once. Two molecules are defined as being in contact if the distance between the headgroup beads is less than 0.9 nm. The left panel represent 5% PE concentration, and the right panel represents the PE concentration of 35%. The colouring scheme goes from beige to dark brown while beige and dark brown represent values closer to zero and one, respectively, Paper II.

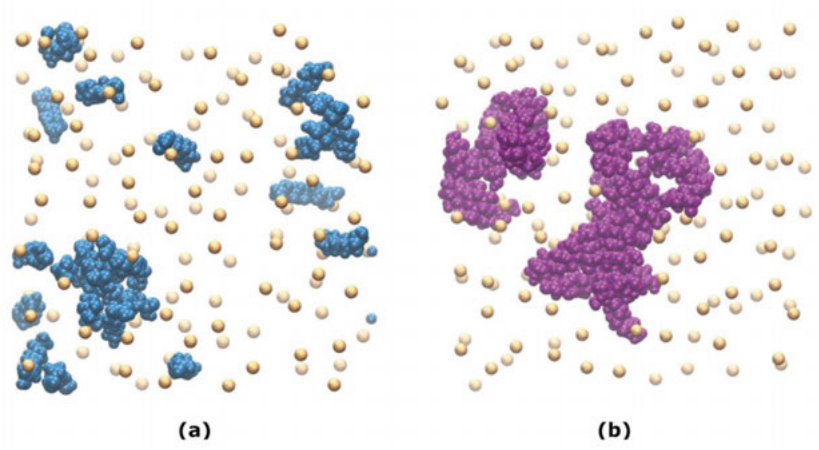

Figure 19. Formation of PE aggregates within the membrane. Top view snapshots showing the PEs with neutral headgroups (a) sodium caprate and (b) sucrose monolaurate formed aggregates within the membrane surface. The images represent both the upper and the lower leaflets. The paler spheres are the phosphate headgroups of the POPC molecules in the lower leaflet (in both a and b), and the paler PE molecules in (a) are the caprate molecules in the lower leaflet. Here in (a), the aggregate in the lower left corner is of interest, and both the aggregates in (b), Paper II.

Other analyses

In Paper I, the results show that the MkVsites toolkit makes it possible to derive virtual site parameters for any molecule, as long as the corresponding molecular topologies can be derived in a manner consistent with the parent force field. Results are presented in Figure 20.

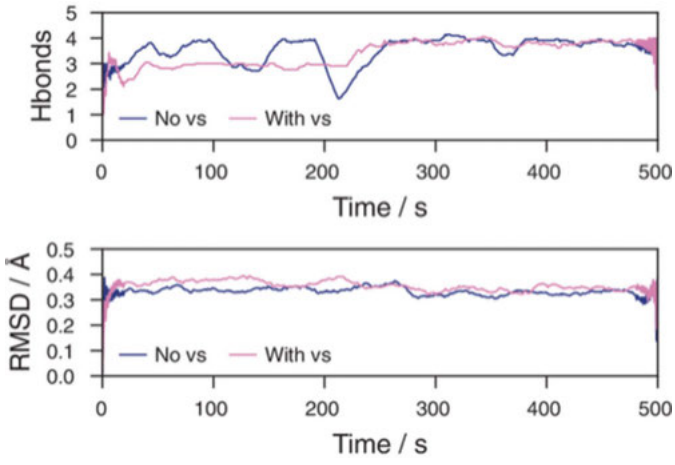

Figure 20. Two simulations, one with virtual sites (pink, 5 fs timestep), and one without (purple, 2 fs timestep), performed on the oestrogen receptor with bound oestrogen. Neither of the results from the 500 ns simulation period show obvious differences, Paper I.

Investigation of interaction patterns between permeation enhancers, peptides, and bile salt

The aggregation behaviour of four different peptides in the presence and absence of SNAC and sodium caprate

In this study, AA-MD simulations were employed to investigate the interaction patterns between different peptides and two different permeability enhancers in the presence of varying concentrations of taurocholate, a bile salt compound. AA-MD simulations can accurately predict the aggregation tendencies for both water-soluble peptides such as octreotide and hexarelin, and peptides with higher aggregation tendencies, such as degarelix and insulin, based on the results from Paper III.

In Paper III, 500 ns long AA-MD simulations were performed to study the aggregation behaviour of four different peptides: degarelix, hexarelin, octreotide and insulin. From these, it was evident that octreotide and hexarelin exhibited a dynamic coexistence as both aggregated species and free monomers in the solution (not stable as aggregates), where trimers and tetramers represented the most prevalent aggregate size. Octreotide and hexarelin are predominantly water-soluble and possess two positively charged residues that work against the formation of stable aggregates. In contrast, degarelix and insulin molecules were present exclusively as aggregates and were formed within the first 50 ns and remained in this aggregated state throughout the 500 ns long simulation. Degarelix has a critical aggregation concentration of

approximately 1 mM, and thus, exhibited a higher aggregation tendency than octreotide and hexarelin. Insulin had also a higher aggregation tendency, compatible with it being observed to form aggregates or fibrils within a pH range of 1.6 and 7.4 and at very low concentrations (0.17 mg mL^{-1}). All peptides carried a net charge, hence, these differences in aggregation propensity between peptides cannot be explained only by electrostatic effects.

In summary, MD simulations can predict the aggregation tendencies of various peptides as it captured the aggregation behaviour of both typical water-soluble peptides, such as octreotide and hexarelin, and peptides with higher aggregation tendencies, such as degarelix and insulin (Figure 21).

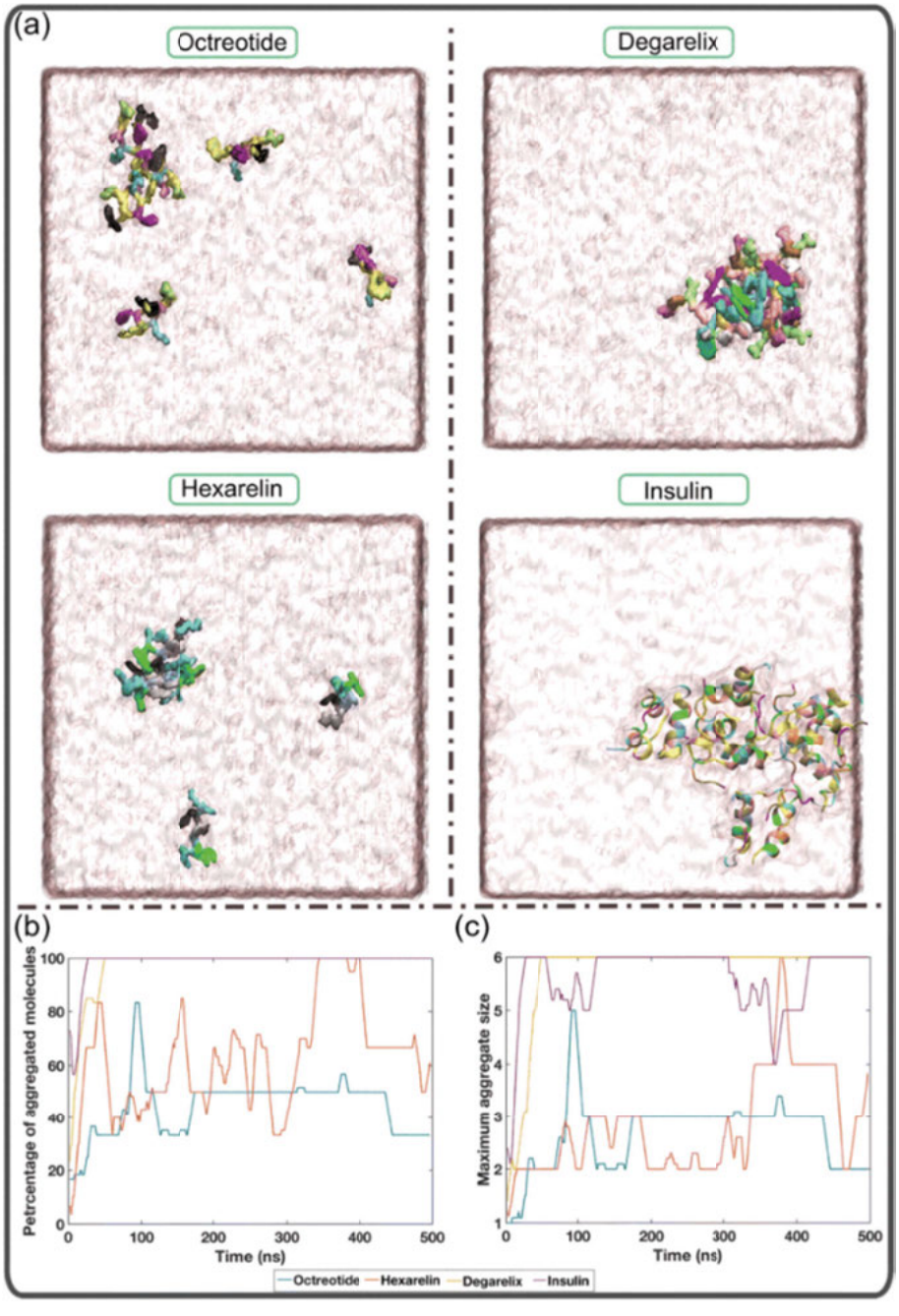

Figure 21. Aggregation tendencies of different peptides. (a) Representative snapshots of each peptide at the end of the simulation (500 ns). The octreotide, hexarelin, and degarelix peptides are shown with a surface representation, and insulin is presented as a cartoon. Panels (b) and (c) show the variation in the percentage of aggregated molecules as well as the maximum aggregate size with time for each peptide. Paper III.

MD simulations provided valuable insights into the behaviour of peptide molecules in the presence of PEs and taurocholate. The simulations demonstrated the formation of mixed colloids, wherein PEs and taurocholate molecules interacted with peptides present in the system. The formation of mixed colloids resulted in a decrease in the amount of free peptide monomers in the aqueous phase, which has also been observed *in vitro* for octreotide[36]. The addition of PEs and taurocholate resulted in larger peptide aggregates in the case of water-soluble peptides (octreotide and hexarelin). For degarelix and insulin, the presence led to the observation of more dynamic molecular aggregation pathways. There was a tendency for the peptides to monomerize, compatible with how SNAC is suggested to induce monomerization for semaglutide[27].

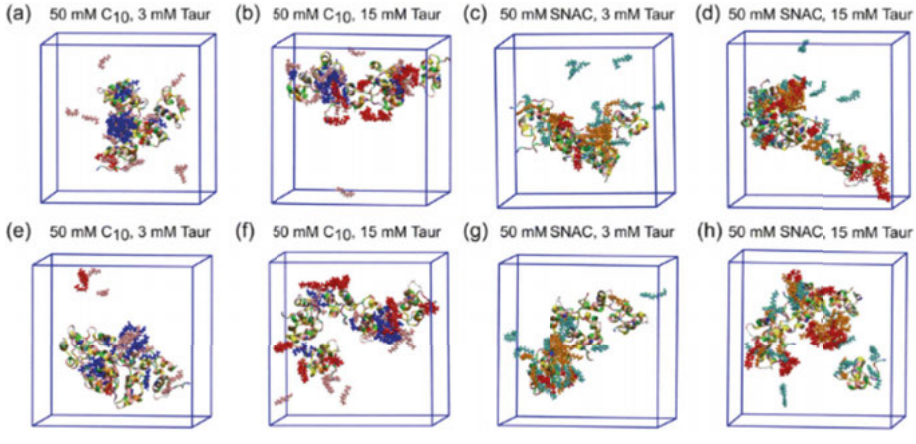

Figure 22. Representative snapshots at the end of the simulations for different systems containing Insulin. Panels (a–d) represent the starting configuration where all the molecules (including the peptides) were randomly placed in the simulation box, and panels (e–h) represent the starting configuration where the peptides are in a pre-aggregated state, but with PE and taurocholate molecules placed randomly. Peptides are shown by the cartoon representation. Caprate, SNAC, and taurocholate molecules are presented by CPK. The neutral and negatively charged caprates are represented by blue and pink, respectively. The neutral and negatively charged SNAC are represented by orange and cyan, respectively. Taurocholate molecules are represented by red colour. Paper III.

Permeation enhancers and taurocholate influence peptide-peptide contact interactions

By investigating the intermolecular hydrogen bond formations, it was found that the presence of PEs and taurocholate reduced the number of bonds for degarelix, those between the 4-S-Phe and 4-D-Phe residues, which play a dominant role in the formation of degarelix aggregates, and between the tryptophan moieties for hexarelin. The presence of PEs and taurocholate did not

significantly impact the formation of hydrogen bonds between the aggregate forming residues in insulin.

In summary, the results from the transition networks, residue-residue contact maps, and hydrogen bond formation analysis provide valuable insights into the influence of PEs and taurocholate on peptide aggregation behaviour. The higher the peptide concentration, the more peptide-peptide interactions, regardless the presence or absence of PEs and taurocholate. However, at higher peptide concentrations (10 mM), PEs and taurocholate can also effectively limit peptide-peptide contact interactions within the mixed colloids, resulting in a reduced propensity of peptides to interact with each other, and forming key interpeptide hydrogen bonds, where SNAC seems to be slightly more effective in that than sodium caprate (C10), which might be due to its larger size with its aromatic ring at the end of the aliphatic chain creating a steric hindrance for the peptides to come in contact within the mixed colloids.

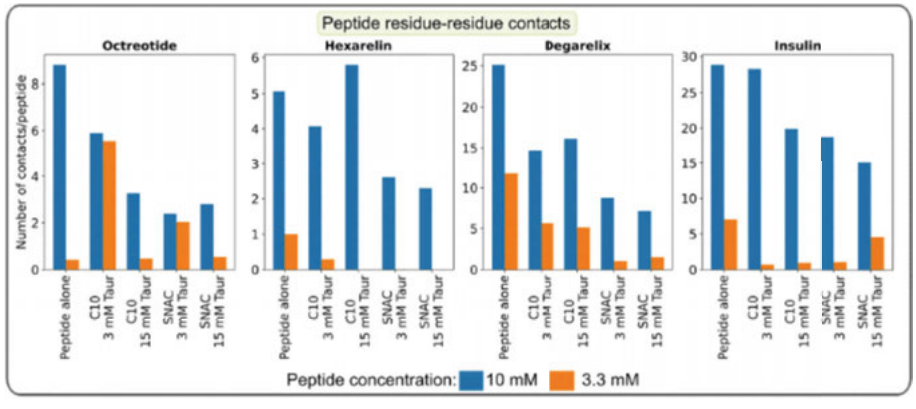

Figure 23. Average number of peptide residue-residue contacts per peptide calculated over the final 100 ns of the simulation. The data represents the systems initiated with a starting configuration where all molecules, including the peptides, were randomly placed within the simulation box. Paper III.

Hydrophobic interactions play a dominant role in the interaction of PEs and taurocholate with peptides

The systems with 10 mM peptide concentration (random starting configuration) were found to reach a plateau and an equilibrium state within 250 ns, for the average number of contacts between peptides and PEs or taurocholate molecules, thus, the simulation time to study this was sufficient. Although each peptide contains positively charged residues, which one would assume to interact more with the negatively charged PEs and taurocholate molecules, the hydrophobic interactions between hydrophobic amino acid residues play a more prominent role in the contact with PEs and taurocholate. Furthermore, it

is rather the neutral form of the PEs that exhibit more contact with peptide residues than their charged counterparts. Also, increasing the concentration of taurocholate enhances the interaction between peptides and taurocholate (fed state, FeSSIF), which impacts the colloid structure and interaction pattern between taurocholate molecules and peptides. In line with the ability of SNAC to reduce the peptide-peptide interactions, SNAC also interacted more with the hydrophobic residues of the peptides compared to sodium caprate (C10). By quantifying the average number of contacts between peptides and PEs or taurocholate, it could be confirmed that SNAC exhibited a higher number of contacts with peptides compared to sodium caprate (C10). Additionally, by increasing the concentration of taurocholate, resulted in more contacts per peptide. Furthermore, the systems with lower peptide concentrations had higher number of contacts per peptide (matching the reduction in peptide-peptide contacts), and the systems with a random starting configuration had higher number of contacts compared to the systems starting with pre-formed peptide aggregates.

In summary, the simulations offered insights into the interactions between peptide residues, permeability enhancers, and taurocholate, in relation to parameters such as concentrations and starting configurations. The hydrophobic peptide residues play a dominant role in the formation of mixed colloids consisting of peptides, PEs, and taurocholates. The analysis of the hydrogen bonds formed between peptide residues and PEs, as well as taurocholate indicates that charged PEs form a higher number of hydrogen bonds with the peptides compared to neutral PEs, particularly with the positively charged residues of the peptides. The number of hydrogen bonds formed between peptides and taurocholate increased as the concentration of taurocholate increased. The number of hydrogen bond formations was only a fraction of the total number of peptide-PE contacts, and therefore, the hydrophobic peptide residues play a dominant role in the formation of mixed colloids (Figure 24-25)

Figure 24. Normalized contact between peptide residues, PEs, and taurocholates for different systems containing 10 mM of octreotide, hexarelin, degarelix and insulin. For each system, the contact values are normalized using the maximum number of contacts found in each case. The data here represents the starting configuration where all the molecules including the peptides were randomly placed in the box. C10 and C10− represent neutral and negatively charged sodium caprate molecules, and SNAC and SNAC− represent neutral and negatively charged SNAC molecules. Taur represents taurocholate molecules. Paper III.

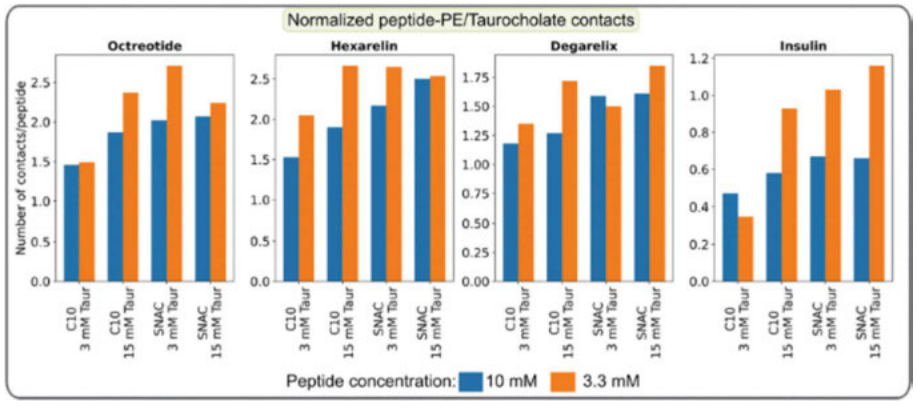

Figure 25. Average number of contacts between peptides and PEs/taurocholates per peptide calculated over the final 100 ns of the simulation and normalized by the number of atoms for each peptide. The data represents the systems initiated with a starting configuration where all molecules, including the peptides, were randomly placed within the simulation box. Paper III.

Permeation enhancers and taurocholate can influence the release of both hydrophobic and water-soluble peptide monomers into the aqueous phase

To investigate the impact of colloid composition on peptide release/expulsion, umbrella sampling (US) simulations were performed to calculate the potential of mean force (PMF), Figure 26. The PMF analysis involved measuring the free energy required to translocate a peptide molecule from either a homogenous peptide aggregate or a mixed colloid to the water phase. Thus, the PMF profiles are highly dependent on the particular peptide conformation, the overall structure of the aggregate, and the location of the peptide within the aggregate. Therefore, replicate simulations (n=3) were performed with different peptides selected within the aggregate. The PMF profiles revealed different patterns for water-soluble and hydrophobic peptides. For octreotide and hexarelin, two to five times more energy was required to separate a peptide molecule from a mixed colloid than from a pure peptide aggregate, and higher energy requirements observed for the separation of a peptide molecule from a pre-formed peptide aggregate where PEs and taurocholate also were present (compared to the random starting configuration). The estimated free energy difference (ΔG) for separating octreotide or hexarelin molecules from mixed colloids (random starting configuration) were within the range of 30-50 kJ mol^{-1}. These findings suggest that PEs and taurocholate can reduce the release of water-soluble peptides such as octreotide and hexarelin, consequently reducing the number of free monomers in the aqueous phase. In addition, this decline in the fraction of free peptide was also found in the transition network analysis and also observed *in vitro* for octreotide[36]. The decreased availability

of free peptides due to their interaction with PEs and taurocholate may have implications for their absorption rate across the intestinal epithelium. When peptides are strongly bound within the mixed colloid, their release into the aqueous environment becomes more challenging, potentially reducing their absorption efficiency. However, this stronger interaction between peptides, the PEs, and taurocholate in the mixed colloids can also serve a beneficial role by protecting the peptides from enzymatic degradation. This reduced enzymatic degradation increases the overall availability of intact peptides for absorption in the intestine. To continue, for degarelix, the PMF profiles indicate that higher energy is required to separate peptide molecules from the mixed colloids when PEs and taurocholates were introduced to the peptide aggregates, compared to the pure peptide aggregates. The ΔG required to separate a degarelix molecule from the pure degarelix aggregate was approximately 140 kJ mol^{-1}, which is nearly nine times higher than the ΔG required to separate octreotide or hexarelin molecules from similar pure peptide aggregates. Interestingly, the opposite trend was observed for the other starting configuration (random starting configuration), and the ΔG values required to separate a degarelix molecule decreased to 40 and 68 kJ mol^{-1} from the mixed colloids containing caprate and SNAC, respectively. This suggests that the PEs and taurocholate can increase the release rate of degarelix, which is a highly hydrophobic peptide, and highlight the importance of understanding and controlling the release conditions of the peptide from the dosage form.

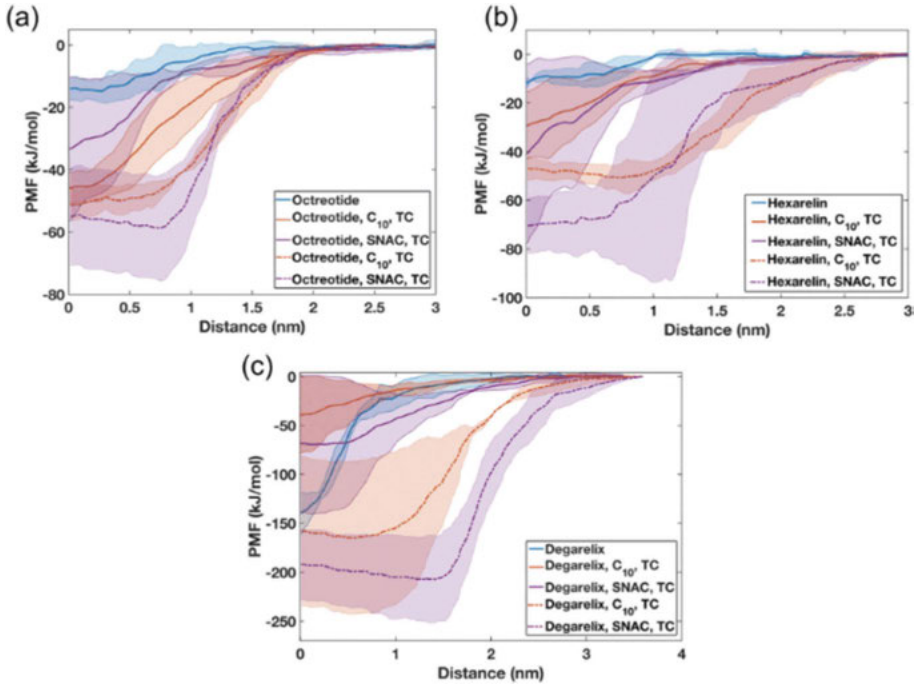

Figure 26. Potential mean force (PMF) profiles observed when pulling a peptide molecule from pure peptide or mixed colloids composed of 10 mM peptides, 50 mM PEs (either caprate or SNAC), and 15 mM TC. PMF profiles depicting the energy required to pull (a) one octreotide, (b) hexarelin, and (c) degarelix molecule from the aggregate surface into the aqueous phase. In the PMF profiles, the lines and shaded regions represent the means and standard deviations, respectively (n=3). The legend describes the constituent components of the aggregate. Solid lines represent the starting configuration, where peptide, PE, and TC molecules were added randomly. The dashed lines represent the starting configuration where PEs and TCs were added randomly, and the peptides were aggregated. Abbreviations: C10: caprate, TC: taurocholate. Paper III.

The FTIR spectra suggest that SNAC can induce insulin fibrillation at pH 6

In Paper III, we looked a little closer at the behaviour of insulin, because any insights into how the oral bioavailability of insulin can be increased would have tremendous therapeutic benefit. By comparing computational experiments with *in vitro* experiments and compare the obtained results from the FTIR experiments with the findings from the simulations, we aimed to validate the simulation outcomes and enhance our understanding of the impact of PEs on the secondary structure of insulin. Insulin is prone to fibrillation under various physiological conditions, such as elevated temperature, different ionic strengths, and low pH[107,108]. The fibril formation of insulin is typically characterized by the presence of β-sheet-rich structures. Using FTIR, Chaaban *et al.*[109] investigated the secondary structure of insulin in the presence of various

concentrations of NaCl at pH 2 and observed a broad peak around 1620-1625 cm^{-1} in the spectra, which corresponded to β-sheet-rich structures. We used their work as validation for our *in vitro* experimental methodology. We detected a peak at approximately 1632 cm^{-1} in the FTIR spectra for various concentrations of NaCl at pH 2. In other studies, peaks in FTIR spectra corresponding to β-sheet-rich structures in the range of 1620 cm^{-1} to 1637 cm^{-1} were observed[110,111]. Then, when we investigated the variation in the secondary structure of insulin in the presence of various NaCl concentrations at pH 6, a peak at approximately 1658 cm^{-1} could be observed. FTIR spectra peaks within the range of 1645 cm^{-1} to 1660 cm^{-1} typically correspond to α-helices and random structures, which are observed in native insulin and systems with relatively higher pH[108,109,110]. In line with native insulin and relatively higher pH, in the systems containing insulin only at pH 6, as well as for the systems with insulin containing sodium caprate and taurocholate, a broad peak was observed around 1650 cm^{-1}. However, in the SNAC-including systems, a shift in the FTIR spectra occurred, from approximately 1650 cm^{-1} to 1637 cm^{-1}, thus, indicative of an increase in the β-sheet-rich structural region and would indicate fibrillation of insulin in the presence of SNAC. Noteworthy, this peak was slightly upshifted compared with that of the samples with pH 2. This upshift is associated with the weakening of hydrogen bonding and more loosely packed β-sheet structures. Similar results were observed by Iannuzzi *et al.* for insulin at pH 7[112].

Lastly, a DSSP analysis on the insulin-containing systems was conducted. The results aligned well with the peaks observed in the FTIR spectra of native insulin and systems with higher pH, indicating the prevalence of α-helices and random structures. Thus, the DSSP results suggest minimal structural rearrangements in the insulin molecules during the simulations, indicating that the timescale for insulin aggregation or fibrillation (in the presence of PEs such as SNAC) is longer than what was simulated. Although, a slightly higher percentage of β-sheet structures was found in the simulations where the starting configuration of the insulin molecules was in the aggregated state.

Permeability

Effect of permeation enhancers on water permeation

The permeation of water molecules into the bilayer was quantified (Figure 27). The effect that different PEs have on water permeation through the membrane was investigated by calculating the amount of water molecules present near the hydrophobic tails of the membrane. For each simulated system, the number of water molecules located near the carbon atoms of the POPC lipid tails was determined. There is a PE concentration-dependent increase in the

number of water molecules near the lipid tails per lipid molecules. The maximum number of water molecules near the lipid tails was observed in the presence of laurate for all concentrations. For the negatively charged fatty acids, an increasing trend in the number of water molecules near the lipid tails with increasing PE chain length could be seen. That is, sodium laurate > sodium caprate > sodium caprylate. This suggests that the presences of higher number of PE molecules inside the membrane at a given concentration would increase the availability of water molecules near the hydrophobic lipid tails. In the systems with neutral caprate (capric acid) and negatively charged SNAC, the number of water molecules near the lipid tails were quite similar and slightly lower than that of the negatively charged fatty acids. We observed that the neutral caprate molecules typically interacted more with the membrane lipid tails compared to the negatively charged fatty acids. The average distance between the bilayer centre and neutral caprate was 0.9 nm, in contrast to 1.52, 1.5 nm, and 1.42 nm for negatively charged caprylate, caprate, and laurate, respectively. Therefore, the neutral caprate molecules restricted the water molecules' contact with the membrane lipid tails compared to the other negatively charged fatty acids. On the other hand, as discussed in the earlier section, SNAC resides typically parallel to the membrane surface and interacts with the POPC headgroup region and thus can restrict the water molecules from going deeper into the model cell membrane. Sucrose monolaurate had the lowest number of water molecules near the lipid tails for most of the PE concentrations used in the study. This is mainly due to the presence of the ester groups in the sucrose monolaurate molecules, which also typically resides near the membrane headgroup region and restricts the water beads to come in contact with the lipid tails.

Overall, the simulation results suggest that the PEs can increase the water molecules' presence inside the membrane with increasing PE concentration. However, depending on the PE structural properties and their interaction pattern with the membrane, the extent of the increase can vary. At least for sodium caprate and laurate with a negative charge, the concentration at which they seem to start induce water permeation is around 15–20 %, corresponding to approximately 70-100 mM concentrations (Figure 28).

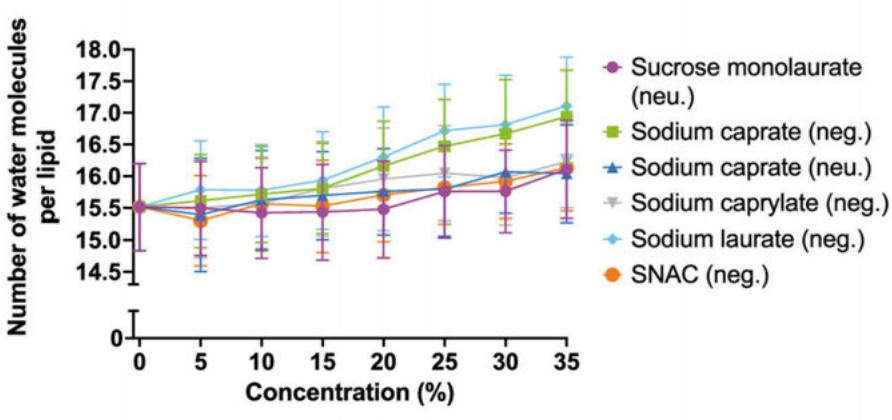

Figure 27. Number of water molecules per lipid (n = 128) near the POPC lipid tails at different PEs concentrations, expressed as averages with standard deviation error bars. The largest increase in the amount of permeating water molecules can be seen for PEs with longer carbon chain and a negative charge. The two neutrally charged PEs, sodium caprate and sucrose monolaurate along with the negatively charged SNAC show less of an increase, but are also able to induce water permeation over a pure POPC bilayer as a baseline, Paper II.

Effective permeability of permeation enhancers

In Paper IV, to calculate the permeability coefficient of PE molecules through each model system, we first determined the free energy profiles associated with pulling a single PE molecule from the water phase to the centre of the model membrane using umbrella sampling simulations. For capric acid (C10) systems (Figure 28a), in the absence of any PEs, there is a slight energy barrier near the membrane surface, approximately 2.5 nm from the membrane centre. In the presence of 30% and 50% capric acid molecules in the membrane, the barrier is diminished. The energy values then progressively decreased as the capric acid molecules approached the membrane centre, reaching a global minimum at around 1.5 nm from the membrane centre in the system without PEs. For the 30% capric acid system, the minimum was located at a similar position. However, in the 50% capric acid system, the minimum shifted closer to the membrane centre at approximately 1-1.1 nm. After reaching the global minimum, the energy values began to increase as the molecules approached the membrane centre. However, the energy at the membrane centre (-2 to -2.2 kcal/mol) remained significantly lower than the initial energy (0 kcal/mol) in the water phase.

In contrast, for SNAC molecules, we observed almost no energy barrier as they entered the membrane (around z=2.5 nm). The global energy minimum for SNAC systems was located closer to the membrane surface than that for capric acid systems (approximately 1.6 nm from the membrane centre).

Beyond this point, the energy profile exhibited a rapid increase, reaching approximately 9-10 kcal/mol for the various SNAC systems (Figure 28b).

We then calculated the effective permeability (P_{eff}) coefficient values for the capric acid and SNAC systems, as shown in Figure 28c (presented as a fold increase over baseline). The results indicated that the P_{eff} values for the capric acid systems increased with higher capric acid concentrations. For 30% SNAC, we observed an increase in P_{eff} compared to the system without PEs, but no further effect was observed when the SNAC concentration was increased from 30% to 50%. The capric acid P_{eff} values obtained for 30% and 50% were 6.347 cm/s and 14.803 cm/s, respectively. A previously reported value for capric acid permeability in lecithin bilayer membranes was 0.221 cm/s[113].

Most importantly, when comparing the magnitude of P_{eff} values across different systems for two different PEs, it is evident that the P_{eff} values are significantly higher – by 6-7 orders of magnitude, for capric acid compared to SNAC.

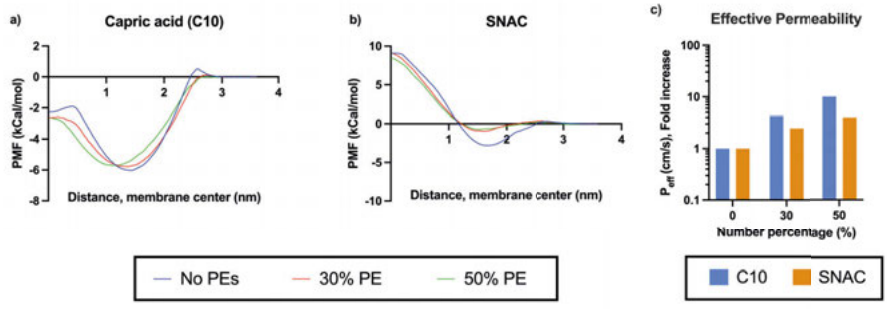

Figure 28. The free energy profiles (kcal/mol), from the umbrella sampling simulations obtained using the gmx WHAM analysis tool, of the PEs (a-b), and the permeability rates (cm/s) presented as fold increases over the baseline of the two PEs caprate acid (C10, blue) and SNAC (yellow), a) capric acid (C10), b) SNAC, and c) effective permeability (P_{eff}) of capric acid (C10) and SNAC, Paper IV.

In summary, both PEs favourably interact below the membrane headgroup region, as indicated by the global minima. However, capric acid molecules tend to remain within the membrane, as its global free energy maxima were always in the water phase when other capric acid molecules were present in the membrane. This was further supported by simulations where capric acid was embedded in the membrane, showing that no capric acid molecules were expelled into the water phased during the 1 microsecond long simulations. In contrast, for SNAC, beyond the global energy minima (around z=1.5 nm, below the membrane headgroup region), there was a very high energy barrier that restricted the movement of SNAC molecules closer to the membrane

centre. This is primarily due to the ring structure at the end of the SNAC lipid tail. SNAC molecules tend to remain at the membrane surface or slightly buried below the membrane headgroup region. In our previous study (Paper II), we observed that SNAC molecules generally orient horizontally at the membrane surface. Such orientation at the membrane limits the number of SNAC molecules interacting with the membrane at any given time and may explain the observation of the concentration threshold beyond which SNAC cannot interact effectively with the membrane.

Effective permeability of peptide drugs

In Paper IV, similar to the determination of P_{eff} values for the PE molecules, we first calculated the free energy profiles associated with the movement of the peptide drugs from the water phase to the membrane centre (Figure 29a-c). We observed similar behaviour in the energy profiles regardless of the specific peptide and PE in the mixed membrane. As the peptide molecule entered the membrane, there was a decrease in free energy, with the PMF profiles reaching a global minimum around 2 nm from the membrane centre. Beyond this point, the energy values began to rise and reached their maximum at the membrane centre. Similar results have been reported by Sugita *et al*.[18]. They studied 100 six-residue cyclic peptides in terms of membrane permeation using MD simulations. They found that the process of crossing the membrane centre is the main obstacle to permeation.

For each peptide, the maximum energy value was highest in the non-PE system, while the 50% capric acid system exhibited the lowest energy values. Additionally, capric acid systems consistently showed lower energy values compared to the corresponding SNAC systems. However, no significant differences were observed between systems containing 30% and 50% SNAC and those with 30% capric acid. The maximum energy values at the membrane centre were highest for desmopressin in each system (Figure 29b).

The P_{eff} values followed the trend: octreotide > triptorelin > desmopressin across all systems (Figure 29d-f). The lowest P_{eff} values were seen in the non-PE systems, while the highest was observed in the 50% capric acid systems. Capric acid exhibited an increasing trend in P_{eff} values with higher concentrations within the membrane. In contrast, P_{eff} values for SNAC systems were similar between 30% and 50% concentrations, aligning with the trends observed in the free energy profiles and the membrane structural characteristics.

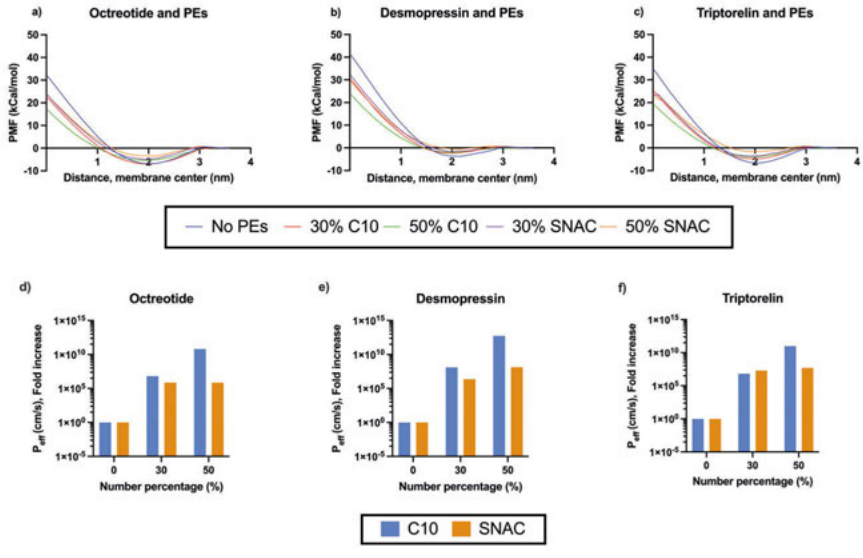

Figure 29. The free energy profiles (kcal/mol), from the umbrella sampling simulations obtained by the gmx WHAM analysis tool, of the pep-des in systems with and without PEs, a) octreotide and PEs, b) desmopressin and PEs, c) triptorelin and PEs. The permeability rates (cm/s) presented as fold increase over baseline of d) octreotide and PEs, e) desmopressin and PEs, and f) triptorelin and PEs, Paper IV.

In summary, the P_{eff} values obtained for the three peptide drugs followed similar trends: a concentration-dependent increase with higher capric acid levels in the membrane. In contrast, the results indicate a critical concentration of SNAC, where 30% SNAC in the membrane increased peptide permeability by several orders of magnitude, but increasing the concentration from 30% to 50% had minimal additional impact, indicating this critical concentration threshold beyond which its ability to enhance membrane permeability plateaus. This limitation is may be due to its inability to significantly impact membrane structural properties above its critical concentration. These findings thus align with our characterization of how PEs affect membrane structural and dynamic properties, as well as their interaction patterns with the membrane surface.

Conclusions

Paper I

- The python-tool MkVsites can create virtual interaction site parameters for an arbitrary molecule containing non-standard atoms, which is not included in the already built-in virtual interaction site technique in GROMACS.

Paper II

- Different chain lengths, sizes, and structural characteristics of permeation enhancers can affect the membrane structural properties. The changes correlated with increasing PE concentrations. SNAC can induce more lipid movement at the membrane surface without significantly changing the overall structural properties inside the membrane. PEs in their neutral form tend to cluster together.

- PEs can increase the number of water molecules in the membrane center, with increasing PE concentration. The effect varies dependent on the PE. The maximum number of water molecules near the lipid tails was observed for laurate over all concentrations. For the negatively charged fatty acids, we can see an increasing trend in the number of water molecules near the lipid tails with increasing PE chain length, i.e., sodium laurate > sodium caprate > sodium caprylate. For sodium laurate and caprate, a PE number percentage concentration of 15-20% seems to be needed to induce the permeation of water into the hydrophobic core of the POPC model bilayer, corresponding to approximately 70-100 mM concentrations.

- There is a PE concentration dependent increase in the number of water molecules near the lipid tails per lipid molecule. The maximum number of water molecules near the lipid tails was observed for laurate at all concentrations. For the negatively charged fatty acids, we can see an increasing trend in the number of water molecules near the lipid tails with increasing PE chain length, i.e., sodium laurate > sodium caprate > sodium caprylate.

Paper III

- PEs and taurocholate were capable of reducing the peptide-peptide contact interactions and key hydrogen bond formations, which are the main driving elements in peptide aggregation.

- The unrestrained simulations also highlighted key interactions between peptide residues leading to aggregation and interactions with peptides and PE/taurocholate within the mixed colloids.

- PEs and taurocholate were found to decrease the release rate of water-soluble peptides, such as octreotide and hexarelin in the aqueous phase, meanwhile the release of the highly hydrophobic degarelix can be enhanced in the presence of PEs and taurocholate.

Paper IV

- Capric acid and SNAC influence membrane structural and dynamic properties by increasing the membrane area per lipid, reducing membrane thickness and lipid tail order, and enhancing flip-flop rates, leading to enhanced membrane leakiness and higher transcellular transport of active components.

- Capric acid molecules affect membrane properties in a clear concentration-dependent manner, whereas SNAC, appears to reach a critical concentration beyond which membrane properties are not significantly altered.

- Peptide permeability also increased with increasing PE concentration. The P_{eff} values followed the trend: octreotide > triptorelin > desmopressin across all systems.

- For each peptide, the lowest P_{eff} values were observed in the no-PE systems, while the highest values were observed in the systems with 50% capric acid.

- In contrast, the peptide P_{eff} values in the SNAC systems were similar between the 30% and 50% concentrations, and similar to the 30% C10 system, aligning with the trends observed in free energy profiles and the membrane structural characteristics. Thus, for SNAC, there seems to be a concentration where the permeability-enhancing effect plateaus.

Populärvetenskaplig sammanfattning

Tänk om personer med allvarliga sjukdomar slapp ta sprutor varje dag och istället kunde svälja en tablett?

Allvarliga sjukdomar som diabetes och cancer behandlas ofta med peptidläkemedel, en grupp biologiska läkemedel baserade på peptider. Exempel på sådana läkemedel är insulin, som är avgörande för behandling av typ 1-diabetes, samt Ozempic, ett läkemedel som fått stort medialt genomslag på senare tid.

Trots att peptidläkemedel kan vara mycket effektiva, administreras de oftast genom injektioner – en metod som innebär regelbundna och ibland smärtsamma stick för patienterna. Injektionerna kan orsaka lokala biverkningar, och för personer med nålskräck kan obehaget leda till att behandlingen inte följs korrekt. Utöver lidandet för patienten medför injektionsbehandling också högre kostnader, både för sjukvården och individen.

En lösning på dessa problem vore att utveckla peptidläkemedel som tas oralt, det vill säga i tablett- eller kapselform. Dock finns det utmaningar med detta. När peptider sväljs, utsätts de för flera biologiska hinder: de bryts ned av enzymer i magtarmkanalen och är känsliga för den sura miljön i magen. Detta leder till ett lågt upptag av läkemedlet genom membranet i magtarmkanalen, vilket kan mätas som permeabilitet.

I den här doktorsavhandlingen har peptiders membranpermeabilitet undersökts med hjälp av datorbaserade simuleringsmodeller, särskilt molekyldynamik (MD), som bygger på fysikens rörelselagar. Ett lovande sätt att förbättra upptaget av peptidläkemedel är att kombinera dem med permeabilitetshöjande molekyler – ämnen som tillfälligt gör membranet mer genomsläppligt. Detta forskningsfält har lett till utvecklingen av totalt två orala peptidläkemedel kombinerade med permeabilitetshöjare, godkända av läkemedelsverket. Det finns stor potential men permeabilitetshöjares verkningsmekanismer och interaktioner med membran och peptider måste studeras närmare för att öka kunskaperna kring detta, och för att slutligen nå optimala kombinationer av dessa, för att således kunna ersätta injektionsbehandlingar med tabletter och kapslar.

Ett exempel på permeabilitetshöjare är det röda färgämnet i jordgubbar, som kan öka upptaget av andra ämnen. I den här avhandlingen har andra sådana molekyler studerats, bland annat dekansyra (C10) och salkaprozat natrium (SNAC), både i närvaro och frånvaro av peptider. Resultaten har bekräftat tidigare kunskaper samt fördjupats inom området och gett insikter om permeabilitetshöjares samspel med och inverkan på membran samt peptidmolekyler.

En viktig slutsats från artikel II är att det krävs en koncentration på omkring 70–100 mM av en permeabilitetshöjare för att öka permeabiliteten för vatten genom modellmembranet. I artikel III visade det sig att permeabilitetshöjares effekt varierar med peptiders fett- respektive vattenlöslighet. Dessutom visade resultaten att permeabilitetshöjare kan minska samspelet mellan peptidmolekyler, vilket kan medföra ett ökat upptag. Från artikel IV kunde slutsatsen dras att C10 påverkar peptider på ett linjärt och koncentrationsberoende sätt. Permeabiliteten för en peptid ökade med ökande koncentrationer av C10. Däremot verkade SNAC ha en begränsad effekt eftersom peptiders permeabilitet planade ut vid högre koncentrationer av SNAC.

Liknande resultat har setts i andra studier av andra forskare. Däremot har det inte påvisats med samma tillvägagångssätt. Molekyldynamiska simuleringar tillåter forskare att studera interaktioner på atom- och molekylnivå. Denna typen av experiment kan ibland kallas för mikroskop i datorn, eller att man är i det ”torra” laboratoriet, till skillnad från i det traditionella våt-laboratoriet. I våt-laboratorier kan man undersöka ämnen på atomnivå, däremot är det utmanade att fånga atomer och molekyler i rörelse, vilket dessa simuleringar kan. I den här avhandlingen har förenklade modeller av verkliga membran byggts vari permeabilitetshöjare och peptider har studerats med hjälp av molekyldynamik.

Framtiden är lovande för forskningsområdet, och möjligheten att kombinera molekylärdynamiska simuleringar med artificiell intelligens (AI) och i synnerhet med maskininlärning öppnar för nya möjligheter. Dessa tekniker kan hjälpa oss att snabbare och mer precist förutsäga hur olika peptider och permeabilitetshöjare interagerar med varandra och med cellmembran, vilket potentiellt skulle påskynda utvecklingen av effektiva orala peptidläkemedel. Genom att kombinera simuleringarnas detaljnivå med AI:s förmåga att analysera enorma datamängder och identifiera mönster kan vi optimera läkemedelsformuleringar, i synnerhet av peptider och permeabilitetshöjare, på ett sätt som tidigare inte varit möjligt.

Acknowledgments

The work presented in this thesis was conducted at the *Department of Pharmacy*, Faculty of Pharmacy, Uppsala University, Sweden. Financial support from VINNOVA (2019-00048) is gratefully acknowledged. I want to express my gratitude to *Apotekarsocieteten* for the travel grants that funded my attendance and trips to research conferences.

***To my main supervisor and co-supervisors**, thank you for your guidance, support, and patience. I deeply appreciate your engagement in the discussions about my research, and I am grateful for every explanation. Your vast knowledge and ability to lead by example have been truly inspiring. I have learned so much from you, and I am incredibly grateful for all efforts, and contributions that made the completion of this PhD thesis possible. This period has been a time of significant growth for me, both professionally and personally. I appreciate working with all of you. **Thank you**.*

To my main supervisor, **Per Larsson**, thank you for believing in me when accepting me as your first PhD student. For continuing believing in me throughout, at times when I didn't. Thank you for leading with openness and a flexible mindset, and for your humble, optimistic, and empathic approach when guiding me in research. I am very grateful for the project becoming a part of the SweDeliver consortium.

To my co-supervisor, **Christel Bergström,** you are a true role model and such an inspiration for everyone, especially for women in science. I still remember how impressed we were by you, as undergrad students, when we heard that you had been able to receive a record high grant! You were a role model and a source of inspiration already then.

To my co-supervisor, **Shakhawath Hossain,** thank you for understanding my chain of thoughts when they have been highly unclear. Yet, surprisingly, you understand my reasoning during those challenging moments. Not only have you understood me when being vague, your competence and intelligence are reflected in everything you do and achieve. Thank you for your unlimited patience with me and our work, for all the teaching and explanations on MD and everything connected to our research, for the constructive feedback and all.

Your help, support, and guidance in this work has been invaluable for me. I am beyond grateful for you officially becoming my co-supervisor.

To my co-supervisor, **Simon Bjerregaard,** thank you for your kindness, for inspiring me, for your enthusiasm, and for taking on the role as industrial co-supervisor. Your expertise as a researcher is truly remarkable. Despite the short duration of your involvement, your contributions have been profound.

I would like to express my gratitude to all members, past and present, of the large Drug delivery group, and to all colleagues, past and present at the **Department of Pharmacy**. Thank you for all fun times during lunch and fika, and for discussing projects and science with me, and everything in between.

Pernilla, thank you for being so kind, warm, and understanding. Thank you for being there for me at work. Your support has been invaluable, and I really appreciate you. **Aleksei**, thank you for setting such a positive, welcoming, and friendly atmosphere. In particular, thank you for reaching out to me on day one with your kindness making me feel included. Not only are you so kind and fun to be around, you are also such an inspiration, competent and successful in everything you do. Thank you for explaining physics and MD to me. Also, I follow your example on how to explain energy minimization to a non-MD user, by resembling it to finding the least crowded place at a rock concert – You're brilliant ☺. Both you **Shakhawath** and you **Aleksei** are so helpful and kind to everyone you meet, and so knowledgeable and competent. I am forever grateful for all help I've received. I really appreciate both of you. **Alexandra,** I am also very impressed and inspired by you. It has been wonderful to connect over our shared Hungarian background. **Patrik Lundquist**, thank you for your welcoming approach, and for discussing peptides with me. To **Lucia Lazorova,** for being the sweetest and kindest person. It's been so nice to talk to you, and to have your support.

I would like to express my gratitude to all I've meet within the **SweDeliver consortium** (Swedish Drug Delivery Centre). It's been such an inspirational environment and I am grateful to have been able to learn from all of you, and for the discussions of science within the consortium. I have gained invaluable experiences from this.

To my **fellow PhD-students** and to **post-docs**, past and present, in the Molecular Pharmaceutics group, included in the SweDeliver consortium, and at the Faculty of Pharmacy: thank you for all fun times, and for all insightful discussions. Thank you for the times within FDR, ULLA, and AAPS as well.

Fanny, thank you for sharing your experiences and knowledge with me, and for listening. Thank you for always being there for me. Thank you for all fun

times, at and outside of work! I really enjoyed working with you in FDR. You made the time as a PhD student so fun. **Frida,** thank you for all spontaneous laughter and for all discussions, and support. For just looking at each other without saying a word and both of us just burst into laughter. And of course, as generally everyone thinks that we are the same person ☺ – we have to go through with our idea about confusing people even more about who is who of us! You know what I mean ;) **Jenny,** thank you for all your kind words, and support. For all fikas and walks in the forest.

To my fellow PhD students in the computational pharmaceutics group, past and present, **Jiaxi, Benyamin, and Shahina,** thank you for all support, and for all discussions, the fun and light-hearted ones and the serious ones.

I am very proud of have being a part of the **BLT group** – the molecular-computational-nano-pharmaceutics group ☺. **Thank you** to all of you, especially for the last years of such a warm, joyful, and welcoming environment in the group. You are all stars and will go far! Thank you, **Malhar** for being such a good lab manager making every day easier with your coordinative and structuring skills, as well as fun talks during fika and lunch. Thank you for surprising me with licorice ☺

To the Pongsters – Sohan, **Irès, Marilena, Julia, Ellen, Marcus, Vahid, Yassir, Shakhawath, Aleksei, and Agnes**, thank you for all fun times at and outside of work. In particular, for all pong sessions at BMC making fika time a true source of joy! **Marcus Wanselius, Agnes Rodler, Vahid, Sana, Randi**, **Lina, Julia, Yassir,** thank you for welcoming me so warmly in D3:4! I really learned a lot from you when I was a newly admitted PhD student. Thank you to the people at the **thesis production, Jesper and Kerri**, for being so nice, understanding, and helpful.

A warm thank you to **my close family and friends**, no one mentioned, no one forgotten❤️. Thank you for all your help, love and support, for always being there for me during this time as a PhD student. It has been invaluable, and I am forever grateful for each and every one of you. I would not have made it through without your love and support. For that, I am forever grateful. To my son **Philip**, you are my sun, my source of happiness, my life. You are everything to me. I am always here for you and I love you unconditionally. Your presence has given me so much joy, strength and happiness, very much needed to complete this PhD. To my grandmother, thank you for inspiring me to follow in your footsteps.

- Rosita, March 2025

References

(1) Lee, E. H.; Hsin, J.; Sotomayor, M.; Comellas, G.; Schulten, K. Discovery Through the Computational Microscope. *Structure* **2009**, *17* (10), 1295–1306. https://doi.org/10.1016/j.str.2009.09.001.

(2) Ingólfsson, H. I.; Arnarez, C.; Periole, X.; Marrink, S. J. Computational 'Microscopy' of Cellular Membranes. *J. Cell Sci.* **2016**, *129* (2), 257–268. https://doi.org/10.1242/jcs.176040.

(3) Moradi, S.; Nowroozi, A.; Shahlaei, M. Shedding Light on the Structural Properties of Lipid Bilayers Using Molecular Dynamics Simulation: A Review Study. *RSC Adv.* **2019**, *9* (8), 4644–4658. https://doi.org/10.1039/C8RA08441F.

(4) Hollingsworth, S. A.; Dror, R. O. Molecular Dynamics Simulation for All. *Neuron* **2018**, *99* (6), 1129–1143. https://doi.org/10.1016/j.neuron.2018.08.011.

(5) Marrink, S. J.; Corradi, V.; Souza, P. C. T.; Ingólfsson, H. I.; Tieleman, D. P.; Sansom, M. S. P. Computational Modeling of Realistic Cell Membranes. *Chem. Rev.* **2019**, *119* (9), 6184–6226. https://doi.org/10.1021/acs.chemrev.8b00460.

(6) Koldsø, H.; Shorthouse, D.; Hélie, J.; Sansom, M. S. P. Lipid Clustering Correlates with Membrane Curvature as Revealed by Molecular Simulations of Complex Lipid Bilayers. *PLOS Comput. Biol.* **2014**, *10* (10), e1003911. https://doi.org/10.1371/journal.pcbi.1003911.

(7) Abraham, M. J.; Murtola, T.; Schulz, R.; Páll, S.; Smith, J. C.; Hess, B.; Lindahl, E. GROMACS: High Performance Molecular Simulations through Multi-Level Parallelism from Laptops to Supercomputers. *SoftwareX* **2015**, *1–2*, 19–25. https://doi.org/10.1016/j.softx.2015.06.001.

(8) Artursson, P.; Karlsson, J. Correlation between Oral Drug Absorption in Humans and Apparent Drug Permeability Coefficients in Human Intestinal Epithelial (Caco-2) Cells. *Biochem. Biophys. Res. Commun.* **1991**, *175* (3), 880–885. https://doi.org/10.1016/0006-291X(91)91647-U.

(9) Wang, L.; Wang, N.; Zhang, W.; Cheng, X.; Yan, Z.; Shao, G.; Wang, X.; Wang, R.; Fu, C. Therapeutic Peptides: Current Applications and Future Directions. *Signal Transduct. Target. Ther.* **2022**, *7* (1), 1–27. https://doi.org/10.1038/s41392-022-00904-4.

(10) Lennernäs, H.; Shah, V. P.; Crison, J. R.; Amidon, G. L. A Theoretical Basis for a Biopharmaceutic Drug Classification: The Correlation of in Vitro Drug Product Dissolution and in Vivo Bioavailability. **1995**. https://doi.org/10.1023/A:1016212804288.
(11) Curatolo, W. Physical Chemical Properties of Oral Drug Candidates in the Discovery and Exploratory Development Settings. *Pharm. Sci. Technol. Today* **1998**, *1* (9), 387–393. https://doi.org/10.1016/S1461-5347(98)00097-2.
(12) Lipinski, C. A.; Lombardo, F.; Dominy, B. W.; Feeney, P. J. Experimental and Computational Approaches to Estimate Solubility and Permeability in Drug Discovery and Development Settings1. *Adv. Drug Deliv. Rev.* **2001**, *46* (1), 3–26. https://doi.org/10.1016/S0169-409X(00)00129-0.
(13) Henninot, A.; Collins, J. C.; Nuss, J. M. The Current State of Peptide Drug Discovery: Back to the Future? *J. Med. Chem.* **2018**, *61* (4), 1382–1414. https://doi.org/10.1021/acs.jmedchem.7b00318.
(14) Söldner, C. A.; Sticht, H.; Horn, A. H. C. Molecular Simulations and Alzheimer′s Disease. In *Systems Medicine*; Wolkenhauer, O., Ed.; Academic Press: Oxford, 2021; pp 54–70. https://doi.org/10.1016/B978-0-12-801238-3.11541-7.
(15) Hjalte, J.; Hossain, S.; Hugerth, A.; Sjögren, H.; Wahlgren, M.; Larsson, P.; Lundberg, D. Aggregation Behavior of Structurally Similar Therapeutic Peptides Investigated by 1H NMR and All-Atom Molecular Dynamics Simulations. *Mol. Pharm.* **2022**, *19* (3), 904–917. https://doi.org/10.1021/acs.molpharmaceut.1c00883.
(16) Maher, S.; Mrsny, R. J.; Brayden, D. J. Intestinal Permeation Enhancers for Oral Peptide Delivery. *Adv. Drug Deliv. Rev.* **2016**, *106*, 277–319. https://doi.org/10.1016/j.addr.2016.06.005.
(17) Sun, X.; Abioye, R. O.; Okagu, O. D.; Udenigwe, C. C. Peptide-Mucin Binding and Biosimilar Mucus-Permeating Properties. *Gels* **2022**, *8* (1), 1. https://doi.org/10.3390/gels8010001.
(18) Sugita, M.; Sugiyama, S.; Fujie, T.; Yoshikawa, Y.; Yanagisawa, K.; Ohue, M.; Akiyama, Y. Large-Scale Membrane Permeability Prediction of Cyclic Peptides Crossing a Lipid Bilayer Based on Enhanced Sampling Molecular Dynamics Simulations. *J. Chem. Inf. Model.* **2021**, *61* (7), 3681–3695. https://doi.org/10.1021/acs.jcim.1c00380.
(19) Maher, S.; Leonard, T. W.; Jacobsen, J.; Brayden, D. J. Safety and Efficacy of Sodium Caprate in Promoting Oral Drug Absorption: From in Vitro to the Clinic. *Adv. Drug Deliv. Rev.* **2009**, *61* (15), 1427–1449. https://doi.org/10.1016/j.addr.2009.09.006.
(20) Maher, S.; Geoghegan, C.; Brayden, D. J. Intestinal Permeation Enhancers to Improve Oral Bioavailability of Macromolecules: Reasons for Low Efficacy in Humans. *Expert Opin. Drug Deliv.* **2021**, *18* (2), 273–300. https://doi.org/10.1080/17425247.2021.1825375.

(21) Castelli, M. C.; Wong, D. F.; Friedman, K.; Riley, M. G. I. Pharmacokinetics of Oral Cyanocobalamin Formulated With Sodium N-[8-(2-Hydroxybenzoyl)Amino]Caprylate (SNAC): An Open-Label, Randomized, Single-Dose, Parallel-Group Study in Healthy Male Subjects. *Clin. Ther.* **2011**, *33* (7), 934–945. https://doi.org/10.1016/j.clinthera.2011.05.088.
(22) Humphrey, W.; Dalke, A.; Schulten, K. VMD: Visual Molecular Dynamics. *J. Mol. Graph.* **1996**, *14* (1), 33–38. https://doi.org/10.1016/0263-7855(96)00018-5.
(23) Wang, C. K.; Swedberg, J. E.; Harvey, P. J.; Kaas, Q.; Craik, D. J. Conformational Flexibility Is a Determinant of Permeability for Cyclosporin. *J. Phys. Chem. B* **2018**, *122* (8), 2261–2276. https://doi.org/10.1021/acs.jpcb.7b12419.
(24) Furukawa, A.; Schwochert, J.; Pye, C. R.; Asano, D.; Edmondson, Q. D.; Turmon, A. C.; Klein, V. G.; Ono, S.; Okada, O.; Lokey, R. S. Drug-Like Properties in Macrocycles above MW 1000: Backbone Rigidity versus Side-Chain Lipophilicity. *Angew. Chem. Int. Ed.* **2020**, *59* (48), 21571–21577. https://doi.org/10.1002/anie.202004550.
(25) Danelius, E.; Poongavanam, V.; Peintner, S.; Wieske, L. H. E.; Erdélyi, M.; Kihlberg, J. Solution Conformations Explain the Chameleonic Behaviour of Macrocyclic Drugs. *Chem. – Eur. J.* **2020**, *26* (23), 5231–5244. https://doi.org/10.1002/chem.201905599.
(26) Kishimoto, H.; Ridley, C.; Thornton, D. J. The Lipophilic Cyclic Peptide Cyclosporin A Induces Aggregation of Gel-Forming Mucins. *Sci. Rep.* **2022**, *12* (1), 6153. https://doi.org/10.1038/s41598-022-10125-y.
(27) Buckley, S. T.; Bækdal, T. A.; Vegge, A.; Maarbjerg, S. J.; Pyke, C.; Ahnfelt-Rønne, J.; Madsen, K. G.; Schéele, S. G.; Alanentalo, T.; Kirk, R. K.; Pedersen, B. L.; Skyggebjerg, R. B.; Benie, A. J.; Strauss, H. M.; Wahlund, P.-O.; Bjerregaard, S.; Farkas, E.; Fekete, C.; Søndergaard, F. L.; Borregaard, J.; Hartoft-Nielsen, M.-L.; Knudsen, L. B. Transcellular Stomach Absorption of a Derivatized Glucagon-like Peptide-1 Receptor Agonist. *Sci. Transl. Med.* **2018**, *10* (467), eaar7047. https://doi.org/10.1126/scitranslmed.aar7047.
(28) Leone-Bay, A.; Santiago, N.; Achan, D.; Chaudhary, K.; DeMorin, F.; Falzarano, L.; Haas, S.; Kalbag, S.; Kaplan, D. N-Acylated .Alpha.-Amino Acids as Novel Oral Delivery Agents for Proteins. *J. Med. Chem.* **1995**, *38* (21), 4263–4269. https://doi.org/10.1021/jm00021a015.
(29) Bohley, M.; Leroux, J.-C. Gastrointestinal Permeation Enhancers Beyond Sodium Caprate and SNAC - What Is Coming Next? *Adv. Sci.* **2024**, *11* (33), 2400843. https://doi.org/10.1002/advs.202400843.
(30) Tuvia, S.; Atsmon, J.; Teichman, S. L.; Katz, S.; Salama, P.; Pelled, D.; Landau, I.; Karmeli, I.; Bidlingmaier, M.; Strasburger, C. J.; Kleinberg, D. L.; Melmed, S.; Mamluk, R. Oral Octreotide Absorption in

Human Subjects: Comparable Pharmacokinetics to Parenteral Octreotide and Effective Growth Hormone Suppression. *J. Clin. Endocrinol. Metab.* **2012**, *97* (7), 2362–2369. https://doi.org/10.1210/jc.2012-1179.

(31) Kim, J. C.; Park, E. J.; Na, D. H. Gastrointestinal Permeation Enhancers for the Development of Oral Peptide Pharmaceuticals. *Pharmaceuticals* **2022**, *15* (12), 1585. https://doi.org/10.3390/ph15121585.

(32) Berg, S.; Krause, J.; Björkbom, A.; Walter, K.; Harun, S.; Granfeldt, A.; Janzén, D.; Nunes, S. F.; Antonsson, M.; Zuydam, N. V.; Skrtic, S.; Hugerth, A.; Weitschies, W.; Davies, N.; Abrahamsson, B.; Bergström, C. A. S. In Vitro and In Vivo Evaluation of 3D Printed Capsules with Pressure Triggered Release Mechanism for Oral Peptide Delivery. *J. Pharm. Sci.* **2021**, *110* (1), 228–238. https://doi.org/10.1016/j.xphs.2020.10.066.

(33) Danielsen, E. M. Intestinal Permeation Enhancers: Lessons Learned from Studies Using an Organ Culture Model. *Biochim. Biophys. Acta BBA - Biomembr.* **2021**, *1863* (1), 183474. https://doi.org/10.1016/j.bbamem.2020.183474.

(34) Maher, S.; Leonard, T. W.; Jacobsen, J.; Brayden, D. J. Safety and Efficacy of Sodium Caprate in Promoting Oral Drug Absorption: From *in Vitro* to the Clinic. *Adv. Drug Deliv. Rev.* **2009**, *61* (15), 1427–1449. https://doi.org/10.1016/j.addr.2009.09.006.

(35) Li, Y.; Duan, Z.; Tian, Y.; Liu, Z.; Wang, Q. A Novel Perspective and Approach to Intestinal Octreotide Absorption: Sinomenine-Mediated Reversible Tight Junction Opening and Its Molecular Mechanism. *Int. J. Mol. Sci.* **2013**, *14* (6), 12873–12892. https://doi.org/10.3390/ijms140612873.

(36) Dening, T. J.; Douglas, J. T.; Hageman, M. J. Do Macrocyclic Peptide Drugs Interact with Bile Salts under Simulated Gastrointestinal Conditions? *Mol. Pharm.* **2021**, *18* (8), 3086–3098. https://doi.org/10.1021/acs.molpharmaceut.1c00309.

(37) Gadgil, P.; Alleyne, C.; Feng, K.-I.; Hu, M.; Gindy, M.; Buevich, A. V.; Fauty, S.; Salituro, G.; Wen, J.; Li, Y.; Nofsinger, R.; Sawyer, T. K.; Buist, N. Assessing the Utility of In Vitro Screening Tools for Predicting Bio-Performance of Oral Peptide Delivery. *Pharm. Res.* **2019**, *36* (10), 151. https://doi.org/10.1007/s11095-019-2682-8.

(38) Pabois, O.; Ziolek, R. M.; Lorenz, C. D.; Prévost, S.; Mahmoudi, N.; Skoda, M. W. A.; Welbourn, R. J. L.; Valero, M.; Harvey, R. D.; Grundy, M. M.-L.; Wilde, P. J.; Grillo, I.; Gerelli, Y.; Dreiss, C. A. Morphology of Bile Salts Micelles and Mixed Micelles with Lipolysis Products, from Scattering Techniques and Atomistic Simulations. *J. Colloid Interface Sci.* **2021**, *587*, 522–537. https://doi.org/10.1016/j.jcis.2020.10.101.

(39) Yoon, B. K.; Jackman, J. A. Medium-Chain Fatty Acids and Monoglycerides: Nanoarchitectonics-Based Insights into Molecular Self-Assembly, Membrane Interactions, and Applications. *Adv. Colloid Interface Sci.* **2025**, 103465. https://doi.org/10.1016/j.cis.2025.103465.
(40) Yoon, B. K.; Jackman, J. A. Medium-Chain Fatty Acids and Monoglycerides: Nanoarchitectonics-Based Insights into Molecular Self-Assembly, Membrane Interactions, and Applications. *Adv. Colloid Interface Sci.* **2025**, *340*, 103465. https://doi.org/10.1016/j.cis.2025.103465.
(41) Wellen, B. A.; Lach, E. A.; Allen, H. C. Surface pKa of Octanoic, Nonanoic, and Decanoic Fatty Acids at the Air–Water Interface: Applications to Atmospheric Aerosol Chemistry. *Phys. Chem. Chem. Phys.* **2017**, *19* (39), 26551–26558. https://doi.org/10.1039/C7CP04527A.
(42) Hossain, M. S.; Berg, S.; Bergström, C. A. S.; Larsson, P. Aggregation Behavior of Medium Chain Fatty Acids Studied by Coarse-Grained Molecular Dynamics Simulation. *AAPS PharmSciTech* **2019**, *20* (2), 61. https://doi.org/10.1208/s12249-018-1289-4.
(43) Rogerson, M. L.; Robinson, B. H.; Bucak, S.; Walde, P. Kinetic Studies of the Interaction of Fatty Acids with Phosphatidylcholine Vesicles (Liposomes). *Colloids Surf. B Biointerfaces* **2006**, *48* (1), 24–34. https://doi.org/10.1016/j.colsurfb.2006.01.001.
(44) Kang, C.; Bernaldez, M.; Stamatis, S. D.; Rose, J. P.; Sun, R. Interaction between Permeation Enhancers and Lipid Bilayers. *J. Phys. Chem. B* **2024**, *128* (7), 1668–1679. https://doi.org/10.1021/acs.jpcb.3c06448.
(45) Twarog, C.; Liu, K.; O'Brien, P. J.; Dawson, K. A.; Fattal, E.; Illel, B.; Brayden, D. J. A Head-to-Head Caco-2 Assay Comparison of the Mechanisms of Action of the Intestinal Permeation Enhancers: SNAC and Sodium Caprate (C10). *Eur. J. Pharm. Biopharm. Off. J. Arbeitsgemeinschaft Pharm. Verfahrenstechnik EV* **2020**, *152*, 95–107. https://doi.org/10.1016/j.ejpb.2020.04.023.
(46) Twarog, C.; Fattah, S.; Heade, J.; Maher, S.; Fattal, E.; Brayden, D. J. Intestinal Permeation Enhancers for Oral Delivery of Macromolecules: A Comparison between Salcaprozate Sodium (SNAC) and Sodium Caprate (C10). *Pharmaceutics* **2019**, *11* (2), 78. https://doi.org/10.3390/pharmaceutics11020078.
(47) Brayden, D. J.; Gleeson, J.; Walsh, E. G. A Head-to-Head Multi-Parametric High Content Analysis of a Series of Medium Chain Fatty Acid Intestinal Permeation Enhancers in Caco-2 Cells. *Eur. J. Pharm. Biopharm.* **2014**, *88* (3), 830–839. https://doi.org/10.1016/j.ejpb.2014.10.008.
(48) Tran, H.; Aihara, E.; Mohammed, F. A.; Qu, H.; Riley, A.; Su, Y.; Lai, X.; Huang, S.; Aburub, A.; Chen, J. J. H.; Vitale, O. H.; Lao, Y.; Estwick, S.; Qi, Z.; ElSayed, M. E. H. In Vivo Mechanism of Action of Sodium Caprate for Improving the Intestinal Absorption of a

GLP1/GIP Coagonist Peptide. *Mol. Pharm.* **2023**, *20* (2), 929–941. https://doi.org/10.1021/acs.molpharmaceut.2c00443.
(49) *MK-0616: The 2023 Molecule of the Year*. Drug Hunter. https://drughunter.com/articles/mk-0616-the-2023-molecule-of-the-year (accessed 2025-03-05).
(50) Burnett, J. R.; Hooper, A. J. MK-0616: An Oral PCSK9 Inhibitor for Hypercholesterolemia Treatment. *Expert Opin. Investig. Drugs* **2023**, *32* (10), 873–878. https://doi.org/10.1080/13543784.2023.2267972.
(51) PubChem. *Enlicitide chloride*. https://pubchem.ncbi.nlm.nih.gov/compound/166642685 (accessed 2025-03-03).
(52) McCartney, F.; Rosa, M.; Brayden, D. J. Evaluation of Sucrose Laurate as an Intestinal Permeation Enhancer for Macromolecules: Ex Vivo and In Vivo Studies. *Pharmaceutics* **2019**, *11* (11), 565. https://doi.org/10.3390/pharmaceutics11110565.
(53) Knudsen, L. B.; Lau, J. The Discovery and Development of Liraglutide and Semaglutide. *Front. Endocrinol.* **2019**, *10*, 155. https://doi.org/10.3389/fendo.2019.00155.
(54) Fattah, S.; Ismaiel, M.; Murphy, B.; Rulikowska, A.; Frias, J. M.; Winter, D. C.; Brayden, D. J. Salcaprozate Sodium (SNAC) Enhances Permeability of Octreotide across Isolated Rat and Human Intestinal Epithelial Mucosae in Ussing Chambers. *Eur. J. Pharm. Sci.* **2020**, *154*, 105509. https://doi.org/10.1016/j.ejps.2020.105509.
(55) Ling, J.; Schroder, R.; Wuelfing, W. P.; Higgins, J.; Kesisoglou, F.; Templeton, A. C.; Su, Y. Molecular Investigation of SNAC as an Oral Peptide Permeation Enhancer in Lipid Membranes via Solid-State NMR. *Mol. Pharm.* **2025**, *22* (1), 459–473. https://doi.org/10.1021/acs.molpharmaceut.4c01061.
(56) Schneebeli, S. T.; Colston, K. J.; Faivre, K. T. Permeation Enhancer-Induced Membrane Defects Assist the Oral Absorption of Peptide Drugs. ChemRxiv January 15, 2025. https://doi.org/10.26434/chemrxiv-2025-n24f8.
(57) Niu, Z.; La Zara, D.; Blaabjerg, L.; Pessi, J.; Raptis, K.; Toftlev, A.; Sauter, M.; Christophersen, P.; Bardonnet, P.-L.; Andersson, V.; Wu, J. X.; Brandt, M.; Fan, L.; Wang, Z.; Hubálek, F.; Wahlund, P.-O.; Norrman, M.; Breusova, K.; Hjaltason, M. S.; Mortensen, N. R.; Bardtrum, L.; Nissen, B.; Naelapää, K.; Sassene, P. J. Combining SNAC and C10 in Oral Tablet Formulations for Gastric Peptide Delivery: A Preclinical and Clinical Study. *J. Controlled Release* **2025**, *378*, 92–102. https://doi.org/10.1016/j.jconrel.2024.11.078.
(58) Hossain, S.; Joyce, P.; Parrow, A.; Jõemetsa, S.; Höök, F.; Larsson, P.; Bergström, C. A. S. Influence of Bile Composition on Membrane Incorporation of Transient Permeability Enhancers. *Mol. Pharm.* **2020**, *17* (11), 4226–4240. https://doi.org/10.1021/acs.molpharmaceut.0c00668.

(59) *Cell - Lipids, Phospholipids, Membranes | Britannica*. https://www.britannica.com/science/cell-biology/Membrane-lipids (accessed 2025-03-03).
(60) Koldsø, H.; Shorthouse, D.; Hélie, J.; Sansom, M. S. P. Lipid Clustering Correlates with Membrane Curvature as Revealed by Molecular Simulations of Complex Lipid Bilayers. *PLoS Comput. Biol.* **2014**, *10* (10), e1003911. https://doi.org/10.1371/journal.pcbi.1003911.
(61) Alberts, B.; Johnson, A.; Lewis, J.; Raff, M.; Roberts, K.; Walter, P. Membrane Proteins. In *Molecular Biology of the Cell. 4th edition*; Garland Science, 2002.
(62) Alberts, B.; Johnson, A.; Lewis, J.; Raff, M.; Roberts, K.; Walter, P. The Lipid Bilayer. In *Molecular Biology of the Cell. 4th edition*; Garland Science, 2002.
(63) Frallicciardi, J.; Melcr, J.; Siginou, P.; Marrink, S. J.; Poolman, B. Membrane Thickness, Lipid Phase and Sterol Type Are Determining Factors in the Permeability of Membranes to Small Solutes. *Nat. Commun.* **2022**, *13* (1), 1605. https://doi.org/10.1038/s41467-022-29272-x.
(64) Lipp, N.-F.; Ikhlef, S.; Milanini, J.; Drin, G. Lipid Exchangers: Cellular Functions and Mechanistic Links With Phosphoinositide Metabolism. *Front. Cell Dev. Biol.* **2020**, *8*. https://doi.org/10.3389/fcell.2020.00663.
(65) *Membrane | Definition, Structure, & Functions | Britannica*. https://www.britannica.com/science/membrane-biology (accessed 2025-03-03).
(66) Bennett, W. F. D.; Tieleman, D. P. Computer Simulations of Lipid Membrane Domains. *Biochim. Biophys. Acta BBA - Biomembr.* **2013**, *1828* (8), 1765–1776. https://doi.org/10.1016/j.bbamem.2013.03.004.
(67) Alder, B. J.; Wainwright, T. E. Phase Transition for a Hard Sphere System. *J. Chem. Phys.* **1957**, *27* (5), 1208–1209. https://doi.org/10.1063/1.1743957.
(68) Verlet, L. Computer "Experiments" on Classical Fluids. I. Thermodynamical Properties of Lennard-Jones Molecules. *Phys. Rev.* **1967**, *159* (1), 98–103. https://doi.org/10.1103/PhysRev.159.98.
(69) Marrink, S.-J.; Berendsen, H. J. C. Simulation of Water Transport through a Lipid Membrane. *J. Phys. Chem.* **1994**, *98* (15), 4155–4168. https://doi.org/10.1021/j100066a040.
(70) Venable, R. M.; Krämer, A.; Pastor, R. W. Molecular Dynamics Simulations of Membrane Permeability. *Chem. Rev.* **2019**, *119* (9), 5954–5997. https://doi.org/10.1021/acs.chemrev.8b00486.
(71) Pronk, S.; Páll, S.; Schulz, R.; Larsson, P.; Bjelkmar, P.; Apostolov, R.; Shirts, M. R.; Smith, J. C.; Kasson, P. M.; van der Spoel, D.; Hess, B.; Lindahl, E. GROMACS 4.5: A High-Throughput and Highly Parallel Open Source Molecular Simulation Toolkit. *Bioinformatics* **2013**, *29* (7), 845–854. https://doi.org/10.1093/bioinformatics/btt055.

(72) Marklund, E. ErikMarklund/Mkvsites, 2024. https://github.com/ErikMarklund/mkvsites (accessed 2025-02-12).
(73) Larsson, P.; Kneiszl, R. C.; Marklund, E. G. MkVsites: A Tool for Creating GROMACS Virtual Sites Parameters to Increase Performance in All-Atom Molecular Dynamics Simulations. *J. Comput. Chem.* **2020**, *41* (16), 1564–1569. https://doi.org/10.1002/jcc.26198.
(74) de Jong, D. H.; Singh, G.; Bennett, W. F. D.; Arnarez, C.; Wassenaar, T. A.; Schäfer, L. V.; Periole, X.; Tieleman, D. P.; Marrink, S. J. Improved Parameters for the Martini Coarse-Grained Protein Force Field. *J. Chem. Theory Comput.* **2013**, *9* (1), 687–697. https://doi.org/10.1021/ct300646g.
(75) Kirkwood, J. G. Statistical Mechanics of Fluid Mixtures. *J Chem Phys* **1935**, *3* (3), 300–313. https://doi.org/10.1063/1.1749657.
(76) Torrie, G. M.; Valleau, J. P. Nonphysical Sampling Distributions in Monte Carlo Free-Energy Estimation: Umbrella Sampling. *J. Comput. Phys.* **1977**, *23* (2), 187–199. https://doi.org/10.1016/0021-9991(77)90121-8.
(77) Kästner, J. Umbrella Sampling. *WIREs Comput. Mol. Sci.* **2011**, *1* (6), 932–942. https://doi.org/10.1002/wcms.66.
(78) Hub, J. S.; de Groot, B. L.; van der Spoel, D. G_wham—A Free Weighted Histogram Analysis Implementation Including Robust Error and Autocorrelation Estimates. *J. Chem. Theory Comput.* **2010**, *6* (12), 3713–3720. https://doi.org/10.1021/ct100494z.
(79) Kumar, S.; Rosenberg, J. M.; Bouzida, D.; Swendsen, R. H.; Kollman, P. A. THE Weighted Histogram Analysis Method for Free-Energy Calculations on Biomolecules. I. The Method. *J. Comput. Chem.* **1992**, *13* (8), 1011–1021. https://doi.org/10.1002/jcc.540130812.
(80) Berendsen, H. J. C.; van der Spoel, D.; van Drunen, R. GROMACS: A Message-Passing Parallel Molecular Dynamics Implementation. *Comput. Phys. Commun.* **1995**, *91* (1), 43–56. https://doi.org/10.1016/0010-4655(95)00042-E.
(81) Case, D. A.; Cheatham III, T. E.; Darden, T.; Gohlke, H.; Luo, R.; Merz Jr., K. M.; Onufriev, A.; Simmerling, C.; Wang, B.; Woods, R. J. The Amber Biomolecular Simulation Programs. *J. Comput. Chem.* **2005**, *26* (16), 1668–1688. https://doi.org/10.1002/jcc.20290.
(82) Phillips, J. C.; Braun, R.; Wang, W.; Gumbart, J.; Tajkhorshid, E.; Villa, E.; Chipot, C.; Skeel, R. D.; Kalé, L.; Schulten, K. Scalable Molecular Dynamics with NAMD. *J. Comput. Chem.* **2005**, *26* (16), 1781–1802. https://doi.org/10.1002/jcc.20289.
(83) Brooks, B. R.; Bruccoleri, R. E.; Olafson, B. D.; States, D. J.; Swaminathan, S.; Karplus, M. CHARMM: A Program for Macromolecular Energy, Minimization, and Dynamics Calculations. *J. Comput. Chem.* **1983**, *4* (2), 187–217. https://doi.org/10.1002/jcc.540040211.

(84) Plimpton, S. Fast Parallel Algorithms for Short-Range Molecular Dynamics. *J. Comput. Phys.* **1995**, *117* (1), 1–19. https://doi.org/10.1006/jcph.1995.1039.
(85) Bowers, K. J.; Chow, E.; Xu, H.; Dror, R. O.; Eastwood, M. P.; Gregersen, B. A.; Klepeis, J. L.; Kolossvary, I.; Moraes, M. A.; Sacerdoti, F. D.; Salmon, J. K.; Shan, Y.; Shaw, D. E. Scalable Algorithms for Molecular Dynamics Simulations on Commodity Clusters. In *Proceedings of the 2006 ACM/IEEE conference on Supercomputing*; SC '06; Association for Computing Machinery: New York, NY, USA, 2006; pp 84-es. https://doi.org/10.1145/1188455.1188544.
(86) Abraham, M.; Alekseenko, A.; Basov, V.; Bergh, C.; Briand, E.; Brown, A.; Doijade, M.; Fiorin, G.; Fleischmann, S.; Gorelov, S.; Gouaillardet, G.; Grey, A.; Irrgang, M. E.; Jalalypour, F.; Jordan, J.; Kutzner, C.; Lemkul, J. A.; Lundborg, M.; Merz, P.; Miletic, V.; Morozov, D.; Nabet, J.; Pall, S.; Pasquadibisceglie, A.; Pellegrino, M.; Santuz, H.; Schulz, R.; Shugaeva, T.; Shvetsov, A.; Villa, A.; Wingbermuehle, S.; Hess, B.; Lindahl, E. GROMACS 2024.1 Manual. **2024**. https://doi.org/10.5281/zenodo.10721192.
(87) Marrink, S. J.; de Vries, A. H.; Mark, A. E. Coarse Grained Model for Semiquantitative Lipid Simulations. *J. Phys. Chem. B* **2004**, *108* (2), 750–760. https://doi.org/10.1021/jp036508g.
(88) Marrink, S. J.; Risselada, H. J.; Yefimov, S.; Tieleman, D. P.; de Vries, A. H. The MARTINI Force Field: Coarse Grained Model for Biomolecular Simulations. *J. Phys. Chem. B* **2007**, *111* (27), 7812–7824. https://doi.org/10.1021/jp071097f.
(89) Jo, S.; Kim, T.; Iyer, V. G.; Im, W. CHARMM-GUI: A Web-Based Graphical User Interface for CHARMM. *J. Comput. Chem.* **2008**, *29* (11), 1859–1865. https://doi.org/10.1002/jcc.20945.
(90) Brooks, B. R.; Brooks, C. L.; Mackerell, A. D.; Nilsson, L.; Petrella, R. J.; Roux, B.; Won, Y.; Archontis, G.; Bartels, C.; Boresch, S.; Caflisch, A.; Caves, L.; Cui, Q.; Dinner, A. R.; Feig, M.; Fischer, S.; Gao, J.; Hodoscek, M.; Im, W.; Kuczera, K.; Lazaridis, T.; Ma, J.; Ovchinnikov, V.; Paci, E.; Pastor, R. W.; Post, C. B.; Pu, J. Z.; Schaefer, M.; Tidor, B.; Venable, R. M.; Woodcock, H. L.; Wu, X.; Yang, W.; York, D. M.; Karplus, M. CHARMM: The Biomolecular Simulation Program. *J. Comput. Chem.* **2009**, *30* (10), 1545–1614. https://doi.org/10.1002/jcc.21287.
(91) Wu, E. L.; Cheng, X.; Jo, S.; Rui, H.; Song, K. C.; Dávila-Contreras, E. M.; Qi, Y.; Lee, J.; Monje-Galvan, V.; Venable, R. M.; Klauda, J. B.; Im, W. CHARMM-GUI *Membrane Builder* toward Realistic Biological Membrane Simulations. *J. Comput. Chem.* **2014**, *35* (27), 1997–2004. https://doi.org/10.1002/jcc.23702.

(92) Jo, S.; Lim, J. B.; Klauda, J. B.; Im, W. CHARMM-GUI Membrane Builder for Mixed Bilayers and Its Application to Yeast Membranes. *Biophys. J.* **2009**, *97* (1), 50–58. https://doi.org/10.1016/j.bpj.2009.04.013.
(93) Jo, S.; Kim, T.; Im, W. Automated Builder and Database of Protein/Membrane Complexes for Molecular Dynamics Simulations. *PLOS ONE* **2007**, *2* (9), e880. https://doi.org/10.1371/journal.pone.0000880.
(94) Vanommeslaeghe, K.; MacKerell, A. D. Jr. Automation of the CHARMM General Force Field (CGenFF) I: Bond Perception and Atom Typing. *J. Chem. Inf. Model.* **2012**, *52* (12), 3144–3154. https://doi.org/10.1021/ci300363c.
(95) Vanommeslaeghe, K.; Raman, E. P.; MacKerell, A. D. Jr. Automation of the CHARMM General Force Field (CGenFF) II: Assignment of Bonded Parameters and Partial Atomic Charges. *J. Chem. Inf. Model.* **2012**, *52* (12), 3155–3168. https://doi.org/10.1021/ci3003649.
(96) Mayne, C. G.; Saam, J.; Schulten, K.; Tajkhorshid, E.; Gumbart, J. C. Rapid Parameterization of Small Molecules Using the Force Field Toolkit. *J. Comput. Chem.* **2013**, *34* (32), 2757–2770. https://doi.org/10.1002/jcc.23422.
(97) *GAFF*. https://ambermd.org/antechamber/gaff.html (accessed 2025-03-09).
(98) Lee, J.; Cheng, X.; Swails, J. M.; Yeom, M. S.; Eastman, P. K.; Lemkul, J. A.; Wei, S.; Buckner, J.; Jeong, J. C.; Qi, Y.; Jo, S.; Pande, V. S.; Case, D. A.; Brooks, C. L.; MacKerell, A. D.; Klauda, J. B.; Im, W. CHARMM-GUI Input Generator for NAMD, GROMACS, AMBER, OpenMM, and CHARMM/OpenMM Simulations Using the CHARMM36 Additive Force Field. *J. Chem. Theory Comput.* **2016**, *12* (1), 405–413. https://doi.org/10.1021/acs.jctc.5b00935.
(99) Huang, J.; MacKerell, A. D. CHARMM36 All-Atom Additive Protein Force Field: Validation Based on Comparison to NMR Data. *J. Comput. Chem.* **2013**, *34* (25), 2135–2145. https://doi.org/10.1002/jcc.23354.
(100) Buchoux, S. FATSLiM: A Fast and Robust Software to Analyze MD Simulations of Membranes. *Bioinformatics* **2017**, *33* (1), 133–134. https://doi.org/10.1093/bioinformatics/btw563.
(101) *do-order.py*. cgmartini.nl. https://cgmartini-library.s3.ca-central-1.amazonaws.com/1_Downloads/tools/other_tools/do-order-gmx5.py (accessed 2025-03-08).
(102) Piggot, T. J.; Allison, J. R.; Sessions, R. B.; Essex, J. W. On the Calculation of Acyl Chain Order Parameters from Lipid Simulations. *J. Chem. Theory Comput.* **2017**, *13* (11), 5683–5696. https://doi.org/10.1021/acs.jctc.7b00643.

(103) Zawada, K. E.; Wrona, D.; Rawle, R. J.; Kasson, P. M. Influenza Viral Membrane Fusion Is Sensitive to Sterol Concentration but Surprisingly Robust to Sterol Chemical Identity. *Sci. Rep.* **2016**, *6* (1), 29842. https://doi.org/10.1038/srep29842.
(104) Hummer, G. Position-Dependent Diffusion Coefficients and Free Energies from Bayesian Analysis of Equilibrium and Replica Molecular Dynamics Simulations. *New J. Phys.* **2005**, *7* (1), 34. https://doi.org/10.1088/1367-2630/7/1/034.
(105) Dickson, C. Callumjd/AMBER-Umbrella_COM_restraint_tutorial, 2024. https://github.com/callumjd/AMBER-Umbrella_COM_restraint_tutorial (accessed 2025-03-08).
(106) Lee, C. T.; Comer, J.; Herndon, C.; Leung, N.; Pavlova, A.; Swift, R. V.; Tung, C.; Rowley, C. N.; Amaro, R. E.; Chipot, C.; Wang, Y.; Gumbart, J. C. Simulation-Based Approaches for Determining Membrane Permeability of Small Compounds. *J. Chem. Inf. Model.* **2016**, *56* (4), 721–733. https://doi.org/10.1021/acs.jcim.6b00022.
(107) Wang, S.-H.; Dong, X.-Y.; Sun, Y. Effect of (−)-Epigallocatechin-3-Gallate on Human Insulin Fibrillation/Aggregation Kinetics. *Biochem. Eng. J.* **2012**, *63*, 38–49. https://doi.org/10.1016/j.bej.2012.02.002.
(108) Manno, M.; Craparo, E. F.; Podestà, A.; Bulone, D.; Carrotta, R.; Martorana, V.; Tiana, G.; San Biagio, P. L. Kinetics of Different Processes in Human Insulin Amyloid Formation. *J. Mol. Biol.* **2007**, *366* (1), 258–274. https://doi.org/10.1016/j.jmb.2006.11.008.
(109) Chaaban, H.; Vallooran, J. J.; van de Weert, M.; Foderà, V. Ion-Mediated Morphological Diversity in Protein Amyloid Systems. *J. Phys. Chem. Lett.* **2022**, *13* (16), 3586–3593. https://doi.org/10.1021/acs.jpclett.2c00182.
(110) Nielsen, L.; Frokjaer, S.; Carpenter, J. F.; Brange, J. Studies of the Structure of Insulin Fibrils by Fourier Transform Infrared (FTIR) Spectroscopy and Electron Microscopy. *J. Pharm. Sci.* **2001**, *90* (1), 29–37. https://doi.org/10.1002/1520-6017(200101)90:1<29::AID-JPS4>3.0.CO;2-4.
(111) Ambrose, E. J.; Elliott, A.; Wilson, A. H. Infra-Red Spectroscopic Studies of Globular Protein Structure. *Proc. R. Soc. Lond. Ser. Math. Phys. Sci.* **1997**, *208* (1092), 75–90. https://doi.org/10.1098/rspa.1951.0145.
(112) Iannuzzi, C.; Borriello, M.; Portaccio, M.; Irace, G.; Sirangelo, I. Insights into Insulin Fibril Assembly at Physiological and Acidic pH and Related Amyloid Intrinsic Fluorescence. *Int. J. Mol. Sci.* **2017**, *18* (12), 2551. https://doi.org/10.3390/ijms18122551.
(113) Kamp, F.; Hamilton, J. A. How Fatty Acids of Different Chain Length Enter and Leave Cells by Free Diffusion. *Prostaglandins Leukot. Essent. Fatty Acids* **2006**, *75* (3), 149–159. https://doi.org/10.1016/j.plefa.2006.05.003.

Acta Universitatis Upsaliensis

Digital Comprehensive Summaries of Uppsala Dissertations from the Faculty of Pharmacy 373

Editor: The Dean of the Faculty of Pharmacy

A doctoral dissertation from the Faculty of Pharmacy, Uppsala University, is usually a summary of a number of papers. A few copies of the complete dissertation are kept at major Swedish research libraries, while the summary alone is distributed internationally through the series Digital Comprehensive Summaries of Uppsala Dissertations from the Faculty of Pharmacy. (Prior to January, 2005, the series was published under the title "Comprehensive Summaries of Uppsala Dissertations from the Faculty of Pharmacy".)

Distribution: publications.uu.se
urn:nbn:se:uu:diva-552025

ACTA UNIVERSITATIS
UPSALIENSIS
2025